Università degli Studi di Pavia

ROSE School

EUROPEAN SCHOOL FOR ADVANCED STUDIES IN REDUCTION OF SEISMIC RISK

Use of Shape-Memory Alloy Devices in Earthquake Engineering: Mechanical Properties, Advanced Constitutive Modelling and Structural Applications

A Thesis Submitted in Partial Fulfilment of the Requirements for the Doctor of Philosophy Degree in

EARTHQUAKE ENGINEERING

by

DAVIDE FUGAZZA

Advisors: Prof. Ferdinando Auricchio (Università degli Studi di Pavia)
Prof. Reginald DesRoches (Georgia Institute of Technology)

Pavia, August 2005

ABSTRACT

Shape-memory alloys (SMAs) are a class of solids showing mechanical properties not present in materials usually utilized in engineering. SMAs have the ability to undergo reversible micromechanical phase transition processess by changing their cristallographic structure. This capacity results in two major features at the macroscopic level which are the *superelasticity* and the *shape-memory effect*. Due to these unique characteristics, SMA materials lend themselves to innovative applications in many scientific fields, ranging from biomedical devices, such as stents or orthodontic archwires, to apparatus for the deployment and control of space structures, such as antennas and satellites.

Recent experimental and numerical investigations have also shown that the use of SMAs as vibration control devices seems to be an effective mean of improving the dynamic response of buildings and bridges subjected to earthquake-induced excitations.

In this respect, the present work focuses on the seismic performance of steel frames equipped with either steel or superelastic SMA braces, in order to evaluate the possibility of adopting an innovative bracing system in place of a traditional one. Also, a contribution on the modelling of superelastic SMA materials for seismic applications is given and two uniaxial rate-dependent constitutive equations are developed, implemented and compared with experimental data.

Finally, preliminary results concerning shake table tests of a reduce-scale frame equipped with superelastic SMA braces are provided and numerical results from the corresponding finite element study are reported and discussed.

Keywords: shape-memory alloys, constitutive modelling, experimental data, seismic protection devices, steel buildings, bracing systems, dynamic analysis, earthquake engineering.

The dissertation is organized in 7 Chapters and 3 Appendices as follows:

Chapter 1 overviews the main features of SMAs. It also explains the reason for the increasing interest in such new materials through a survey of the most important applications nowadays exploited.

Chapter 2 investigates the mechanical properties of SMAs by reviewing the experimental works available in the literature. The structural behavior of SMA wires, bars and plates is discussed in view of their potential use as innovative seimic devices.

Chapter 3 proposes an updated state-of-the-art review on the use of SMA-based devices in earthquake engineering. Attention is devoted to numerical, experimental and existing applications.

Chapter 4 concentrates on the structural applications. An extensive campaign of numerical simulations is performed on steel buildings equipped with either traditional steel braces or innovative superelastic SMA braces for the evaluation of their seismic performance.

Chapter 5 focuses on the constitutive modelling of SMAs for seismic applications. Two rate-dependent uniaxial constitutive models for superelastic SMAs are developed and implemented and their ability to simulate experimental data is assessed.

Chapter 6 shows the preliminary results of an experimental investigation dealing with shake table tests of a reduced-scale frame endowed with superelastic SMA wires as bracing system. Comparisons with a finite element study are also provided.

Chapter 7 concludes the dissertation by summarizing the most important findings as well as by proposing some ideas for further research.

Appendix A reports the acceleration time-histories of the seismic inputs used for the numerical simulations as well as a summary of their characteristics.

Appendix B provides the mathematical expressions needed to integrate the proposed constitutive models via iterative strategy.

Appendix C lists the algebraic coefficients needed to integrate the proposed constitutive models in closed-form.

ACKNOWLEDGMENTS

I wish to express my most sincere gratitude to my advisors, Professor Ferdinando Auricchio and Professor Reginald DesRoches. I have had a great and fruitful experience working with them and I really hope that our collaboration can continue in the future.

I am indebted with Professor Auricchio for his continuous help, assistance and advice during these years and since the first time I met him. I also thank him for introducing me to the Rose School and to Georgia Tech.

I am very grateful to Professor DesRoches for giving me the possibility of working with him in the United States. That was a dream come true. I did have a good time in Atlanta and I really thank him so much for his kindness.

I would like to thank the Italian National Seismic Survery for providing the Ph.D. scholarship as well as the University of Pavia for the research fundings provided through the PRIN Project "Shape-memory alloys: constitutive modeling, structural behavior, experimental validation and design of biomedical devices" and the Progetto Giovani Ricercatori - Bando 2002. Also, the support offered by the School of Civil and Environmental Engineering of the Georgia Institute of Technology is kindly acknowledged.

Finally, a very special thank goes to my family and to my closest friends for their continuous support and encouragement, specially when I was abroad.

Pavia, August 2005

TABLE OF CONTENTS

LIST OF TABLES

LIST OF FIGURES

1. GENERAL CHARACTERISTICS OF SHAPE-MEMORY ALLOYS

1.1 Introduction

In the 1960s, Buehler and Wiley developed a series of nickel-titanium alloys, with a composition of 53 to 57% nickel by weight, that exhibited an unusual effect: severely deformed specimens of the alloys, with residual strain of 8-15%, regained their original shape after a thermal cycle. This effect became known as the *shape-memory effect* and the alloys exhibiting it were named *shape-memory alloys* (SMAs). It was later found that at sufficiently high temperatures such materials also possess the property of *superelasticity*, that is, the ability of recovering large deformations during mechanical loading-unloading cycles performed at constant temperature.

Due to their unique properties, not present in most traditional materials, in recent years SMAs have attracted significant attention from the scientific community. SMAs have been widely used in many different fields, in particular for aerospace, automotive and biomedical applications. Recent numerical and experimental studies have also highlighted the possibility of utilizing such materials in earthquake engineering, as innovative seismic devices for the protection of buildings and bridges.

1.2 General Features and Phase Transformations

The unique properties of SMAs are related to reversible martensitic phase transformations, that is, solid-to-solid diffusionless processes between a crystallographically more-ordered phase, the *austenite* and a crystallographically less-ordered phase, the *martensite*. The latter may be present in single or multiple *variants*[1]. Typically, the austenite is stable at low stresses and high temperatures, while the martensite is stable at high

[1]The martensite can be present in different but crystallographically equivalent forms (variants). If there is no preferred direction along which the martensite variants tend to align, then multiple variants are formed. If, instead, there is a preferred direction for the formation of martensite, just one (single) variant is formed.

stresses and at low temperatures. These transformations can be either thermal-induced or stress-induced [Duerig *et al.*, 1990].

In the stress-free state, an SMA is characterized by four transformation temperatures: M_s and M_f during cooling and A_s and A_f during heating. The former two (with $M_s > M_f$) indicate the temperatures at which the transformation from the austenite into martensite, also named as *parent phase*, respectively starts and finishes, while the latter two (with $A_s < A_f$) are the temperatures at which the inverse transformation, also named as *reverse phase*, starts and finishes.

1.3 Superelasticity and Shape-Memory Effect

The phase transformations between austenite and martensite are the keys to explain the superelasticity and the shape-memory effect. For the simple case of uniaxial tensile stress, a brief explanation follows.

- **Superelasticity** (Figure 1.1). Consider a specimen in the austenitic state and at a temperature grater than A_f. Accordingly, at zero stress only the austenite is stable. If the specimen is loaded, while keeping the temperature constant, the material presents a nonlinear behavior (ABC) due to a stress-induced conversion of austenite into single-variant martensite. Upon unloading, while again keeping the temperature constant, a reverse transformation from single-variant martensite to austenite occurs (CDA) as a result of the instability of the martensite at zero stress. At the end of the loading-unloading process no permanent strains are present and the stress-strain path is a closed hysteresis loop.
- **Shape-memory effect** (Figure 1.2). Consider a specimen in the multiple-variant martensitic state and at temperature lower than M_s. Accordingly, at zero stress only the martensite is stable, either in a single-variant or in a multiple-variant composition. During loading, the material has a nonlinear response (AB) due to a stress-induced conversion of the multiple-variant martensite into a single-variant martensite. During unloading (BC) residual deformations appear (AC). However, the residual (apparently inelastic) strain may be recovered by heating the material to a temperature above A_f, thus inducing a temperature-driven conversion of martensite into austenite. Finally, upon cooling, the austenite is converted back into multiple-variant martensite.

1.4 An Example of Shape-Memory Alloy Material: Nitinol

The *nickel-titanium*[2] (NiTi) system is based on the equiatomic compound of nickel and titanium. Besides the ability of tolerating quite large amounts of shape-memory strain, NiTi alloys show high stability in cyclic applications, possess an elevate electrical resistivity and are corrosion resistant (Table 1.1).

For commercial exploitation and in order to improve its properties, a third metal is usually added to the binary system. In particular, a nickel quantity up to an extra 1% is the most common modification. This increases the yield strength of the austenitic phase while, simultaneously, depressing the transformation temperatures.

The manifacturing process of NiTi alloys is not an easy task and many machining techniques can only be used with difficulty. This explains the reason for the elevated cost of such a system. Anyway, despite this disatvantage, the excellent mechanical properties of NiTi alloys (Table 1.2) have made them the most frequently used SMA material in commercial applications.

1.5 Applications

As previously described, SMAs possess properties which are not present in materials traditionally utilized in engineering practice. Accordingly, their use opens the possibility of designing and proposing innovative commercial products based on their unique characteristics. In particular, the present section reviews, through practical examples, the most important applications exploiting both the superelasticity and the shape-memory effect [Auricchio, 1995; Humbeeck, 1999a,b].

Actuators.

SMA materials have mainly been used for on/off applications such as cooling circuit valves, fire detection systems and clamping devices. For instance, commercial on/off applications are available in very small sizes such as *miniature actuators*, which are devices electrically actuated. SMAs offer important advantages in actuation mechanisms: simplicity, compactness and safety. They also create clean, silent, spark-free and zero gravity working conditions. High power/weight (or power/volume) ratios can be obtained

[2]Sometimes the nickel-titanium alloy is called Nitinol (pronounced night-in-all). The name represents its elemental components and place of origin. The “Ni” and “Ti” are the atomic symbols for nickel and titanium. The “NOL” stands for the Naval Ordinance Laboratory where it was discovered.

as well. However, some drawbacks of SMA actuators such as low energy efficiency and limited bandwidth due to heating and cooling restrictions should be considered.

Adaptive materials and hybrid composites.

The use of a *torsion tube* for trailing the edge trim tab control on helicopter rotors is a typical example of the smart blade technology, whose main task is the attenuation of noise and vibrations in the surrounding environment.

Another example of application is the *smart wing* for airplanes. For similar reasons as in the helicopter rotor blades, the shape of the wing should be adaptive, depending for instance on the actual speed of the plane and able to improve the overall efficiency.

Medicine and Biomechanics.

A number of products that have been brought to the market uses the superelastic property of SMAs. The most important ones are medical guidewires, stents and orthodontic devices.

A *medical guidewire* is a long, thin, metallic wire passed into the human body through a natural opening or a small incision. It serves as a guide for the safe introduction of various therapeutic and diagnostic devices. The use of superelastic alloys may (a) reduce the complications of the guidewire taking a permanent kink, which may be difficult to remove from the patient without injury and (b) increase steerability, that is, the ability to transmit a twist at one end of the guidewire into a rotation of identical degree at the other end.

Stent (Figure 1.3) is the technical word indicating self-expanding micro-structures, which are currently investigated for the treatment of hollow-organ or duct-system occlusions. The stent is initially stretched out to reach a small profile, which facilities a safe, atraumatic insertion of the device itself. After being released from the delivery system, the stent self-expands to over twice its compressed diameter and exerts a nearly constant, gentle, radial force on the vessel wall.

During orthodontic therapy, tooth movement is obtained through a bone remodeling process, resulting from forces applied to the dentition. Such forces are usually created by elastically deforming an *orthodontic wire* and allowing its stored energy to be released to the dentition over a period of time. Recently, coil springs made of superelastic materials have been realized. As experimentally demonstrated, they produce excellent results due

to the constant stress that SMAs are able to exert during a substantial part of the transformation.

Applications based on the damping capacity of SMAs.

A Swiss ski producer studied composite skis in which *laminated strips* made of CuZnAl alloys are embedded. The strips have the martensitic transformation temperatures slightly above 0 ^oC. Once in contact with snow, the skis cool down while the CuZnAl elements transform into martensite. In this way, vibrations are damped significantly giving the skis a much better performance.

Recent experimental and numerical investigations have also shown the possibillity of using SMA materials as innovative devices for the protection of civil engineering structures, such as buildings and bridges, against earthquake-induced vibrations. Intelligent *bracing systems* for framed structures as well as smart *restrainer cables* for bridges seem to be the most promising applications in the field.

Fashion, decoration and gadgets.

In this area some of the applications are: *eyeglass frames* (Figure 1.4), *frames for brasseries* and *antennas* for portable cellular telephones. All these items realize their goals and comfort by means of the superelastic behavior.

Apart from lingerie, NiTi alloys are also applied in other *clothing parts* such as, for instance, the use of a superelastic wire as the core wire of a wedding dress petticoat. This wire can be folded into a compact size for storage and transport.

An elegant application is the *lamp shade*. A shape-memory spring heated by an electrical light opens a lamp shade. This simple mechanism creates a sticking elegant movement of the object.

Another invention (gadget) is a *cigarette holder* of an ash-tray, that drops a burning cigarette into the ash-tray preventing it falling at the other side on a table cloth when left in the cigarette holder.

Table 1.1. Properties of binary NiTi SMAs.

Melting temperature	1300	$[^oC]$
Density	6.45	[g/cm^3]
Resistivity of austenite	$\approx$ 100	$[\mu\Omega\, cm]$
Resistivity of martensite	$\approx$ 70	$[\mu\Omega\, cm]$
Thermal conductivity of austenite	18	[W/(cm^oC)]
Thermal conductivity of martensite	8.5	[W/(cm^oC)]
Corrosion resistance	similar to Ti alloys	
Young's modulus of austenite	$\approx$ 80	[MPa]
Young's modulus of martensite	$\approx$ 20 to 40	[MPa]
Yield strength of austenite	190 to 700	[MPa]
Yield strength of martensite	70 to 140	[MPa]
Ultimate tensile strength	$\approx$ 900	[MPa]
Transformation temperature	-200 to 110	$[^o]$
Shape-memory strain	8.5	[%]

Table 1.2. Nitinol SMAs versus typical structural steel: comparison of the mechanical properties. Letters A and M stand for, respectively, austenite and martensite while abbreviations f.a. and w.h. respectively refer to the names "fully annealed" and "work hardened" which are two types of treatment.

Property		**NiTi SMA**	**Steel**
Recoverable elongation	[%]	8	2
Modulus of elasticity	[MPa]	8.7x10^4 (A), 1.4x10^4 (M)	2.07x10^5
Yield strength	[MPa]	200-700 (A), 70-140 (M)	248-517
Ultimate tensile strength	[MPa]	900 (f.a.), 2000 (w.h.)	448-827
Elongation at failure	[%]	25-50 (f.a.), 5-10 (w.h.)	20
Corrosion performance	[-]	Excellent	Fair

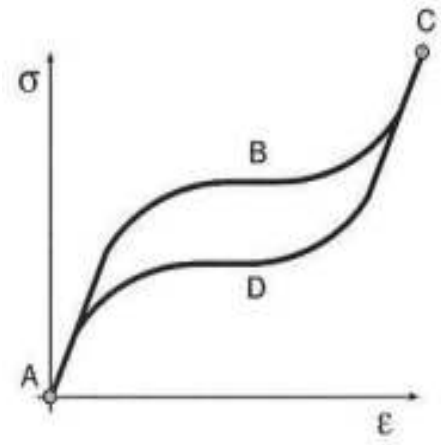

Figure 1.1. Superelasticity. At a constant high temperature the material is able to undergo large deformations with zero final permanent strain. Note the closed hysteresis loop.

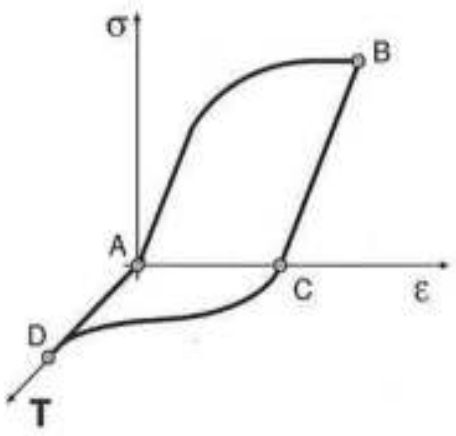

Figure 1.2. Shape-memory effect. At the end of a loading-unloading path (ABC) performed at a constant low temperature, the material presents residual deformations (AC) which can be recovered through a thermal cycle (CDA).

Figure 1.3. Self-expandable superelastic stent.

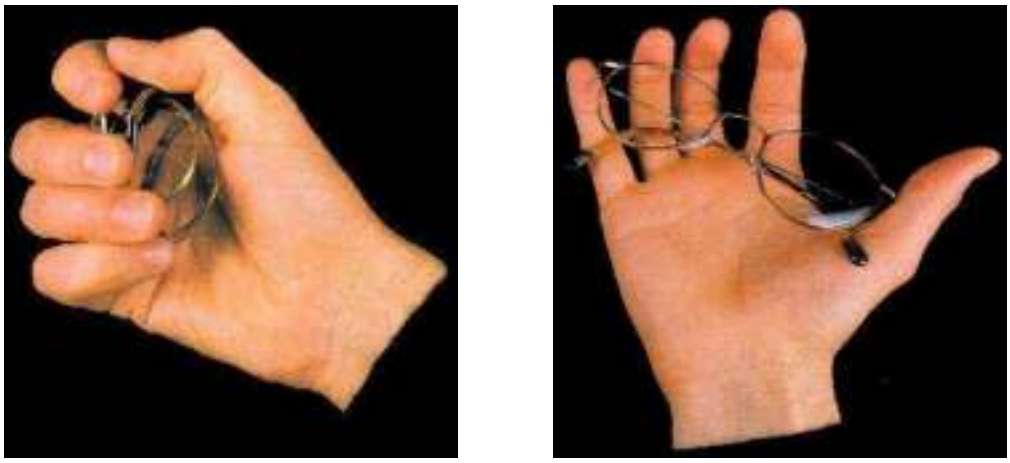

Figure 1.4. Superelastic eyeglass frame. Note the ability to recover the original shape (right) after being deformed (left).

2. MECHANICAL BEHAVIOUR OF SHAPE-MEMORY ALLOY ELEMENTS

2.1 Introduction

The mechanical behavior of SMA elements, such as wires, bars and plates, has been studied by many authors [Graesser and Cozzarelli, 1991; Lim and McDowell, 1995; Strnadel *et al.*, 1995; Piedboeuf *et al.*, 1998; Tobushi *et al.*, 1998; Wolons *et al.*, 1998; Dolce and Cardone, 2001a,b; Moroni *et al.*, 2002; Tamai and Kitagawa, 2002; DesRoches *et al.*, 2004; Fugazza, 2005] in order to understand the response of such elements under various loading conditions. In the following, we present a state-of-the-art review of the most recent experimental investigations, focusing only on works dealing with a material characterization.

2.2 Mechanical Behaviour of SMA Wires, Bars and Plates

Graesser and Cozzarelli [1991] focused on Nitinol samples machined from a raw stock of cylindrical bar having a 15.1 mm diameter. The tests were carried out at different strain rates ($\dot{\epsilon}$ equals to $1.0{\cdot}10^{-4}$ sec^{-1} and $3.0{\cdot}10^{-4}$ sec^{-1}) and up to a 3% strain in tension and compression. The researchers summarized different points of interest.

1. The stress levels at which both phase transformations take place do not show a pronounced sensitivity to the varying levels of strain rate applied.
2. The inelastic response of Nitinol is rate-dependent and affects the overall shape of the fully developed cyclic hysteresis.

Lim and McDowell [1995] analyzed the path dependence of superelastic SMAs by performing experimental tests on 2.54 mm diameter wires. In particular, they focused attention on both the cyclic uniaxial tension behavior and the cyclic uniaxial tension-compression behavior. The most significant results they found were the following.

1. Under condition of cycling loading with a maximum imposed strain, the critical stress to initiate stress-induced martensite transformation decreases, the residual strain accumulates and the hysteresis energy progressively decreases over many cycles of loading.
2. The stress at which both forward and reverse transformation occurs depends on the strain level prior to the last unloading event. This behavior is attributed to the distribution and configuration of austenite-martensite interfaces which evolve during the transformation.

Strnadel *et al.* [1995] tested both NiTi and NiTiCu thin plates in their superelastic phase to evaluate the cyclic stress-strain characteristics of the selected alloys. They also devoted particular attention to the effect of the variation of the nickel content in the specimens' mechanical response. Interesting were the conclusions of the research group.

1. Ternary NiTiCu alloys display lower transformation deformations and transformation stresses than binary NiTi alloys.
2. In both NiTi and NiTiCu alloys, the higher the nickel content, the lower the residual deformation as the number of cycles increases.

Piedboeuf *et al.* [1998] studied the damping behavior of superelastic SMA wires. They performed experiments on 100 μm diameter NiTi wires at three levels of amplitudes (2, 3 and 4% of strain), over four frequency values (0.01, 0.1, 1, 5 and 10 Hz) and at two different temperatures (25 and 35 ^{o}C). Different were the findings that worth discussion.

1. An increase in temperature causes a linear increase in transformation stresses and a shift of the stress-strain curve upward.
2. Up to a frequency of 0.1 Hz and for a fixed value of deformation of 4%, the stress difference between the two superelastic plateaus increases, producing an increase in the dissipated energy as well. For higher frequencies, instead, the lower plateau stress level rises, causing a pronounced reduction of the surface hysteresis.

3. Frequency interacts with the deformation amplitude. In particular, at 2% strain there is only a slight variation in the dissipated energy by varying the frequency, while at 4% the variation is more important and the maximum occurs at around 0.1 Hz. For higher values of frequency the dissipated energy decreases.

Tobushi *et al.* [1998] investigated the influence of the strain rate in the properties of 0.75 mm diameter superelastic NiTi wires. The tensile tests were conducted at strain rates ranging from $1.67{\cdot}10^{-3}\% \cdot \sec^{-1}$ to $1.67\% \cdot \sec^{-1}$. They also took into account the effects of the temperature variation in the wires' mechanical response. Their main considerations were the following.

1. When $\dot{\epsilon} \geq 1.67{\cdot}10^{-1}\% \cdot \sec^{-1}$, the larger $\dot{\epsilon}$, the higher the stress at which the forward transformation starts and the lower the stress at which the reverse transformation starts.
2. For each temperature level considered, the larger $\dot{\epsilon}$, the larger the residual strain after unloading. Also, the higher the temperature, the larger the residual strain.
3. As the number of cyclic deformation increases, the stress at which forward and reverse transformation starts decreases with a different amount of variation. Also, the irrecoverable strain which remains after unloading increases.
4. The strain energy increases with an increase in temperature, while the dissipated work slightly depends on the temperature variation. Also, at each temperature level, it is observed that both quantities do not depend on the strain rate for values of $\dot{\epsilon} \leq 3.33{\cdot}10^{-2}\% \cdot \sec^{-1}$. Instead, for values of $\dot{\epsilon} \geq 1.67{\cdot}10^{-1}\% \cdot \sec^{-1}$, the dissipated work increases and the strain energy decreases.

Wolons *et al.* [1998] tested 0.5 mm diameter superelastic NiTi wires in order to understand their damping characteristics. They studied in detail the effect of cycling, oscillation frequency (from 0 to 10 Hz), temperature level (from about 40 ^{o}C to about 90 ^{o}C) and static strain offset (i.e. strain level from which the cycling deformation starts). On the basis of the experimental data, they made several observations.

1. A significant amount of mechanical cycling is required for an SMA wire to reach a stable hysteresis loop shape. The amount of residual strain is dependent on both temperature and strain amplitude, but it is not a function of the cycling frequency.
2. The shape of hysteresis loop changes significantly with frequency. The reverse transformation is affected more than the forward transformation.

3. Energy dissipation is a function of frequency, temperature, strain amplitude and static strain offset. The energy dissipated per unit volume initially decreases up to 1-2 Hz, then appears to approach a stable level at 10 Hz. Dissipation capacity at 6-10 Hz is about 50% lower than the corresponding value at very low frequencies. Moreover, it decreases as the temperature increases above 50 ^{o}C.
4. By reducing the static strain offset, the energy dissipated per unit volume increases.
5. Energy dissipation, per unit volume, of SMA wires undergoing cyclic strains at moderate strain amplitudes (about 1.5%) is about 20 times bigger than that exhibited by typical elastomers undergoing cyclic shear strain.

Dolce and Cardone [2001a] investigated the mechanical behaviour of several NiTi SMA bars in both austenitic and martensitic phase subjected to torsion. The SMA elements were different in size (diameter of 7-8 and 30 mm), shape (round and hexagonal bars) and physical characteristics (alloy composition and thermomechanical treatment). The experimental results were carried out by applying repeated cyclic deformations. Strain rate, strain amplitude, temperature and number of cycles were considered as test parameters. The most important findings of the experimental investigation can be summarized as follows.

1. The mechanical behaviour of SMA bars subjected to torsion is independent from loading frequency in case of martensite, or slightly dependent on it in case of austenite.
2. The effectiveness in damping vibrations is good for martensite (up to 17% in terms of equivalent damping), but rather low for austenite (of the order of 5-6% in terms of equivalent damping).
3. Austenite bars present negligible residual deformations at the end of the action, being of the order of 10% of the maximum attained deformation.
4. The fatigue resistance under large strains is considerable for austenite bars (hundreds of cycles) and extraordinary for martensitic bars (thousands of cycles). In both cases, the cyclic behaviour is highly stable and repeatable.

Dolce and Cardone [2001b] concentrated on the mechanical behaviour of superelastic NiTi wires subjected to tension. The experimental tests were carried out on austenite wire samples with diameter of 1-2 mm and length of 200 mm. Several kinds of wires were considered, differing in alloy composition and/or thermomechanical treatment. Firstly,

cyclic tests on pre-tensioned wires at room temperature ($\approx 20\ ^oC$), frequency of loading ranging from 0.01 to 4 Hz and strain amplitude up to 10% were performed. Secondly, loading-unloading tests under temperature control, between 40 ^oC and 10 ^oC (step 10 ^oC), at about 7% strain amplitude and 0.02-0.2 Hz frequency of loading were conducted. The authors deeply investigated the superelastic behaviour, focusing on the dependence of the mechanical properties on temperature, loading frequency and number of cycles. In the following, their most important considerations are listed.

1. The dependence on temperature of the tested materials appears compatible with the normal range of ambient temperature variations, if this is assumed to be of the order of 50 ^oC.
2. Loading frequency affects the behaviour of SMAs, specially when passing from very low frequency levels (0.01 Hz or even less) to higher frequency levels (0.2-4 Hz). A considerable decrease of energy loss and equivalent damping occurs because of the increase of temperature, due to the latent heat of transformation, which cannot be dissipated in case of high strain rates.
3. The number of undergone cycles considerably affects the superelastic behaviour of austenitic SMAs, worsening the energy dissipating capability and increasing the cyclic strain hardending.

Moroni *et al.* [2002] tried to use copper-based SMA bars as energy dissipation devices for civil engineering structures. They performed cyclic tension-compression tests on martensitic elements, with a diameter of 5 and 7 mm, characterized by different processing hystories (hot rolled or extrusion) and grain size composition. The experimental investigation was conducted both in strain and stress control at different frequencies of loading (from 0.1 to 2 Hz). On the basis of the results, the researchers drew the following major conclusions.

1. The martensitic CuZnAlNi alloy dissipates substantial energy through repeated cycling.
2. Damping is a function of strain amplitude and it tends to stabilize for large strains. Also, frequency (0.1-2 Hz) has a small influence on the damping values.
3. The considered mechanical treatments (rolling and extrusion) do not influence the bars' mechanical behavior.
4. Observed fractures are due to tensile actions and present a brittle intergranular morphology.

Tamai and Kitagawa [2002] observed the behavior of 1.7 mm diameter superelastic NiTi wires for a possible use of SMAs in innovative bracing systems as weel as exposed-type column base for buildings. Monotonic and pulsating tension loading tests were performed with constant, increasing and decreasing strain amplitudes. Also, the effects of the ambient temperature was taken into consideration. As a result of the experimental observations, they provided the following comments.

1. A spindle shaped hysteresis loop without residual deformation is observed
2. The stress which starts the phase transformation is very sensitive to ambient temperature. Furthermore, wire temperature varies during cyclic loading due its latent heat.
3. The residual deformation increment and dissipated energy decrement per cycle decreases with the number of loading cycles.
4. The rise and fall of the wire temperature during forward and reverse transformation has almost the same intensity. In particular, the forward transformation is exothermal while the reverse transformation is endothermal.

DesRoches *et al.* [2004] performed several experimental tests on superelastic NiTi wires and bars to assess their potential for applications in seismic resistant design and retrofit. In particular, they studied the effects of the cycling loading on residual strain, forward and reverse transformation stress levels and energy dissipation capability. Specimens were different in diameters (1.8, 7.1, 12.7 and 25.4 mm respectively) with nearly identical composition. The loading protocol used consisted of increasing strain cycles of 0.5%, 1% to 5% by increments of 1%, followed by four cycles at 6%. The research group considered two series of tests. The first one, in quasi-static conditions, was performed at a frequency of 0.025 Hz, while the second one was conducted at frequencies of 0.5 and 1 Hz in order to simulate dynamic loads. After carrying out the experiments, they proposed several points of interest.

1. Nearly ideal superelastic properties are obtained in both wires and bars. The residual strain generally increases from an average of 0.15% following 3% strain to an average of 0.65% strain following 4 cycles at 6% strain. It seems to be independent on both section size and loading rate.
2. Values of equivalent damping range from 2% for the 12.7 mm bars to a maximum of 7.6% for the 1.8 mm wires and are in agreement with the values found by other

authors [Dolce and Cardone, 2001a]. Bars show a lower dissipation capability than wires.

3. The initial modulus of elasticity and the stress level at which the forward transformation starts in the 25.4 mm diameter bars are lower by about 30% than the corresponding values in the wires.
4. Increase of the loading rates leads to lower values of the equivalent damping but has negligible influence on the superelastic effect.

Fugazza [2005] tested a number of superelastic NiTi wires and bars of different size (diameter of 0.76, 1 and 8 mm) and chemical composition. He focused on the cyclic behaviour of such elements and performed both static and dynamic tests at loading frequencies of 0.001 and 1 Hz respectively. The maximum deformation attained during the experiments was 6%, reached by subsequent increments of 1%. The author investigated the seismic performance of such elements by evaluating those quantities which are of interest in earthquake engineering, such as damping properties, material strength and recentering capability. In the following, the main results coming from the analysis of the experimental outcomes are reported.

1. Both wires and bars show very good superelastic behavior by almost recovering all the imposed deformation. Failure has been observed for deformations of approximatively 9%.
2. Under dynamic loading conditions, SMA elements display a consistent reduction of the damping capacity and narrower hysteresis loops are noticed. Furthermore, the material hardens and the upper plateau shifts upwards. As a consequence, the corresponding stress level are higher than those obtained under static loadings.
3. Chemical composition plays a foundamental role in the material behavior. For the same loading protocol, the considered SMAs evidence substantial differences in terms of both phase transformation stress levels and elastic properties.
4. The material seems to stabilize after a limited number of cycles which is of the same order of that experienced by a structure during an earthquake.

3. USE OF SHAPE-MEMORY ALLOYS IN EARTHQUAKE ENGINEERING

3.1 Introduction

This section presents a state-of-the-art of the applications of the SMA technology in earthquake engineering, where such innovative materials are being considered as both vibration control devices and isolation systems for buildings and bridges. The chapter intends to provide comments on the works available in the recent literature, starting from the reviews by Sadat *et al.* [2002], Fugazza [2003], DesRoches *et al.* [2004] and Wilson and Wesolowsky [2005].

3.2 Numerical Applications

Baratta and Corbi [2002] and Corbi [2003] investigated the influence of SMA tendon elements collaborating to the overall strength of a simple portal frame model (Figure 3.1 left) undergoing horizontal shaking. The basic structure was assumed to exhibit an elastic-perfectly plastic material behaviour while the tendons were supposed to behave according to a superelastic model. The performance of such a system was compared with the response of a similar structure, where the tendons were supposed to be fully elastic-plastic, as the main structure, or, alternatively, unilaterally plastic then unable to sustain compression forces. Numerical results showed that the structure endowed with superelastic tendons decisively improved the dynamic response with respect to the case in which the tendons were made by elastic-plastic wires. More precisely, SMA tendons produced smaller response amplitude, much smaller residual drift and excellent performance in attenuating P-Δ effects.

Bruno and Valente [2002] presented a comparative analysis of different passive seismic protection strategies, aiming at quantifying the improvement achievable with the use of innovative devices based on SMAs in place of traditional steel or rubber devices (i.e. bracing and base isolation systems). They considered new and existing RC buildings to be protected either with base isolation devices or dissipating braces (Figure 3.1 right). As

concerns the comparison between conventional and innovative devices, the researchers found that SMA-based devices were more effective than rubber isolators in reducing seismic vibrations. On the other hand, the same conclusions could not be drawn for SMA braces if compared to steel braces because of the similar structural performance. However, SMA braces proved preferable considering the recentering capabilities not possessed by steel braces as well as the reduced functional and maintenance requirements.

Wilde *et al.* [2000] proposed a smart isolation system for bridge structures (Figure 3.2 left) which combined a laminated rubber bearing (LRB) with a device made of SMA bars, working in tension and compression, attached to the pier and the superstructure. The new isolation system was mathematically modelled and analytically studied for earthquakes with different accelerations. For the smallest earthquake, the system provided a stiff connection between the pier and the deck. For the medium earthquake, the SMA bars provided increased damping capabilities to the system due to the stress induced martensite transformation of the alloy. Finally, for the largest seismic event, the SMA bars provided hysteretic damping and acted as a displacement control device due to the hardening of the alloy after the phase transformation was completed. The research group also compared the performance of the new isolation system with that of a conventional isolation system consisting of a LRB with a lead core equipped with an additional stopper device. Numerical tests showed that the damage energy of the bridge endowed with the SMA isolation system was small, although the input energy to the structure was large compared to the bridge isolated with LRB. Possible drawback of the new system was the need of additional devices to prevent the possible buckling of the long SMA bars utilized.

Seelecke *et al.* [2002] reported on the influence of a superelastic SMA element on the dynamic response of a single-degree-of-freedom system (Figure 3.2 right) representing a multi-storey building undergoing earthquake excitation. The main goal of the work was to numerically study the variation of the SMA element's geometry in order to find the optimal system performance. Comparisons made with the same system equipped with the SMA element not experiencing any phase transformations highlighted how the superelastic hysteresis was effective in reducing the oscillations caused by the ground motion.

DesRoches and Delemont [2003] considered the application of superelastic SMA restrainers to a multi-span bridge. The structure under investigation (Figure 3.3) consisted of three spans supported on multi-column bents. The SMA restrainers were connected from the pier cap to the bottom flange of the beam in a manner similar to typical cable restrainers. They were used in a tension-only manner. The results that the researchers

obtained showed that the SMA restrainers reduced relative hinge displacements at the abutment much more effectively than conventional steel cable restrainers. The large elastic strain range of the SMA devices allowed them to undergo large deformations while remaining elastic. In addition, the superelastic properties of the SMA restrainers resulted in energy dissipation at the hinges. Also, for unexpexted strong earthquakes, the increased stiffness that SMAs exhibit at large strains provided additional restraint to limit the relative openings in the bridge. Before this work, a prelimiary study on the same topic was conducted by DesRoches [1999], who also performed parametric analyses for simulating the seismic response of typical bridge frames endowed with conventional and innovative restrainers.

3.3 Experimental Applications

Clark *et al.* [1995] performed an extensive testing program on a wire-based SMA devices (Figure 3.4 left) to evaluate the effects of temperature and loading frequency on their cyclic behavior. The tested devices used a basic configuration of multiple loops of superelastic wires wrapped around cyclindrical supports. Two pairs of devices were tested and each of the four devices had identical hardware but different wire configuration. In particular, one of the two pairs used only a single layer of wires while the second one had fewer loops wrapped around three different layers. The proposed dampers exhibited stable hysteresis with minor variations due to frequency of loading and device configuration (single layer versus multiple layers of wires). Moreover, the research highlighted that the temperature effects were substantial in the single-sided device.

Krumme *et al.* [1995] examined the performance of a sliding SMA device (Figure 3.4 right) in which resistance to sliding was achieved by opposite pairs of SMA tension elements. Experimental results reported temperature insensitivity, frequency independence and excellent cyclic behavior. Furthermore, numerical analyses showed the good performance of the new isolation system in limiting the interstorey drift of concrete buildings.

Adachi and Unjoh [1999] developed an energy dissipation device for bridges using SMA plates (Figure 3.5). The device was designed to take the load only in bending and its damping characteristics were determined through both cycling loadings and shake table tests. Experiments successfully showed that the SMA damper, which worked as a cantilever beam, could reduce the seismic response of the bridge and that its performance was more effective and efficient if the SMA material displayed the shape-memory effect. Finally, numerical simulations of a simplified bridge model further confirmed the feasibility of such a device.

Castellano [2000] and Indirli *et al.* [2000] realized different brick masonry wall mock-ups (Figure 3.6), simulating a portion of a cultural heritage structure, to be tested on the shake table. The aim of the experimental investigation was to evaluate the effectiveness of innovative techniques based on the use of SMAs as ties for the prevention of the out-of-plane collapse of such walls. Results from the tests showed that the new tying system could be highly effective to prevent the out-of-plane collapse of peripheral walls, such as church façades, poorly connected at floor level. Furthermore, unlike traditional steel ties, SMA ties were also able to protect tympanum structures from seismic-induced damage.

Valente *et al.* [1999], Dolce *et al.* [2000] and Bruno and Valente [2002] studied in great detail the possibility of using special braces for framed structures utilizing SMAs (Figure 3.8). Due to their extreme versatility, they could obtain a wide range of cyclic behaviour (from supplemental and fully recentering to highly dissipating) by simply varying the number and/or the characteristics of the SMA components. In particular, they proposed three categories of devices which were realized and then tested:

- *Supplemental re-centering devices*: typically based on the recentering group only, they presented zero residual displacement at the end of the action and further capability to provide an auxiliary re-centering force, which compensates possible reacting forces external to the device, such as friction of bearings (for isolation system) or plastic forces of structural elements (for bracing systems).
- *Not re-centering devices*: based on the dissipating group only, they presented large dissipation capabilities but also large residual displacements at the end of the action.
- *Re-centering devices*: including both re-centering devices and dissipating group, they presented zero or negligible residual displacement but were not capable of recovering the initial configuration if reacting forces external to the device existed.

The idea of using a SMA-based bracing system as a damper device for the structural vibration control of a frame was also considered by Han *et al.* [2003]. They carried out an experimental test on a two-storey steel frame equipped with eight SMA wires (Figure 3.9 left). The researchers focused on free-vibrations, concentrating on the decay history shown by the frame with and without the SMAs. Results highlighted that the frame equipped with the innovative damper took much shorter time to reduce its initial displacement than the uncontrolled frame (i.e. frame without the damper). Furthermore, finite element analyses of both the uncontrolled and controlled frame subjected to the El Centro ground motion confirmed the effectiveness of the innovative device in reducing

the structural oscillations.

Ocel *et al.* [2004] evaluated the feasibility of a new class of partially restrained connections by using SMAs in their martensitic form (Figure 3.7). The proposed connection consisted of four large diameter SMA bars connecting the beam flange to the column flange and was serving as the primary moment transfer mechanism. The researchers tested it in both quasi-static and dynamic conditions and focused attention on its cyclic performance. The connection exhibited a high level of energy dissipation, large ductility capacity and no strength degradation after being subjected to cycles up to 4% drift. Following the initial testing series, the tendons were then heated above the transformation temperature to evaluate the potential for recovering the residual deformation. The connection was then retested and exhibited nearly identical behavior to the original one with repeatable and stable hysteretic behavior. Moreover, additional tests performed under dynamic loadings carried out to examine the effects of the strain-rate in the performance displayed similar behavior to quasi-static tests, except for a decrease in the energy dissipation capacity.

Dolce *et al.* [2005] performed shake table tests on reduced-scale RC frames endowed with either steel or superelastic SMA braces (Figure 3.9 right). The experimental outcomes showed that the new bracing system based on SMAs may provide performances at least comparable to those provided by currently used devices, also in abscence of design criteria and methods specifically addressed to the new technology. With respect to steel braces, the innovative bracing configuration presented excellent fatigue resistance and recentering ability. Due to this property, since the vertical-load-resisting structural system is always restored at its initial shape at the end of the action, it was then possible to allow for great ductility demand in RC members. Accordingly, such approach highlighted the advantage of needing no strengthening of the frame then resulting more attractive from an economic point of view.

3.4 Existing Applications

The Basilica of St Francis in Assisi was severely damaged during the 1999 earthquake occurred in central Italy [Croci *et al.*, 2000; Mazzolani and Mandara, 2002]. The main challenge of the restoration was to obtain an adequate safety level while mantaining the original concept of the structure. In order to reduce the seismic forces transferred to the tympanum, a connection between it and the roof was created using superelastic SMA rods (Figure 3.10). The SMA devices demonstrated different structural properties for different horizontal force levels. Under low horizontal forces (wind, small intensity seismic events) they are stiff and allow for no significant displacements, under high horizontal actions their stiffness reduces for controlled displacements of the masonry walls, whereas

under extremely intense horizontal loads their stiffness increases to prevent collapse.

The rehabilitation of the bell tower of the church of San Giorgio in Trignano, Italy, is another important example of seismic retrofit utilizing SMAs [Indirli, 2000; Mazzolani and Mandara, 2002]. The structure is very old (XIV century), it is made of masonry and it was seriuosly damaged during the 1996 earthquake. The innovative intervention consisted in the insertion of four vertical prestressing steel tie bars in the internal corners of the structure with the aim of increasing its flexural strength (Figure 3.11). The tie bars were formed by six tight-screwing segments placed in series with four SMA devices made of several superelastic wires. The main goal of the restoration was to guarantee constant compression on the masonry by post-tensioning the SMA devices.

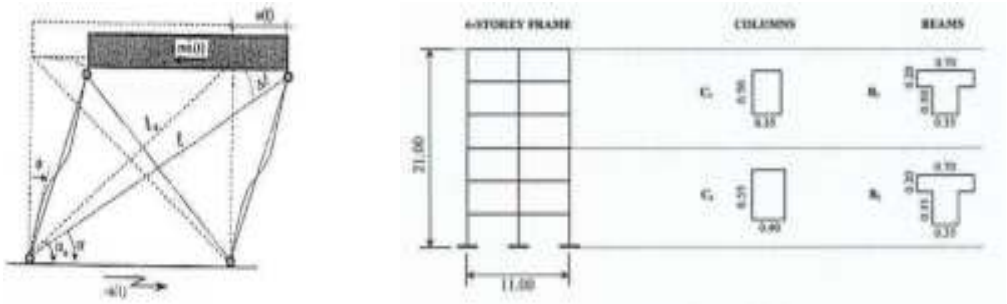

Figure 3.1. Framed structure equipped with superelastic SMA tendons considered by Baratta and Corbi [2002] and Corbi [2003] (left) and RC frames studied by Bruno and Valente [2002] (right).

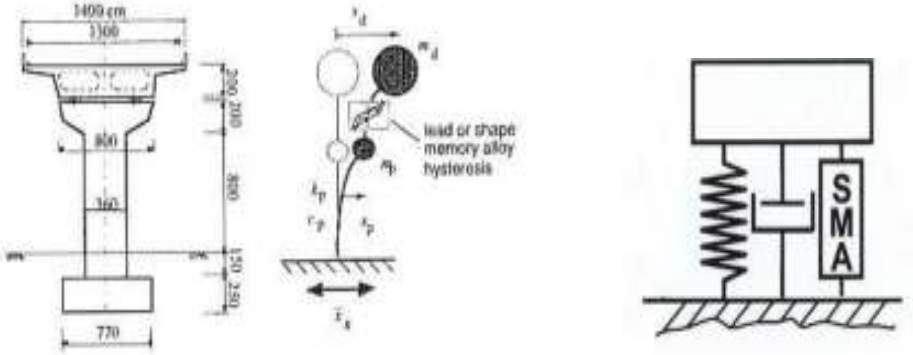

Figure 3.2. Isolation device for bridges studied by Wilde *et al.* [2000] (left) and single-degree-of-freedom structure investigated by Seelecke *et al.* [2002] (right).

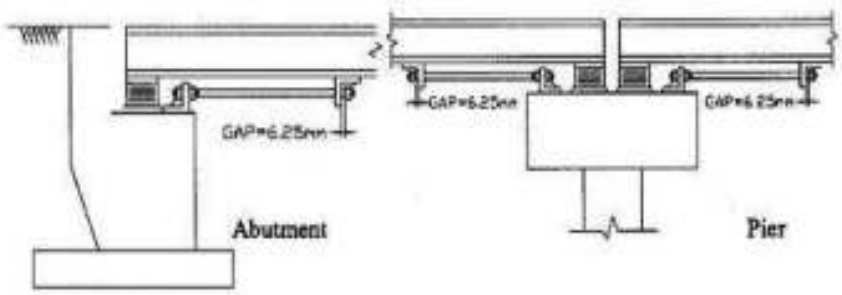

Figure 3.3. Multi-span bridge equipped with superelastic SMA restrainers studied by Ocel *et al.* [2004].

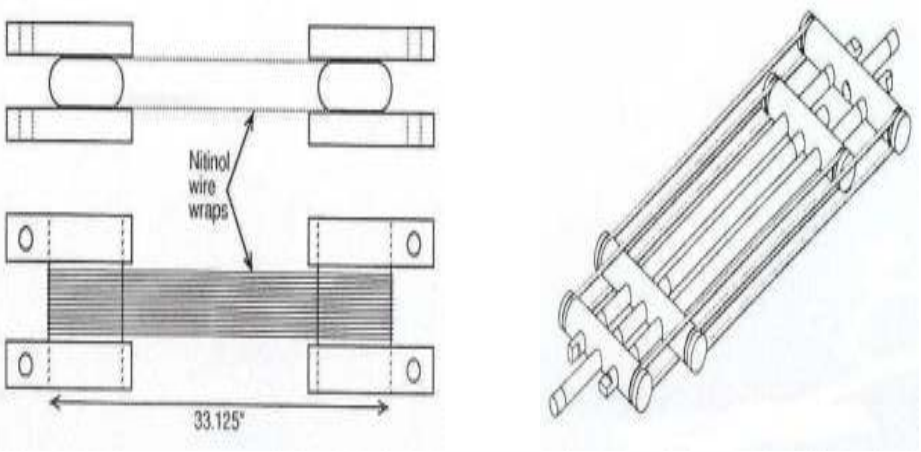

Figure 3.4. SMA devices proposed by Clark *et al.* [1995] (left) and Krumme *et al.* [1995] (right).

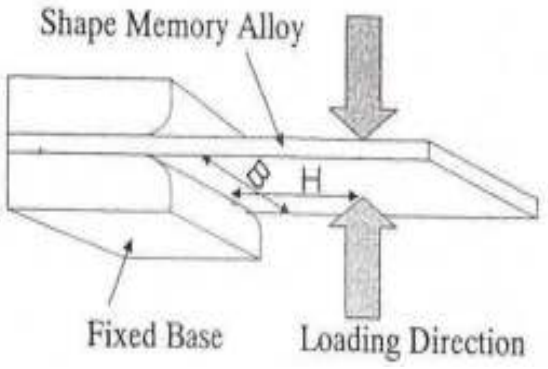

Figure 3.5. SMA device proposed by Adachi and Unjoh [1999].

Figure 3.6. Masonry wall tested by Castellano [2000] and Indirli *et al.* [2000] (left) and wall connection with superelastic SMA devices (right).

Figure 3.7. The smart beam-column connection studied by Ocel *et al.* [2004].

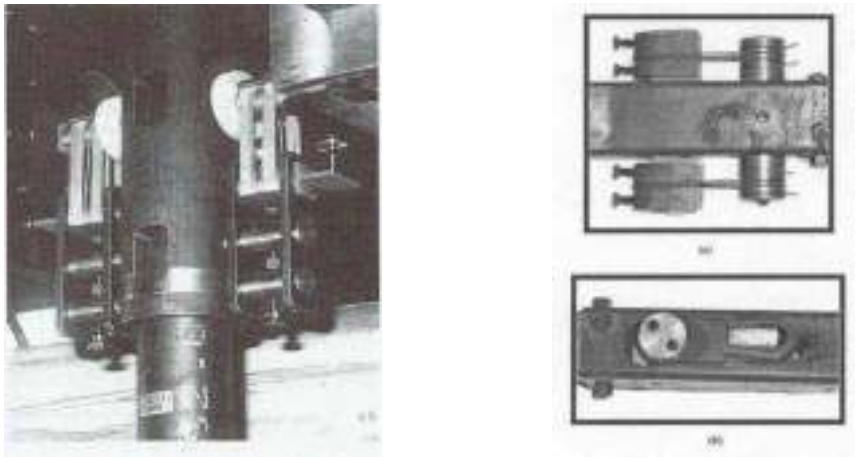

Figure 3.8. Particulars of the bracing systems studied by Dolce *et al.* [2000].

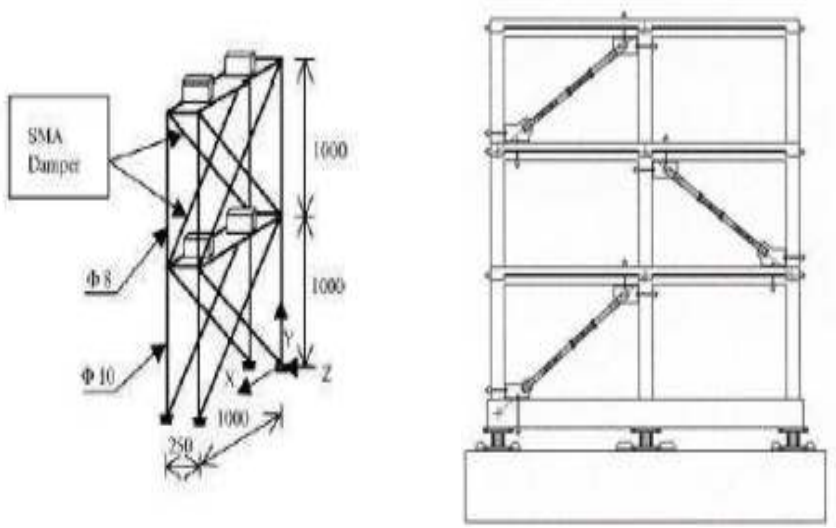

Figure 3.9. Damper device based on SMAs investigated by Han *et al.* [2003] (left) and RC frame endowed with SMA braces experimentally studied by Dolce *et al.* [2005] (right).

Figure 3.10. Particular of the SMA device utilized for the seismic upgrading of the Basilica of St Francis in Assisi, Italy.

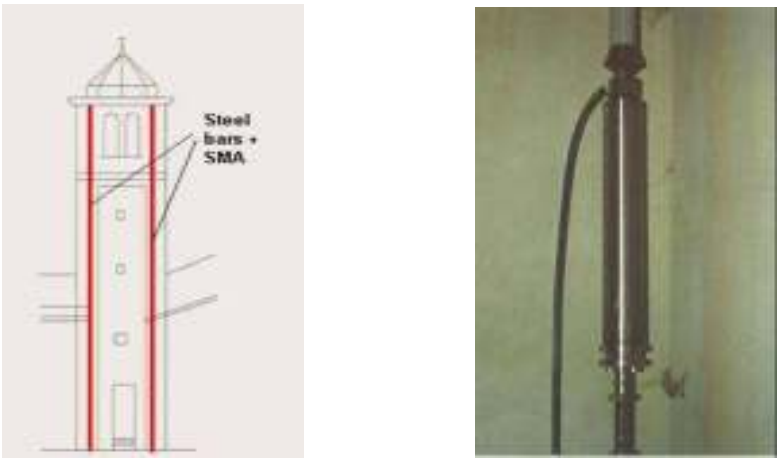

Figure 3.11. Schematic view of bell tower of the church of San Giorgio in Trignano (left), Italy and particular of the SMA device used for its seismic retrofit (right).

4. SEISMIC PERFORMANCE OF STEEL FRAMES EQUIPPED WITH TRADITIONAL AND INNOVATIVE BRACES

4.1 Introduction

In this chapter, we study the dynamic behavior of steel frames equipped with traditional steel braces, both buckling-allowed and buckling-restrained, and innovative superelastic SMA braces. The seismic performance of the structures under investigation is judged through the evaluation of the maximum interstorey drift and the residual drift of the top floor.

4.2 Earthquake Records and Frame Characteristics

All the steel frames under investigation are studied by using the ground motions developed for the SAC Steel Project [Sabelli, 2001]. These consist of twenty records and represent a suite of seismic inputs having a 10% probability of exceedence in a 50-year period. These records were derived either from historical recordings or from simulations of physical fault rupture processes. Later, for the numerical simulations, they will be scaled based on the average spectral acceleration of all twenty at the foundamental period of the frame being analyzed. Characteristics of such seismic events (Table A.1) as well as acceleration time-histories (Figures A.1-A.20) are reported in Appendix A.

Among the several steel buildings analyzed by Sabelli [2001], two of them are considered. In particular, we concentrate on one 3-storey frame and one 6-storey frame, both designed to be equipped with either buckling-allowed steel braces or buckling-restrained steel braces oriented in a stacked chevron (inverted V) pattern. Geometric dimensions of the structures are given in Figures 4.1-4.3, while member sizes are provided in Tables 4.1-4.4.

4.3 Overview on the Constitutive Modelling of Shape-Memory Alloys for Seismic Applications

We now focus attention on the constitutive modelling of SMAs, by reviewing the material laws that have been adopted for describing the response of SMA-based devices for seismic applications. In view of numerical simulations, for each model we briefly summarize advantages and disatvantages, in order to select the constitutive equation that better meets the requirements needed for an appropriate description of SMA materials in earthquake engineering.

Graesser and Cozzarelli [1991] were among the first to take into consideration the possibility of using SMAs for seismic applications and proposed an equation able to capture both the superelastic effect and the martensitic hysteresis. Drawbacks of the formulation were the inability to predict the material behavior after phase transition completion as well as the rate- and temperature-independence.

Bernardini and Brancaleoni [1999] studied a constitutive law able to simulate the rate- and temperature-dependent response of SMAs, with the aim of predicting the dynamic response of frames equipped with SMA-based devices undergoing seismic excitations. In the proposed equation, SMAs were represented as a mixture of two solid phases whose individual behavior was modelled as a linear isotropic thermoelastic material.

Wilde *et al.* [2000] proposed an innovative device made of SMA bars for bridge isolation. They improved the Graesser and Cozzarelli model by describing the material behavior also after phase transformation completion. However, the model was still rate- and temperature-independent and most of the material parameters did not have a physical meaning.

Tamai and Kitagawa [2002] considered a temperature-dependent model in which the phase transformation stress levels were depending on the martensite fraction. The constitutive law was rate-independent and required a large number of experimental data. It was used for evaluating the seismic response of SMA elements.

Fugazza [2003] concentrated on the performance of a superelastic SMA single-degree-of-freedom system undergoing different loading conditions. He implemented a modification of the model for superelastic SMAs previously introduced by Auricchio and Sacco [1997] as well as a robust integration algorithm. The advantages of the constitutive equation were the simplicity, the limited number of material parameters and the ability to describe partial and complete transformation patterns. The main disatvantages were the rate- and

temperature-independence.

4.4 Finite Element Platform and Modelling Assumptions

We perform non-linear dynamic analyses by use of the Open System for Earthquake Engineering Simulations framework [Mazzoni *et al.*, 2003]. OpenSEES is a PEER-sponsored project aimed at the development of a software platform able to simulate the seismic response of structural and geotechnical systems. It is an open source code and, among its features, allows the users to implement their own material model.

Due to the symmetry of the structures (Figures 4.1 and 4.2), only one braced bay is studied and the seismic weight is computed dividing the total floor weight by the number of braced frames in each principal direction.

Beams and columns are modelled using *nonlinearBeamColumn* elements with fiber sections and, apart from the roof level where there are hinges between the columns and the beams, fixed connections are assumed among elements. Braces are pinned at both ends so that they can ideally carry axial loads only. P-Δ effects are taken into consideration. Also, a 5% Rayleigh damping is specified, according to the usual values adopted for steel construction [Sabelli, 2001; Sabelli *et al.*, 2003].

The uniaxial material model *steel01* is used to model columns, beams and buckling-restrained steel braces, while a modified version of the *hysteretic* model is utilized to simulate the response of buckling-allowed steel braces. Mechanical properties of structural steel such as elastic modulus, E^{steel}, and yielding stress, σ_y, are assumed to be the same as the ones considered by Sabelli [2001] and Sabelli *et al.* [2003] and are summarized in Table 4.7.

For representing the superelastic behavior of the SMA braces, we choose the constitutive model proposed by Fugazza [2003]. Such a model is capable of describing the material behavior under arbitrary loadings such as those involved in seimic excitations, where the response is mainly composed by sub-hysteresis loops internal to the main one associated to complete phase transformations. Its formulation, developed in the small deformation regime, relies on the assumption that the relationship between stresses and strains is represented by a series of straight lines whose form is determined by the extent of the transformation being experienced. Further assumptions made, in agreement with previous studies, are that no strength degradation occurs during cycling [Bernardini and Brancaleoni, 1999] and that austenite and martensite branches have the same modulus

of elasticity [Andrawes *et al.*, 2004]. In order to avoid repetitions, the model formulation as well as the algorithmic solution is provided in detail in Chapter 5. With respect to its original version, developed using the MATLAB environment, the model required additional programming work for its coding into the new finite element platform.

4.5 Design of Superelastic Shape-Memory Alloy Braces

For comparison purposes, superelastic SMA braces are designed to provide the same yielding strength, F_y, and the same axial stiffness, K, as steel braces (Figure 4.5). In such a way, the structure endowed with SMA braces will have the same natural period of the one endowed with steel braces and both steel and SMA elements will yield at the same force level. In order to guarantee such properties, we need to perform the following steps:

1. Obtain yielding force, F_y, and axial stiffness, K, of the steel brace under consideration from the original structural design.
2. Obtain elastic modulus, E^{SMA}, of the considered SMA material and stress level, σ_s^{AS}, at which it enters the inelastic range (i.e. stress level to initiate the forward transformation).
3. Compute area, A^{SMA}, of the corresponding SMA brace:

$$A^{SMA} = \frac{F_y}{\sigma_s^{AS}} \tag{4.1}$$

4. Compute length, L^{SMA}, of the corresponding SMA brace:

$$L^{SMA} = \frac{E^{SMA}\, A^{SMA}}{K} \tag{4.2}$$

In Tables 4.5 and 4.6 we provide the required geometric properties (i.e. cross-sectional area and element length) of the superelastic SMA braces. Since such members appear to be shorter than steel braces, in order to guarantee the actual brace length rigid elements are connected to each SMA member (Figure 4.4). By doing so, we ensure all the deformation to occur in the SMA. Throughout this study, it is also assumed that the proposed smart braces are made of a number of large diameter superelastic bars able to undergo compressive loads without buckling.

Their mechanical properties, provided in Table 4.7, are selected on the basis of the uniaxial tests carried out by DesRoches *et al.* [2004], who studied the cyclic behavior

of large diameter superelastic SMA bars for seismic applications. In particular, for the numerical simulations, we choose those obtained from the dynamic tests, in order to correctly consider the reduced energy dissipation capability of such materials at high frequency loadings [Tobushi *et al.*, 1998; Dolce and Cardone, 2001b; DesRoches *et al.*, 2004; Fugazza, 2005].

4.6 Results and Discussion

In this section, the most important findings obtained from the non-linear dynamic analyses of the structures under investigation are discussed. As previously mentioned, attention is paid to the computation of both the maximum interstorey drift and residual drift of the top floor, two quantities traditionally considered for the evaluation of the seismic performance of buildings undergoing earthquake motions. Also, since the structures with steel braces have the same period as the corresponding structures with superelastic SMA braces, a good comparison can be made on the effectiveness of using the proposed innovative bracing system in place of a traditional one. In particular, the structural performance is judged by distinguishing two cases:

- buckling-allowed steel braces vs. superelastic SMA braces,
- buckling-restrained steel braces vs. superelastic SMA braces.

4.6.1 Buckling-allowed steel braces vs. superelastic SMA braces

Outcomes from the overall study lead to the following main conclusions:

- The plot of the maximum interstorey drift (Figures 4.6 and 4.8) shows that superelastic SMA braces are far more effective than buckling-allowed steel braces. Although steel braces provide wider hysteresis loops, therefore possessing bigger energy dissipation capacity, the superelastic effect of SMAs makes them desirable for vibration response reduction. In particular, the ability of the SMA elements to regain the imposed deformations (i.e. recentering ability) strongly reduces the interstorey drift to an average value of approximatively 1% for both the 3- and 6-storey frame. The same structures designed to carry traditional steel braces are instead characterized by average values of interstorey drift of approximatively 4.93% and 2.05% respectively.

- As displayed in Figures 4.7 and 4.9 and again due to the recentering ability of superelastic SMAs, the frames equipped with superelastic SMA braces show much lower values of residual drift than those exhibited by the same structures equipped with buckling-allowed steel braces. The superelasticity allows the SMA elements to bring the structure back to their undeformed shape after the ground motion is over and diminishes the permanent deformations in other steel members even in the case where yielding occurs in the columns.

4.6.2 Buckling-restrained steel braces vs. superelastic SMA braces

Outcomes from the overall study lead to the following main conclusions:

- By observing Figure 4.10, which is related to the 3-storey frame, we notice that superelastic SMA braces and buckling-restrained steel braces provide similar performance in terms of maximum interstorey drift. In particular, its average value is 1.36% if we use superlastic SMA braces and 1.52% in case we use steel braces. Despite the fact that traditional steel braces may account for a much higher energy dissipation capability, the recentering property of superelastic SMA braces still plays a foundamental role in reducing the structural oscillations.
- In the 6-storey frame (Figure 4.12), the innovative bracing system shows better behavior and a more uniform distribution of the maximum interstorey drift for all the considered seismic inputs. More precisely, its average value decreases of approximatively 20% (from 1.35% when using steel braces to 1.08% when using superelastic SMA braces) with respect to the case in which the frame is endowed with a traditonal bracing system.
- As far as the residual drift of the top floor is concerned (Figures 4.11 and 4.13), results highlight that in most of the cases superelastic SMA braces have a much better performance than buckling-restrained steel braces, in agreement with the results obtained for the case of steel frames with buckling-allowed steel braces.
- Numerical tests related to the 3-storey frame undergoing record LA14 and to the 6-storey frame undergoing records LA03 and LA10, show that the damage level occured at the top floor of both structures (Figures 4.11 and 4.13) is higher if we adopt the new bracing system in place of the traditional one. This is probably due to the post-inelastic behavior (i.e. branch observed at the end of the upper plateau) of the superelastic braces, which in their fully martensitic phase transmit high values of forces to columns and/or beams with consequent structural problems caused by yielding.

Table 4.1. Model information of the 3-storey frame equipped with buckling-allowed steel braces (frame 3BA).

Storey	Element Size		
	Column	Beam	Brace
1	W 12×96	W 30×90	HSS 8×8×1/2
2	W 12×96	W 27×84	HSS 8×8×1/2
3	W 12×96	W 18×46	HSS 6×6×3/8

Table 4.2. Model information of the 6-storey frame equipped with buckling-allowed steel braces (frame 6BA).

Storey	Element Size		
	Column	Beam	Brace
1	W 14×211	W 36×150	HSS 10×10×1/2
2	W 14×211	W 30×116	HSS 8×8×1/2
3	W 14×211	W 30×116	HSS 8×8×1/2
4	W 14×211	W 30×116	HSS 8×8×1/2
5	W 14×211	W 30×99	HSS 6×6×1/2
6	W 14×211	W 27×94	HSS 5×5×1/2

Table 4.3. Model information of the 3-storey frame equipped with buckling-restrained steel braces (frame 3BR).

Storey	Element Size			
	Column	Beam	Brace F_y [kip]	Brace K [kip/in]
1	W 12×96	W 14×48	324	1450
2	W 12×96	W 14×48	259	1248
3	W 12×96	W 14×48	157	791

Table 4.4. Model information of the 6-storey frame equipped with buckling-restrained steel braces (frame 6BR).

Storey	Element Size			
	Column	Beam	Brace F_y [kip]	Brace K [kip/in]
1	W 14×211	W 14×48	511	1907
2	W 14×211	W 14×48	389	1886
3	W 14×211	W 14×48	349	1707
4	W 14×132	W 14×48	317	1566
5	W 14×132	W 14×48	288	1432
6	W 14×132	W 14×48	173	888

Table 4.5. Geometry of the superelastic SMA braces for the 3- and 6-storey frame.

Storey	SMA braces for frame 3BA		SMA braces for frame 6BA	
	Length [mm]	Area [mm^2]	Length [mm]	Area [mm^2]
1	504	5259	595	6701
2	504	5259	504	5259
3	504	2953	504	5259
4	-	-	504	5259
5	-	-	504	3795
6	-	-	504	3070

Table 4.6. Geometry of the superelastic SMA braces for the 3- and 6-storey frame.

Storey	SMA braces for frame 3BR		SMA braces for frame 6BR	
	Length [mm]	Area [mm^2]	Length [mm]	Area [mm^2]
1	378	3481	453	5491
2	351	2783	349	4180
3	336	1687	346	3750
4	-	-	343	3406
5	-	-	340	3094
6	-	-	330	1859

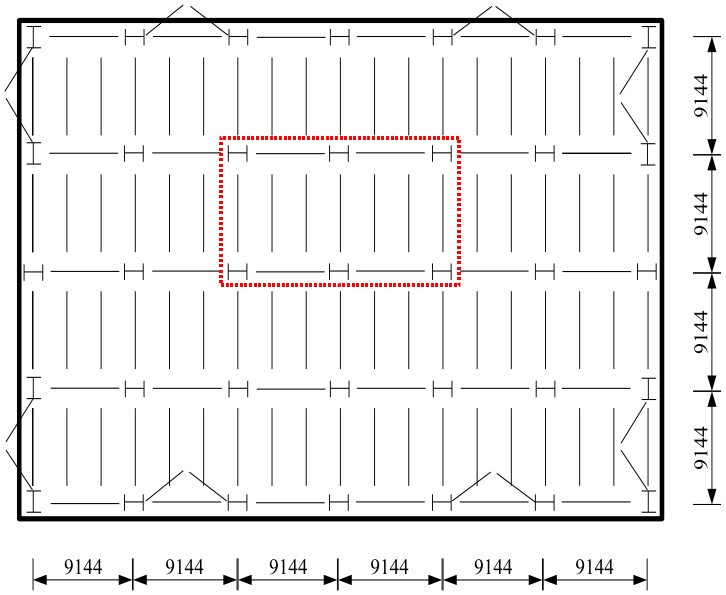

Figure 4.1. Plan view of the 3-storey frame. The penthouse is indicated with a dashed line. Dimensions are expressed in mm.

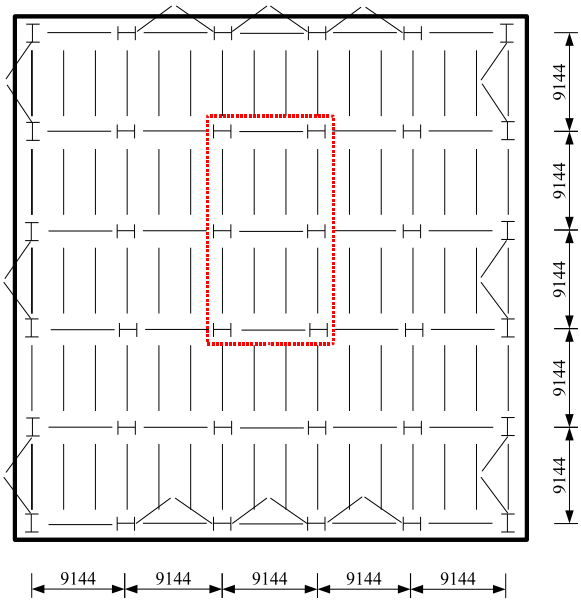

Figure 4.2. Plan view of the 6-storey frame. The penthouse is indicated with a dashed line. Dimensions are expressed in mm.

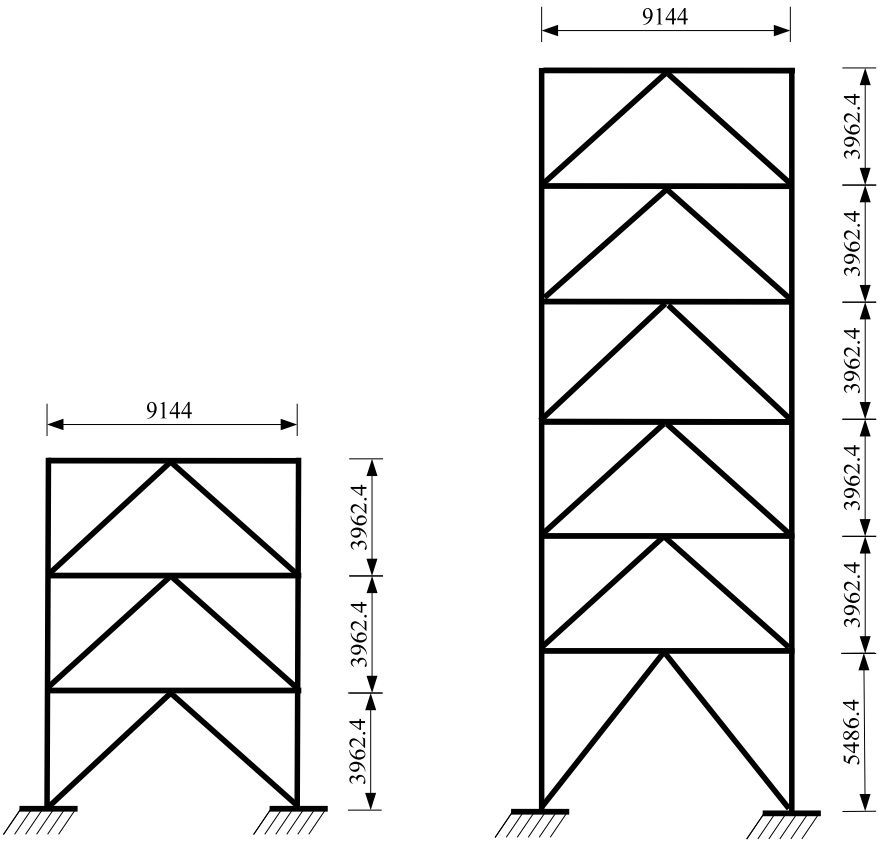

Figure 4.3. Elevation view of the 3- and 6-storey frame. Dimensions are expressed in mm.

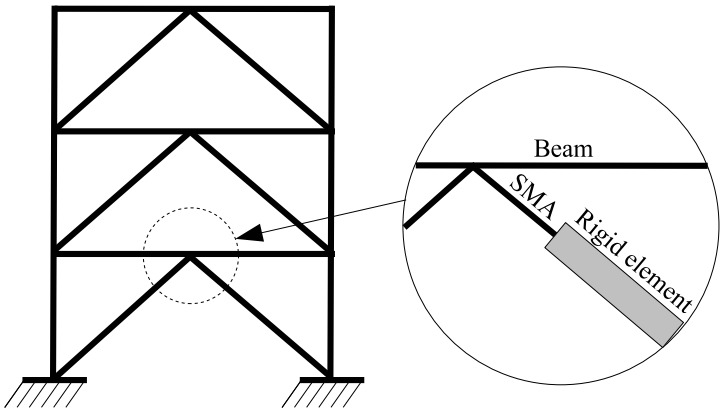

Figure 4.4. Particular of the SMA brace installed in the 3-storey frame.

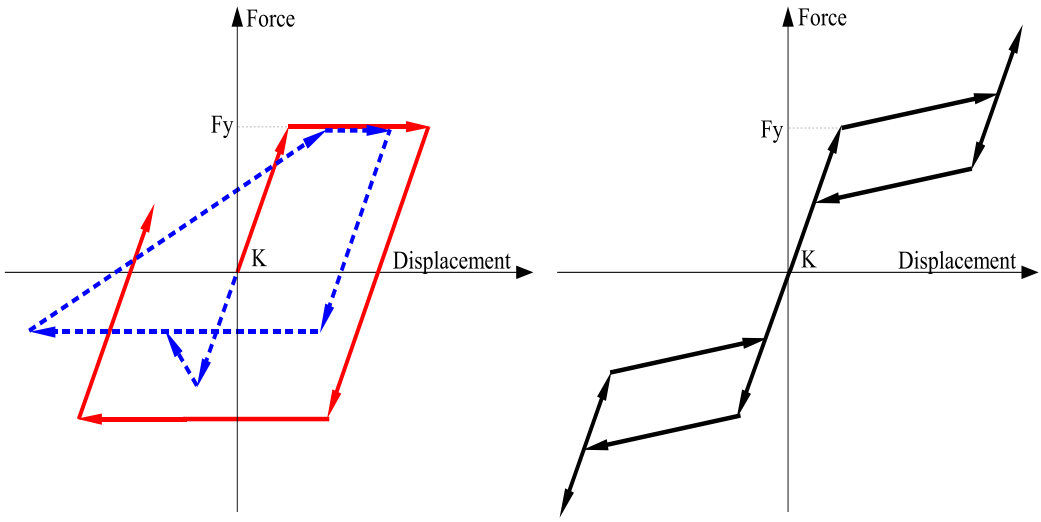

Figure 4.5. Material models: buckling-allowed steel braces (dashed line, left), buckling-restrained steel braces (continuous line, left) and superelastic SMA braces (continuous line, right).

Table 4.7. Material properties adopted for the numerical simulations.

Quantity		Value
E^{steel}	[MPa]	200000
E^{SMA}	[MPa]	27579
σ_y^{braces}	[MPa]	250
σ_y^{beams}	[MPa]	345
$\sigma_y^{columns}$	[MPa]	345
σ_s^{AS}	[MPa]	414
σ_f^{AS}	[MPa]	550
σ_s^{SA}	[MPa]	390
σ_f^{SA}	[MPa]	200
ϵ_L	[%]	3.50

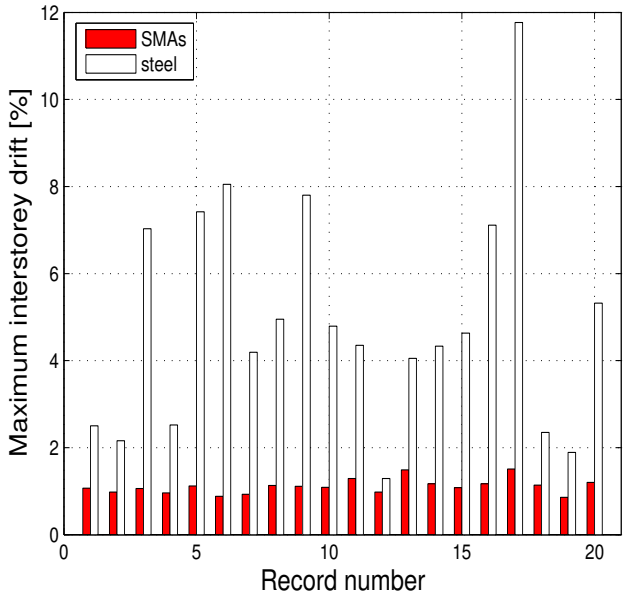

Figure 4.6. Maximum interstorey drift exhibited by the 3-storey frame equipped with either buckling-allowed steel braces or superelastic SMA braces.

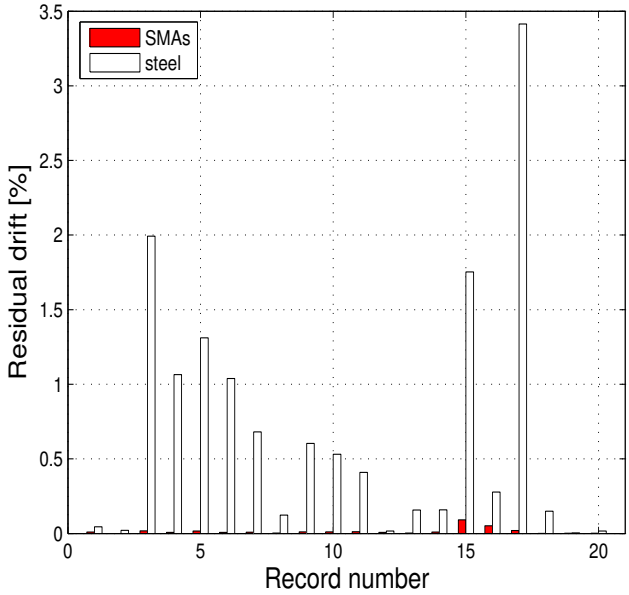

Figure 4.7. Residual drift of the top floor exhibited by the 3-storey frame equipped with either buckling-allowed steel braces or superelastic SMA braces.

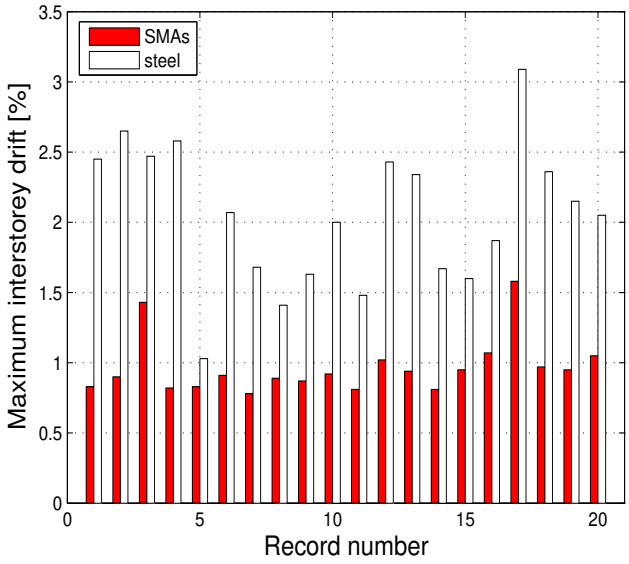

Figure 4.8. Maximum interstorey drift exhibited by the 6-storey frame equipped with either buckling-allowed steel braces or superelastic SMA braces.

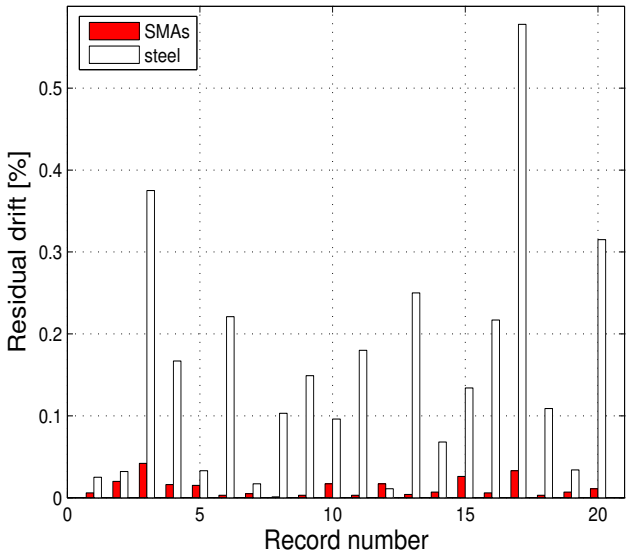

Figure 4.9. Residual drift of the top floor exhibited by the 6-storey frame equipped with either buckling-allowed steel braces or superelastic SMA braces.

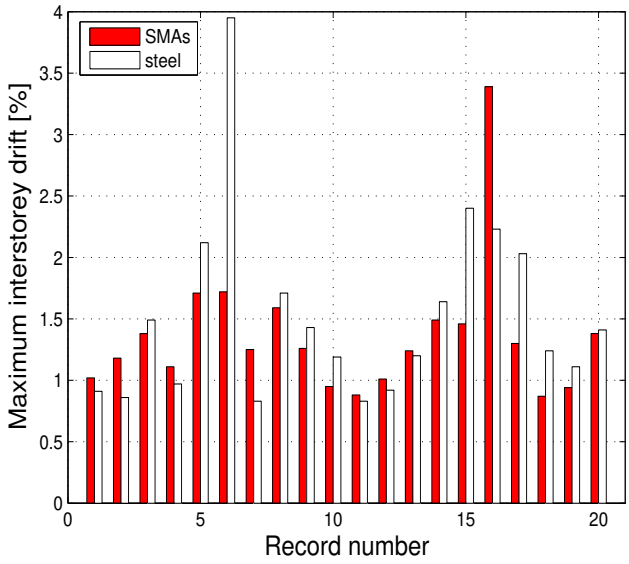

Figure 4.10. Maximum interstorey drift exhibited by the 3-storey frame equipped with either buckling-restrained steel braces or superelastic SMA braces.

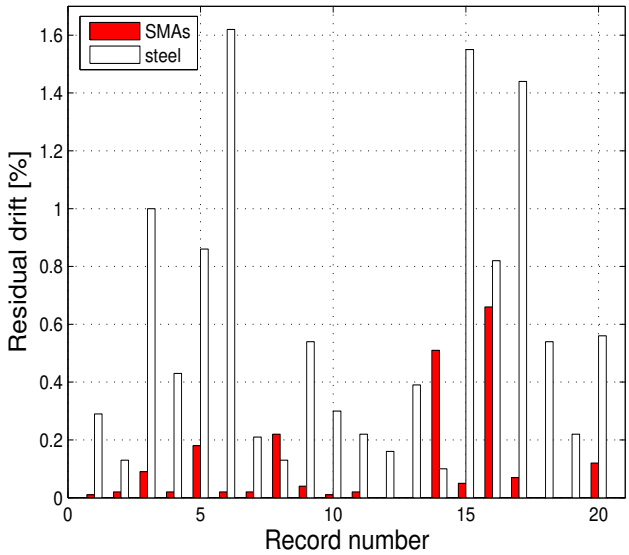

Figure 4.11. Residual drift of the top floor exhibited by the 3-storey frame equipped with either buckling-restrained steel braces or superelastic SMA braces.

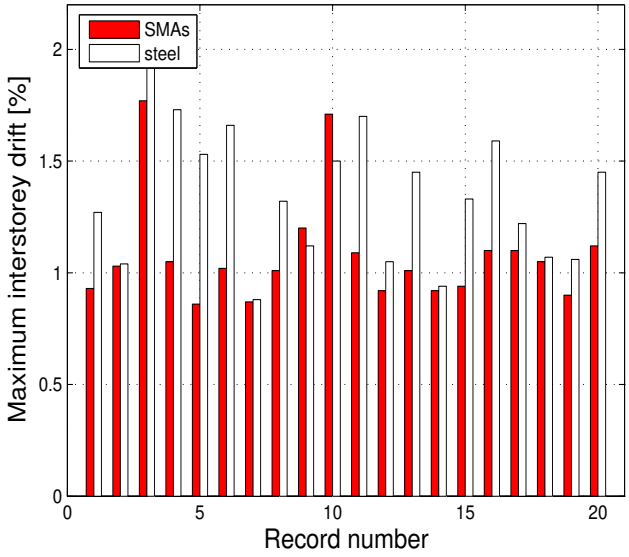

Figure 4.12. Maximum interstorey drift exhibited by the 6-storey frame equipped with either buckling-restrained steel braces or superelastic SMA braces.

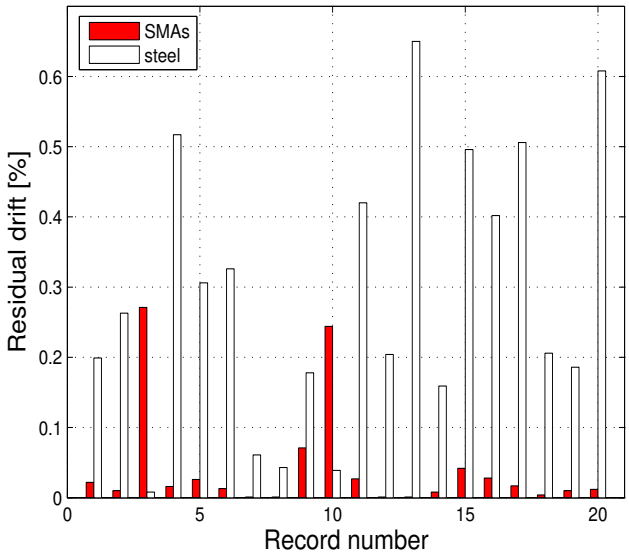

Figure 4.13. Residual drift of the top floor exhibited by the 6-storey frame equipped with either buckling-restrained steel braces or superelastic SMA braces.

5. ADVANCED UNIAXIAL CONSTITUTIVE MODELS FOR SUPERELASTIC SHAPE-MEMORY ALLOYS

5.1 Introduction

Experimental investigations on superelastic SMAs show a dependency of the stress-strain relationship on the loading-unloading rate. This feature is of particular importance in view of the use of such materials in earthquake engineering where the loading rate may affect the structural response. Motivated by this observation and by the limited number of available works on the modelling of SMAs for seismic applications, the present chapter addresses two constitutive models able to describe the rate-dependent behavior of superelastic SMAs. Besides their formulation and implementation, the ability of the models to simulate experimental data from tests conducted on SMA wires and bars at different frequency levels is assessed. As highlighted in Chapter 3, since SMA-based seismic devices are typically made as a combination of wires and bars, both models are developed under the hypothesis of uniaxial state of stress.

5.2 Development of a Rate-Dependent Viscous Constitutive Model

In the following, starting from the work by Auricchio and Sacco [1999], we present a viscous constitutive equation able to describe the rate-dependent superelastic behavior of SMA materials. It will be developed in the small deformation regime.

5.2.1 Time-continuous general framework

The material crystallographic state of the SMA material is described through two scalar internal variables, the *static martensite fraction*, ξ_{ST}, and the *dynamic martensite fraction*, ξ. The former represents the fraction which would be obtained for static loading conditions or, equivalently, for a very small ratio between the loading rate and a characteristic *material internal time*, τ. Accordingly, the possible differences between ξ_{ST} and ξ should model either the presence of rate effects in the phase transformations or their

dependence on rate phenomena, such as heat exchanges with the surrounding or other transient thermal processes.

Consistently with the introduction of a static and a dynamic martensite fraction, we also introduce two different stresses, the static one, σ_{ST}, and the dynamic one, σ, the former representing the stress which would be obtained for the case of static loading conditions.

In terms of phase transformations, we assume to work with two processes:

- the conversion of austenite into martensite A $\rightarrow$ S (i.e. forward transformation),
- the conversion of martensite into austenite S $\rightarrow$ A (i.e. reverse transformation).

For each one, we propose the possibility of choosing between three different kinetic rules, indicated as *linear*, *power* and *exponential* and herein presented according to an increasing order of complexity. Clearly, we assume that both evolutionary processes may produce variations of both the static and dynamic martensite fraction.

5.2.2 Kinetic Rules

The kinetic rules govern the evolution in time of the martensite fractions and are expressed as first order differential equations. For each rule, we now resent the corresponding evolutionary equations for both phase transformations.

Conversion of austenite into martensite.

$$\textit{Linear} \quad \begin{cases} \dot{\xi}_{ST} &= -\left(1-\xi_{ST}\right) \dfrac{\dot{\overline{|\sigma_{ST}|}}}{|\sigma_{ST}| - \sigma_{f,ST}^{AS}} \; \mathcal{H}_{ST}^{AS} \\ \dot{\xi} &= -\left(1-\xi\right) \quad \dfrac{\dot{\overline{|\sigma|}}}{|\sigma| - \sigma_{f}^{AS}} \quad \mathcal{H}^{AS} - \dfrac{\xi-\xi_{ST}}{\tau} \; \mathcal{H}_v \end{cases} \tag{5.1}$$

$$\textit{Power} \quad \begin{cases} \dot{\xi}_{ST} &= -\pi_{ST}^{AS}\left(1-\xi_{ST}\right) \dfrac{\dot{\overline{|\sigma_{ST}|}}}{|\sigma_{ST}| - \sigma_{f,ST}^{AS}} \; \mathcal{H}_{ST}^{AS} \\ \dot{\xi} &= -\pi^{AS}\left(1-\xi\right) \quad \dfrac{\dot{\overline{|\sigma|}}}{|\sigma| - \sigma_{f}^{AS}} \quad \mathcal{H}^{AS} - \dfrac{\xi-\xi_{ST}}{\tau} \; \mathcal{H}_v \end{cases} \tag{5.2}$$

$$\textit{Exponential} \quad \begin{cases} \dot{\xi}_{ST} &= \beta_{ST}^{AS}\left(1-\xi_{ST}\right) \dfrac{\dot{\overline{|\sigma_{ST}|}}}{(|\sigma_{ST}| - \sigma_{f,ST}^{AS})^2} \; \mathcal{H}_{ST}^{AS} \\ \dot{\xi} &= \beta^{AS}\left(1-\xi\right) \quad \dfrac{\dot{\overline{|\sigma|}}}{(|\sigma| - \sigma_{f}^{AS})^2} \quad \mathcal{H}^{AS} - \dfrac{\xi-\xi_{ST}}{\tau} \; \mathcal{H}_v \end{cases} \tag{5.3}$$

where $\mathcal{H}^{AS}$, $\mathcal{H}^{AS}_{ST}$ and $\mathcal{H}_v$ are zero unless the conditions described in the following are satisfied:

$$\left\{\begin{array}{rlllll} \mathcal{H}^{AS}_{ST} & = 1 & \text{when} & \dot{\sigma_{ST}} > 0 & \text{and} & \sigma^{AS}_{s,ST} \leq \sigma_{ST} \leq \sigma^{AS}_{f,ST} \\ \mathcal{H}^{AS} & = 1 & \text{when} & \dot{\sigma} > 0 & \text{and} & \sigma^{AS}_{s} \leq \sigma \leq \sigma^{AS}_{f} \\ \mathcal{H}_v & = 1 & \text{when} & \sigma > \sigma_{ST} & & \end{array}\right. \tag{5.4}$$

where $\sigma^{AS}_{s,ST}$, $\sigma^{AS}_{f,ST}$, σ^{AS}_{s} and σ^{AS}_{f} are the material properties representing, respectively, the stress levels at which the static and dynamic forward transformations start and finish. Finally, π^{AS}_{ST}, β^{AS}_{ST}, π^{AS} and β^{AS} are material constants which govern, respectively, the form of the static and dynamic forward phase transition evolution.

Conversion of martensite into austenite.

Linear

$$\left\{\begin{array}{rcl} \dot{\xi}_{ST} & = & \xi_{ST}\, \dfrac{\dot{\overline{|\sigma_{ST}|}}}{|\sigma_{ST}| - \sigma^{SA}_{f,ST}}\, \mathcal{H}^{SA}_{ST} \\ \dot{\xi} & = & \xi \quad \dfrac{\dot{\overline{|\sigma|}}}{|\sigma| - \sigma^{SA}_{f}} \quad \mathcal{H}^{SA} - \dfrac{\xi - \xi_{ST}}{\tau}\, \mathcal{H}_v \end{array}\right. \tag{5.5}$$

Power

$$\left\{\begin{array}{rcl} \dot{\xi}_{ST} & = & \pi^{SA}_{ST}\, \xi_{ST}\, \dfrac{\dot{\overline{|\sigma_{ST}|}}}{|\sigma_{ST}| - \sigma^{SA}_{f,ST}}\, \mathcal{H}^{SA}_{ST} \\ \dot{\xi} & = & \pi^{SA}\, \xi \quad \dfrac{\dot{\overline{|\sigma|}}}{|\sigma| - \sigma^{SA}_{f}} \quad \mathcal{H}^{SA} - \dfrac{\xi - \xi_{ST}}{\tau}\, \mathcal{H}_v \end{array}\right. \tag{5.6}$$

Exponential

$$\left\{\begin{array}{rcl} \dot{\xi}_{ST} & = & \beta^{SA}_{ST}\, \xi_{ST}\, \dfrac{\dot{\overline{|\sigma_{ST}|}}}{(|\sigma_{ST}| - \sigma^{SA}_{f,ST})^2}\, \mathcal{H}^{SA}_{ST} \\ \dot{\xi} & = & \beta^{SA}\, \xi \quad \dfrac{\dot{\overline{|\sigma|}}}{(|\sigma| - \sigma^{SA}_{f})^2} \quad \mathcal{H}^{SA} - \dfrac{\xi - \xi_{ST}}{\tau}\, \mathcal{H}_v \end{array}\right. \tag{5.7}$$

where $\mathcal{H}_v$ is defined as above while $\mathcal{H}^{SA}$ and $\mathcal{H}^{SA}_{ST}$ are zero unless the conditions described in the following are satisfied:

$$\left\{\begin{array}{rlllll} \mathcal{H}^{SA}_{ST} & = 1 & \text{when} & \dot{\sigma_{ST}} < 0 & \text{and} & \sigma^{SA}_{f,ST} \leq \sigma_{ST} \leq \sigma^{SA}_{s,ST} \\ \mathcal{H}^{SA} & = 1 & \text{when} & \dot{\sigma} < 0 & \text{and} & \sigma^{SA}_{f} \leq \sigma \leq \sigma^{SA}_{s} \end{array}\right. \tag{5.8}$$

where $\sigma^{SA}_{s,ST}$, $\sigma^{SA}_{f,ST}$, σ^{SA}_{s} and σ^{SA}_{f} are material properties representing, respectively, the stress levels at which the static and dynamic reverse transformations start and finish. Finally, π^{SA}_{ST}, β^{SA}_{ST}, π^{SA} and β^{SA} are material constants which govern, respectively, the form of the static and dynamic reverse phase transition evolution.

5.2.3 Evolution of elastic modulus

Experimental tests show large differences between the elastic properties of austenite and martensite [Auricchio and Sacco, 1997; Dolce and Cardone, 2001a,b; DesRoches *et al.*, 2004; Fugazza, 2005]. To model this aspect, we introduce a static and a dynamic elastic modulus, respectively indicated as E_{ST} and E, function of the corresponding martensite fractions:

$$E_{ST} = E_{ST}(\xi_{ST}) \qquad \text{and} \qquad E = E(\xi) \tag{5.9}$$

Valid expressions can be obtained regarding the SMA as a composite material made of a volume fraction of martensite and a volume fraction of austenite. Next, the composite elastic properties can be recovered through the homogenization theory. Addressing the reader to more specific works regarding such a topic, for the specific problem under investigation (i.e. uniaxial state of stress of wires and bars subject to cyclic loadings), we follow Auricchio and Sacco [1999] and Ikeda *et al.* [2004] and adopt a Reuss scheme. In particular, by knowing the elastic modulus of the pure austenite, E_A, and the elastic modulus of the pure martensite, E_S, the equivalent moduli are expressed as:

$$E_{ST} = \frac{E_A E_S}{E_S + (E_A - E_S)\,\xi_{ST}} \tag{5.10a}$$

$$E = \frac{E_A E_S}{E_S + (E_A - E_S)\,\xi} \tag{5.10b}$$

5.2.4 Stress-strain relationship

Consistently with the previous considerations, we introduce two different inelastic strains, the *static inelastic strain*, ϵ^{in}_{ST}, and the *dynamic inelastic strain*, ϵ^{in}, the former representing the inelastic strain that would be obtained in the case of static loading conditions. These inelastic strains are related to the corresponding martensite fractions as follows:

$$\epsilon^{in}_{ST} = \epsilon_L\,\xi_{ST}\,\mathrm{sgn}(\sigma_{ST}) \tag{5.11a}$$

$$\epsilon^{in} = \epsilon_L\,\xi\,\mathrm{sgn}(\sigma) \tag{5.11b}$$

where ϵ_L is the maximum residual strain (i.e. a measure of the maximum deformation obtainable aligning all the single-variant martensites in one direction), $\mathrm{sgn}(\cdot)$ is the sign function defined as:

$$\mathrm{sgn(x)} = \begin{cases} -1 & \text{if} \quad \mathrm{x} < 0 \\ 0 & \text{if} \quad \mathrm{x} = 0 \\ +1 & \text{if} \quad \mathrm{x} > 0 \end{cases} \tag{5.12}$$

and σ_{ST} and σ are the static and the dynamic stress, respectively. Recalling that we are limiting the discussion to a small deformation regime, for the total strain ϵ we may

introduce two additive decompositions:

$$\epsilon = \epsilon_{ST}^{el} + \epsilon_{ST}^{in} \tag{5.13a}$$

$$\epsilon = \epsilon^{el} + \epsilon^{in} \tag{5.13b}$$

where ϵ_{ST}^{el} represents the *static elastic strain* and ϵ^{el} represents the *dynamic elastic strain.* Finally, by assuming the previous stress states to be linearly related to the corresponding elastic deformations, we can write:

$$\sigma_{ST} = E_{ST}\,\epsilon_{ST}^{el} = E_{ST}\,(\epsilon - \epsilon_{ST}^{in}) = E_{ST}\,\left[\epsilon - \epsilon_L\,\xi_{ST}\,\mathrm{sgn}(\sigma_{ST})\right] \tag{5.14a}$$

$$\sigma = E\,\epsilon^{el} \quad = E\,(\epsilon - \epsilon^{in}) \quad = E\,\left[\epsilon - \epsilon_L\,\xi\,\mathrm{sgn}(\sigma)\right] \tag{5.14b}$$

5.2.5 Time-discrete model

During the development of the time-continuous model we assumed the stresses as control variables. However, for the development of the time-discrete model we assume the strain as the control variable. This choice is consistent with the fact that, from the integration scheme point of view, the time-discrete problem is interpreted as strain-driven.

Accordingly, we consider two instants, t_n and $t_{n+1} > t_n$, such that t_{n+1} is the first time value of interest after t_n. Next, knowing the strain at time t_{n+1} and the solution at time t_n, we should compute the new solution at time t_{n+1}. To minimize the appearence of subscripts and to make the equations more readable, we introduce the convention:

$$a_n = a(t_n), \qquad a = a(t_{n+1}) \tag{5.15}$$

where a is a generic quantity. Therefore, the subscript n indicates a quantity evaluated at time t_n while no subscript indicates a quantity evaluated at time t_{n+1}. Before proceeding, we wish to observe that from Equations 5.14a and 5.14b it is possible to conclude that $\mathrm{sgn}(\sigma_{ST}) = \mathrm{sgn}(\sigma) = \mathrm{sgn}(\epsilon)$. This consideration is of interest since, in a time-discrete setting, ϵ is assumed to be known at any instant.

5.2.5.1 Integration of kinetic rules.

We can obtain the time-discrete phase-transition rules by writing Equations $5.1-5.3$ and Equations $5.5-5.7$ in residual form. Introducing the notations $\lambda_{ST} = \xi_{ST}$ - $\xi_{ST,n}$ and $\lambda = \xi$ - ξ_n and after clearing the fractions, we obtain the following algebraic expressions.

Conversion of austenite into martensite.

$$\textit{Linear} \quad \begin{cases} \mathcal{R}_{ST}^{AS} &= \lambda_{ST}\left(|\sigma_{ST}| - \sigma_{f,ST}^{AS}\right) + \\ &\quad + (1-\xi_{ST})\left(|\sigma_{ST}| - |\sigma_{ST,n}|\right)\mathcal{H}_{ST}^{AS} = 0 \\ \mathcal{R}^{AS} &= \lambda\left(|\sigma| - \sigma_f^{AS}\right) + (1-\xi)\left(|\sigma| - |\sigma_n|\right)\ \mathcal{H}^{AS} + \\ &\quad + \frac{\Delta t}{\tau}\left(\xi - \xi_{ST}\right)\left(|\sigma| - \sigma_f^{AS}\right)\ \mathcal{H}_v = 0 \end{cases} \tag{5.16}$$

$$\textit{Power} \quad \begin{cases} \mathcal{R}_{ST}^{AS} &= \lambda_{ST}\left(|\sigma_{ST}| - \sigma_{f,ST}^{AS}\right) + \\ &\quad + \pi_{ST}^{AS}(1-\xi_{ST})\left(|\sigma_{ST}| - |\sigma_{ST,n}|\right)\mathcal{H}_{ST}^{AS} = 0 \\ \mathcal{R}^{AS} &= \lambda\left(|\sigma| - \sigma_f^{AS}\right) + \pi^{AS}(1-\xi)\left(|\sigma| - |\sigma_n|\right)\ \mathcal{H}^{AS} + \\ &\quad + \frac{\Delta t}{\tau}\left(\xi - \xi_{ST}\right)\left(|\sigma| - \sigma_f^{AS}\right)\ \mathcal{H}_v = 0 \end{cases} \tag{5.17}$$

$$\textit{Exponential} \quad \begin{cases} \mathcal{R}_{ST}^{AS} &= \lambda_{ST}\left(|\sigma_{ST}| - \sigma_{f,ST}^{AS}\right)^2 + \\ &\quad - \beta_{ST}^{AS}(1-\xi_{ST})\left(|\sigma_{ST}| - |\sigma_{ST,n}|\right)\mathcal{H}_{ST}^{AS} = 0 \\ \mathcal{R}^{AS} &= \lambda\left(|\sigma| - \sigma_f^{AS}\right)^2 - \beta^{AS}(1-\xi)\left(|\sigma| - |\sigma_n|\right)\mathcal{H}^{AS} + \\ &\quad + \frac{\Delta t}{\tau}\left(\xi - \xi_{ST}\right)\left(|\sigma| - \sigma_f^{AS}\right)^2\mathcal{H}_v = 0 \end{cases} \tag{5.18}$$

Conversion of martensite into austenite.

$$\textit{Linear} \quad \begin{cases} \mathcal{R}^{SA}_{ST} &= \lambda_{ST}\,(|\sigma_{ST}| - \sigma^{SA}_{f,ST}) + \\ & \quad - \xi_{ST}\,(|\sigma_{ST}| - |\sigma_{ST,n}|)\,\mathcal{H}^{SA}_{ST} = 0 \\ \mathcal{R}^{SA} &= \lambda\,(|\sigma| - \sigma^{SA}_{f}) - \xi\,(|\sigma| - |\sigma_n|)\,\mathcal{H}^{SA} + \\ & \quad + \frac{\Delta t}{\tau}\,(\xi - \xi_{ST})\,(|\sigma| - \sigma^{SA}_{f})\;\mathcal{H}_v = 0 \end{cases} \tag{5.19}$$

$$\textit{Power} \quad \begin{cases} \mathcal{R}^{SA}_{ST} &= \lambda_{ST}\,(|\sigma_{ST}| - \sigma^{SA}_{f,ST}) + \\ & \quad - \pi^{SA}_{ST}\,\xi_{ST}\,(|\sigma_{ST}| - |\sigma_{ST,n}|)\,\mathcal{H}^{SA}_{ST} = 0 \\ \mathcal{R}^{SA} &= \lambda\,(|\sigma| - \sigma^{SA}_{f,ST}) - \pi^{SA}\xi\,(|\sigma| - |\sigma_n|)\,\mathcal{H}^{SA} + \\ & \quad + \frac{\Delta t}{\tau}\,(\xi - \xi_{ST})\,(|\sigma| - \sigma^{SA}_{f})\;\mathcal{H}_v = 0 \end{cases} \tag{5.20}$$

$$\textit{Exponential} \quad \begin{cases} \mathcal{R}^{SA}_{ST} &= \lambda_{ST}\,(|\sigma_{ST}| - \sigma^{SA}_{f,ST})^2 + \\ & \quad - \beta^{SA}_{ST}\,\xi_{ST}\,(|\sigma_{ST}| - |\sigma_{ST,n}|)\,\mathcal{H}^{SA}_{ST} = 0 \\ \mathcal{R}^{SA} &= \lambda\,(|\sigma| - \sigma^{SA}_{f})^2 - \beta^{SA}\xi\,(|\sigma| - |\sigma_n|)\,\mathcal{H}^{SA} + \\ & \quad + \frac{\Delta t}{\tau}\,(\xi - \xi_{ST})\,(|\sigma| - \sigma^{SA}_{f})^2\,\mathcal{H}_v = 0 \end{cases} \tag{5.21}$$

5.2.6 Solution algorithms

To solve the time-discrete evolutionary equations, we can either adopt an interative strategy (1) or a closed-form solution approach (2), as briefly discussed in the following.

1. *Solution by iterative strategy.* As an iterative scheme, we select the Newton-Raphson strategy. To guarantee the method a quadratic convergence, the derivatives of the evolutionary equations written in residual form are required to obtain the tangent modulus consistent with the time-discrete model. Since the computation needs long algebra, we include them in Appendix B.

2. *Solution in closed form.* Substitution of Equations 5.14*a* and 5.14*b* into the time-discrete evolutionary equations written in residual form, returns expressions of the following type:

$$A\,\xi^2 + B\,\xi + C = 0 \qquad \text{and} \qquad A\,\xi^3 + B\,\xi^2 + C\,\xi + D = 0 \tag{5.22}$$

whose roots can be easily found in closed-form. In particular, we obtain a quadratic expression when considering both linear and power rules and a cubic expression

when considering the exponential rules. The coefficients are not reported here for brevity but can be found in Appendix C. Moreover, due to their complexity, it does not seem reasonable to perform a discussion of the equation roots. As a consequence, the admissible root is chosen as the one bounded between 0 (phase transformation not started yet) and 1 (phase transformation completed).

Finally, in Table 5.1 we summarize the main steps concerning the overall strain-driven algorithm and in Tables 5.2 and 5.3 we provide the solution schemes of the two transformation processes.

Remark: the static version of the presented model (i.e. we neglect the contribution of the viscous term) with linear kinetic rules is the constitutive equation that has been selected to model the behavior of the superelastic SMA braces.

5.3 Development of a Rate-Dependent Thermo-Mechanical Constitutive Model

In the following, we present a uniaxial thermo-mechanical constitutive model for superelastic SMAs, cast within the theory of irreversible thermodynamics and developed in the small deformation regime.

5.3.1 Time-continuous general framework

We assume that at each time istant the thermodynamic state of a volume element is characterized by a set of external (controllable) and internal variables. More precisely, we choose as external variables the uniaxial strain, ϵ, and the absolute temperature, T, and as internal variable a scalar quantity, ξ, representing the volume of *martensite fraction*. A necessary ingredient will then be the *free energy*, named as ψ, depending on both internal and external variables.

5.3.2 Kinetic rules

We still assume to work with two processes which may produce variations of the martensite fraction:

- the conversion of austenite into martensite A $\rightarrow$ S (i.e. forward transformation),
- the conversion of martensite into austenite S $\rightarrow$ A (i.e. reverse transformation).

For each process, the evolution of the martensite fraction is expressed in terms of the associated driving force:

$$F = |\sigma| - TA \tag{5.23}$$

where

$$A = \frac{\Delta\eta}{\epsilon_L} \tag{5.24}$$

consistently with experimental evidences showing that both processes can be either stress and/or temperature driven [Duerig *et al.*, 1990] and that they may occur in regions delimited, with good approximations, by straight lines. Again, we propose *linear*, *power* and *exponential* kinetic rules to model the evolution in time of the martensite fraction.

Conversion of austenite into martensite.

$$\textit{Linear} \qquad \dot{\xi} = - (1-\xi) \frac{\dot{F}}{F - R_f^{AS}} \mathcal{H}^{AS} \tag{5.25}$$

$$\textit{Power} \qquad \dot{\xi} = - \pi^{AS} (1-\xi) \frac{\dot{F}}{F - R_f^{AS}} \mathcal{H}^{AS} \tag{5.26}$$

$$\textit{Exponential} \qquad \dot{\xi} = \beta^{AS} (1-\xi) \frac{\dot{F}}{(F - R_f^{AS})^2} \mathcal{H}^{AS} \tag{5.27}$$

The term $\mathcal{H}^{AS}$ is the activation factor relative to the A $\rightarrow$ S transformation and it is defined as:

$$\mathcal{H}^{AS} = \begin{cases} 1 & \text{when} \quad \dot{F} > 0 \quad \text{and} \quad R_s^{AS} < F < R_f^{AS} \\ 0 & \text{otherwise} \end{cases} \tag{5.28}$$

where

$$R_s^{AS} = \sigma_s^{AS} - T_R A \qquad R_f^{AS} = \sigma_f^{AS} - T_R A \tag{5.29}$$

The quantities σ_s^{AS} and σ_f^{AS} are material properties representing the stress level at which, respectively, the forward transformation starts and finishes at temperature T_R. Also, coefficients π^{AS} and β^{AS} are material constants which govern the form of the considered phase transformation.

Conversion of martensite into austenite.

$$\textit{Linear} \qquad \dot{\xi} = \xi \frac{\dot{F}}{F - R_f^{SA}} \mathcal{H}^{SA} \tag{5.30}$$

$$\textit{Power} \qquad \dot{\xi} = \pi^{SA} \xi \frac{\dot{F}}{F - R_f^{SA}} \mathcal{H}^{SA} \tag{5.31}$$

$$\textit{Exponential} \qquad \dot{\xi} = \beta^{SA} \xi \frac{\dot{F}}{(F - R_f^{SA})^2} \mathcal{H}^{SA} \tag{5.32}$$

The term $\mathcal{H}^{SA}$ is the activation factor relative to the forward phase transformation and it is defined as:

$$\mathcal{H}^{SA} = \begin{cases} 1 & \text{when} \quad \dot{F} < 0 \quad \text{and} \quad R_f^{SA} < F < R_s^{SA} \\ 0 & \text{otherwise} \end{cases} \tag{5.33}$$

where

$$R_s^{SA} = \sigma_s^{SA} - T_R A \qquad R_f^{SA} = \sigma_f^{SA} - T_R A \tag{5.34}$$

The quantities σ_s^{SA} and σ_f^{SA} are material properties representing the stress level at which, respectively, the reverse transformation starts and finishes at temperature T_R. Also, coefficients π^{SA} and β^{SA} are material constants which govern the form of the considered phase transformation.

5.3.3 Evolution of elastic modulus

As for the case of the previously developed constitutive equation, we still model the modulus of elasticity of the SMA material according to the Reuss scheme. Again, by knowing the values E_A, E_S and the martensite fraction, ξ, the overall equivalent elastic modulus is given by:

$$E = \frac{E_A E_S}{E_S + (E_A - E_S)\,\xi} \tag{5.35}$$

5.3.4 Free energy

Based on the work by Auricchio and Sacco [2001], we consider the following free energy:

$$\begin{aligned} \psi &= [(u_A - T\eta_A) - \xi(\Delta u - T\Delta\eta)] + C\left[(T - T_0) - T\log\frac{T}{T_0}\right] \\ &+ \frac{1}{2}\,E[\epsilon - \epsilon_L\,\xi\,\mathrm{sgn}(\sigma)]^2 - (T - T_0)\,[\epsilon - \epsilon_L\,\xi\,\mathrm{sgn}(\sigma)]\,E\alpha \end{aligned} \tag{5.36}$$

where

- u_A and η_A are the internal energy and entropy of the austenite,
- Δu and $\Delta\eta$ are the internal energy difference and the entropy difference between the austenite and the martensite,
- C is the material heat capacity,
- T_0 is the natural or reference state temperature,
- σ is the uniaxial stress,
- α is the thermal expansion factor.

5.3.5 Stress-strain relationship

The stress is defined as the partial derivative of the free-energy with respect to the total strain:

$$\sigma = \frac{\partial \psi}{\partial \epsilon} = E\ [\epsilon - \epsilon_L\, \xi\, \mathrm{sgn}(\sigma)] - E\, \alpha\, (T - T_0) \tag{5.37}$$

We still assume an additive decomposition of the total strain, ϵ, of the form:

$$\epsilon = \epsilon^{el} + \epsilon^{in} \tag{5.38}$$

with the inelastic strain again expressed by:

$$\epsilon^{el} = \epsilon_L\, \xi\, \mathrm{sgn}(\sigma) \tag{5.39}$$

Furthermore, by recalling that the term ϵ^{el} includes contributions such as the pure elastic term as well as the thermo-elastic expansion term and by considering Equation 5.39, we can observe that there is a linear relationship between stress and elastic strain:

$$\sigma = E\, \epsilon^{el} \tag{5.40}$$

Finally, substitution of Equation 5.40 into Equation 5.38 indicates that we still have $\mathrm{sgn}(\sigma) = \mathrm{sgn}(\epsilon)$. This last equality will be particularly useful during the development of the solution algorithm.

5.3.6 Heat equation

According to the classical literature [Lemaitre and Chaboche, 1990], the heat equation can be written as:

$$C\, \dot{T} + \mathrm{div}\, \mathbf{q} = b - \gamma\, (T - T_{ext}) \tag{5.41}$$

where div indicates the divergence operator, a superposed dot indicates a time-derivative, $\mathbf{q}$ is the heat flux, b is the heat source and γ a material constant linking the temperature difference between the element being considered and the surrounding. Since for this specific study we are considering elements with small size cross sections (i.e. wires and bars), in the previous equation we may neglect the contribution given by the heat flux. Accordingly:

$$C\, \dot{T} = b - \gamma\, (T - T_{ext}) \tag{5.42}$$

with the heat source that can be described as the sum of two contributions:

$$b = \mathcal{H}_{tmc} + \mathcal{D}_{mec} \tag{5.43}$$

where

- $\mathcal{H}_{tmc}$ represents the heat production associated to the thermo-mechanical coupling and it is defined as:

$$\mathcal{H}_{tmc} = T\,\frac{\partial^2\psi}{\partial T\partial\epsilon}\,\dot{\epsilon} + T\,\frac{\partial^2\psi}{\partial T\partial\xi}\,\dot{\xi} \tag{5.44}$$

- $\mathcal{D}_{mec}$ represents the heat production associated to the dissipative mechanical processes and it is defined as:

$$\mathcal{D}_{mec} = \sigma\dot{\epsilon} - \left(\frac{\partial\psi}{\partial\epsilon}\,\dot{\epsilon} + \frac{\partial\psi}{\partial\xi}\,\dot{\xi}\right) \tag{5.45}$$

Due to the specific form of the free energy chosen, we have:

$$\mathcal{H}_{tmc} = T\{-E\,\alpha\,\dot{\epsilon} + [\Delta\eta + E\,\alpha\,\epsilon_L\,\mathrm{sgn}(\sigma)]\;\dot{\xi}\} \tag{5.46}$$

$$\mathcal{D}_{mec} = \Pi_1\,\dot{\xi} \tag{5.47}$$

with

$$\Pi_1 = \Delta u - T\Delta\eta + \epsilon_L|\sigma| \tag{5.48}$$

modelling the thermodynamic force associated to ξ.

5.3.7 Time-discrete model

As in the case of the viscous model, the time-discrete model is obtained by integrating the time-continuous model over the time-interval $[t_n, t_{n+1}]$ through a backward-Euler integration scheme. To minimize the appearence of subscripts, the subscript n still indicates a quantity that is evaluated at time t_n while no subscript still indicates a quantity that is evaluated at time t_{n+1}, with $t_n < t_{n+1}$.

5.3.7.1 Integration of kinetic rules.

We can obtain the time-discrete phase-transition rules by writing Equations $5.25 - 5.27$ and Equations $5.30 - 5.32$ in residual form. Recalling the notation $\lambda = \xi - \xi_n$ and after clearing the fractions, we obtain the following algebraic expressions.

Conversion of austenite into martensite.

$$\textit{Linear} \quad \mathcal{R}^{AS} = \lambda\left(F - R_f^{AS}\right) + (1-\xi)\,(F - F_n)\,\mathcal{H}^{AS} = 0 \tag{5.49}$$

$$\textit{Power} \quad \mathcal{R}^{AS} = \lambda\left(F - R_f^{AS}\right) + \pi^{AS}\,(1-\xi)\,(F - F_n)\,\mathcal{H}^{AS} = 0 \tag{5.50}$$

$$\textit{Exponential} \quad \mathcal{R}^{AS} = \lambda\left(F - R_f^{AS}\right)^2 - \beta^{AS}\,(1-\xi)\,(F - F_n)\,\mathcal{H}^{AS} = 0 \tag{5.51}$$

Conversion of martensite into austenite.

$$\textit{Linear} \quad \mathcal{R}^{SA} = \lambda \left(F - R_f^{SA}\right) - \xi \left(F - F_n\right) \mathcal{H}^{SA} = 0 \tag{5.52}$$

$$\textit{Power} \quad \mathcal{R}^{SA} = \lambda \left(F - R_f^{SA}\right) - \pi^{SA} \xi \left(F - F_n\right) \mathcal{H}^{SA} = 0 \tag{5.53}$$

$$\textit{Exponential} \quad \mathcal{R}^{SA} = \lambda \left(F - R_f^{SA}\right)^2 - \beta^{SA} \xi \left(F - F_n\right) \mathcal{H}^{SA} = 0 \tag{5.54}$$

In order to improve the robustness of the solution procedure, we introduce one modification to the model. In particular, we scale the phase transition driving force, F, with respect to a temperature upper limit value T_U. Accordingly, its new expression becomes:

$$F = |\sigma| - (T - T_U)\, A \tag{5.55}$$

where the temperature T_U is an arbitrary value such that $T < T_U$. By means of Equation (5.55), we then guarantee the constant sign of F.

5.3.7.2 Integration of heat equation.

Integration of Equation 5.42 leads to:

$$C \frac{T - T_n}{t - t_n} - b_d + \gamma \left(T - T_{ext}\right) = 0 \tag{5.56}$$

where

$$b_d = \frac{1}{t - t_n} \left[\Pi_1 \lambda + T \Gamma_1\right] \tag{5.57}$$

with

$$\lambda = \xi - \xi_n \tag{5.58}$$

$$\Pi_1 = \Delta u - T \Delta \eta + \epsilon_L |\sigma| \tag{5.59}$$

$$\Gamma_1 = -E\, \alpha \left(\epsilon - \epsilon_n\right) + \left[E\, \epsilon_L\, \alpha\, \mathrm{sgn}(\sigma) + \Delta \eta\right] \lambda \tag{5.60}$$

with ϵ and ϵ_n assumed to be known.

5.3.8 Solution algorithms

Equations $5.49 - 5.51$ and Equations $5.52 - 5.54$ can be solved in general by means of an iterative strategy or, in the specific case in which $\alpha = 0$, in closed-form. Since the same observations drawn in section 3.3.6 still apply, we address the reader to Appendices B and C for the computations involved. Again, in view of the computer implementation of the constitutive model, in Table 5.4 we summarize the main steps concerning the overall solution procedure and in Tables 5.5 and 5.6 we provide the solution schemes related to the two transformation processes.

5.4 Numerical Simulations

We investigate the ability of the models to simulate typical superelastic SMA stress-strain response by considering two test cases:

- **Test 1**: strain-controlled loading-unloading cycle performed in static conditions up to a 7% strain. The goal of this test is to understand the role of the speed parameters (i.e. π's and β's) that both power and exponential rules contain.

- **Test 2**: simple strain-driven loading-unloading cycle performed initially in 10^3 seconds and then, in a subsequent simulation, in 10^{-3} seconds in order to reproduce, respectively, very slow and very fast loading conditions. As in the previous test, the maximum strain attained is 7%. With this way of proceeding, we keep the same type of loading-unloading history while changing only the strain-rate at which it is applied. The goal of this test is to study the rate-dependent response of the models under investigation.

Furthermore, the capability of the models to describe the material behavior also for more complex loading histories (such as partial loading-unloading patterns with the description of inner hysteresis loops) has been numerically tested, but not reported here for brevity.

For the numerical simulations, we consider the following material parameters.

Parameters common to both models:

$$E_A = 40000\,\text{MPa} \qquad E_S = 20000\,\text{MPa} \qquad \epsilon_L = 5\%$$

Parameters related to the viscous model only:

$$\begin{aligned} \sigma^{AS}_{s,ST} &= 200\,\text{MPa} & \sigma^{AS}_{f,ST} &= 300\,\text{MPa} \\ \sigma^{SA}_{s,ST} &= 200\,\text{MPa} & \sigma^{SA}_{f,ST} &= 100\,\text{MPa} \\ \sigma^{AS}_{s} &= \sigma^{AS}_{s,ST} & \sigma^{AS}_{f} &= 1000\,\text{MPa} \\ \sigma^{SA}_{f} &= 800\,\text{MPa} & \sigma^{SA}_{f} &= \sigma^{SA}_{f,ST} \\ \tau &= 0.5\,\text{sec} \end{aligned}$$

Parameters related to the thermo-mechanical model only:

$$\begin{aligned} \sigma_s^{AS} &= 200\,\text{MPa} & \sigma_f^{AS} &= 300\,\text{MPa} \\ \sigma_s^{SA} &= 200\,\text{MPa} & \sigma_f^{SA} &= 100\,\text{MPa} \\ \Delta u &= 30\,\text{MPa} & \Delta\eta &= 0.20\,\text{MPaK}^{-1} \\ C &= 4\,\text{MPaK}^{-1} & T_{ext} &= T_0 = T_R = 293\,\text{K} \\ T_U &= 573\,\text{K} & \alpha &= 0\,\text{K}^{-1} \\ \gamma &= 0.1 \end{aligned}$$

It is important to observe that, as far as the viscous model is concerned, the stress level at which the austenite-to-martensite phase transformation starts and the stress level at which the martensite-to-austenite phase transformation finishes is the same for both the static and the dynamic case.

Moreover, for most of the numerical simulations performed in the present section and unless explicitly stated, we adopt constant values for the static and dynamic speed parameters (i.e. we set $\pi_{ST}^{AS} = \pi^{AS} = \pi_{ST}^{SA} = \pi^{SA} = \pi$ for the power rules and $\beta_{ST}^{AS} = \beta^{AS} = \beta_{ST}^{SA} = \beta^{SA} = \beta$ for the exponential rules). This choice is done to reduce the number of results to be reported but, as it is clear from them, it is quite limiting and, hence, it will be removed when studying the ability of the models to simulate experimental data.

5.4.1 Model response

Numerical results from Test 1 (static loadings) are reported in Figures 5.1-5.3 in terms of stress-strain relationships, for the three different kinetic rules and for both models. From the result examination, we may draw the following considerations.

- Under static loading conditions both models display identical results (Figures 5.1-5.3). This is justified by the fact that the effect of the viscous term, in the viscous model and of the heat equation, in the thermo-mechanical model (Figure 5.4), are negligible. Therefore, no dynamic effetcs are produced.
- The linear rules (Figure 5.1) describe the superelastic behavior by linearly connecting the corresponding start and finish transformation stress levels, therefore without reproducing the typical smooth behavior displayed by most superelastic SMAs during the phase transitions.
- The power rules (Figure 5.2) show different behaviors according to the values of the π-parameters. In particular, for π below or above 1 the curve representing

the phase transition evolution changes convexity. In fact, the smaller the π-values, the faster is the model response in reaching the final transformation stress levels while the higher the π-values, the slower is the model response to reach the final transformation stress levels. Finally, also from a numerical point of view, the power rules reproduce a linear kinetic upon setting $\pi = 1$.

- The exponential rules (Figure 5.3) show different behaviors according to the values of the β-parameters. In particular, by choosing β in the positive range it is possible to control the speed of the phase transition saturation, without however having the possibility of changing the convexity of the phase transition evolution as for the power rules.

Numerical results from Test 2 (very slow vs. very fast loading conditions) are reported in Figures 5.5-5.10 in terms of stress-strain relationships, for the three different kinetic rules and, again, for both models. From the result examination, we may draw the following considerations.

- Both models are able to reproduce the experimentally observed [Dolce and Cardone, 2001b; DesRoches *et al.*, 2004; Fugazza, 2005] increase of the stress level at which, respectively, the forward and reverse transformation finishes and starts as the loading frequency increases.
- The linear rules (Figures 5.5 and 5.6) are able to reproduce the experimentally observed hysteresis size reduction [Dolce and Cardone, 2001b; DesRoches *et al.*, 2004; Fugazza, 2005] with the increase of the loading rate. Furthermore, the higher the speed of the test, the faster the response approaches the final phase transformation stress levels.
- When considering the viscous model, we observe that the power rules (Figures 5.7 and 5.8) do not seem to reproduce the hysteresis size reduction, meaning that there is a dissipated energy overestimation. However, this effect is also due to the arbitrary choice of setting $\pi_{ST}^{AS} = \pi^{AS} = \pi_{ST}^{SA} = \pi^{SA} = \pi$. In fact, by choosing different values for the static and the dynamic speed factors, it would be possible to model a significant hysteresis size reduction. In the thermo-mechanical model, instead, we notice a narrower hysteresis cycle than that obtained after running the same test under very slow loading conditions.
- As in the previous case, we observe that if we adopt exponential rules (Figure 5.9 and 5.10) in the viscous model, we still cannot simulate the hysteresis size reduction. Again, this effect is also due to the arbitrary choice of setting $\beta_{ST}^{AS} =$

$\beta^{AS} = \beta^{SA}_{ST} = \beta^{SA} = \beta$. By choosing instead different values for the static and the dynamic speed factors, it would still be possible to predict a significant hysteresis size reduction. On the other hand, the thermo-mechanical model seems to provide a more realistic trend of the material behavior.

5.5 Experimental Investigation and Material Parameter Selection

We now want to test the ability of the models to simulate experimental data. In particular, we consider four sets of experiments.

- **Set 1**: The material is a commercial superelastic NiTi straight wire with circular cross section of diameter 1.00 mm provided by CNR-IENI (Lecco, Italy). The testing frequencies were 0.001 Hz (static) and 1 Hz (dynamic).
- **Set 2**: The material is a commercial superelastic NiTi straight wire with circular cross section of diameter 0.76 mm provided by Memry Corp. (Menlo Park, USA). The testing frequencies were 0.001 Hz (static) and 0.1 Hz (dynamic).
- **Set 3**: The material is a commercial superelastic NiTi bar with circular cross section of diameter 7.1 mm provided by Special Metals Corporations (New Hartford, USA). The testing frequencies were 0.0025 Hz (static) and 1 Hz (dynamic).
- **Set 4**: The material is a commercial superelastic NiTi bar with circular cross section of diameter 12.7 mm provided by Special Metals Corporations (New Hartford, USA). The testing frequencies were 0.0025 Hz (static) and 1 Hz (dynamic).

Tests relative to the first two sets were performed by Fugazza [2005] at the Parco Scientifico Tecnologico e delle Telecomunicazioni in Valle Scrivia (Tortona, Italy) while tests considered in Sets 3 and 4 were performed by DesRoches *et al.* [2004] at the Georgia Institute of Technology (Atlanta, USA). Both experimental studies were aimed at investigating the cyclic properties of superelastic SMA wires and bars for seismic applications.

Besides the development of the constitutive models and their algorithmic implementation, the other goal of this study is to try to reproduce the rate-dependent superelastic behavior of the considered SMA elements. In the following two sections, we propose a methodology for selecting the material parameters of each model by including the list of the steps that should be sequentially performed. The important task is to judge the ability of both constitutive equations to simulate the dynamic behavior of the SMA material being considered, starting from its static experimental stress-strain relationship.

5.5.1 Material parameter selection for viscous model

As far as the viscous model is concerned and recalling that a priori we set $\sigma_s^{AS} = \sigma_{s,ST}^{AS}$ and $\sigma_f^{SA} = \sigma_{f,ST}^{SA}$, for each set of experimental data we need to:

1. Obtain mechanical parameters E_A, E_S, ϵ_L common to all the experimental curves belonging to the same set.
2. Obtain mechanical parameters $\sigma_{s,ST}^{AS}$, $\sigma_{f,ST}^{AS}$, $\sigma_{s,ST}^{SA}$ and $\sigma_{f,ST}^{SA}$ from the experimental tests performed in static loading conditions (these data may vary according to the considered kinetic rules).
3. Find values π_{ST}^{AS} and π_{ST}^{SA} when considering power rules and values β_{ST}^{AS} and β_{ST}^{SA} when considering exponential rules in such a way to best fit the experimental curve performed in static loading conditions.
4. Obtain mechanical parameters σ_f^{AS} and σ_s^{SA} as well as speed parameters π^{AS} and π^{SA} when considering power rules or β^{AS} and β^{SA} when considering exponential rules from the tests performed in dynamic loading conditions.
5. Run numerical simulations for all the strain-rates considered using the same material parameters throughout the analyses.
6. Compare experimental data and numerical results.

5.5.2 Material parameter selection for thermo-mechanical model

As far as the thermo-mechanical model is concerned, for each set of experimental data we need to:

1. Obtain mechanical parameters E_A, E_S and ϵ_L common to all experimental curves belonging to the same set.
2. Obtain mechanical parameters σ_s^{AS}, σ_f^{AS}, σ_s^{SA} and σ_f^{SA} from the experimental tests performed in static loading conditions (these data may vary according to the considered kinetic rules).
3. Obtain thermodynamic parameters Δu, $\Delta\eta$, C, α and γ.
4. Find values of π^{AS} and π^{SA} when considering power rules and values of β^{AS} and β^{SA} when considering exponential rules in such a way to best fit the experimental curve obtained in static loading conditions.

5. Run numerical simulations for all the strain-rates considered using the same material parameters throughout the analyses.
6. Compare experimental data and numerical results.

5.6 Ability of the Models to reproduce Experimental Data

After performing several experimental tests, we now want to simulate them using the proposed model. We only focus on one loading-unloading cycle up to a 6% strain and we address the reader to Tables 5.7 and 5.8 for the material parameters. Also, since thermodynamic coefficients were not determined experimentally, we use the same as those adopted in the section "Numerical Simulations". Finally, to avoid repetitions, we recall that the static transformation stress levels related to the viscous model correspond to the actual ones in the thermo-mechanical model. Therefore $\sigma^{AS}_{s,ST} = \sigma^{AS}_{s}$, $\sigma^{AS}_{f,ST} = \sigma^{AS}_{f}$, $\sigma^{SA}_{s,ST} = \sigma^{SA}_{s}$ and $\sigma^{SA}_{f,ST} = \sigma^{SA}_{f}$.

In the following, we list and discuss the most important results.

- From the static tests (Figures 5.11-5.14), we observe an excellent match between experiments and numerical results, specially when power and exponential rules are used to model the evolution of the martensite fraction during the deformation process. Under these loading conditions both models provide the same mechanical response. In fact, as previously reported, the viscous term and the heat equation do not provide rate-dependent effects.
- When exploiting the dynamic conditions, we note that the ability of the models to reproduce experimental data strongly depends on the type of SMA material under investigation. More precisely, when we consider the first set of data (Figures 5.15 and 5.16) we observe a very good fit of the model response with the experimental curve. On the other hand, we do not observe the same trend for the other sets of data (Figures 5.17 and 5.22) where, however, the models compute with good approximation the maximum stress level reached at the end of the loading phase.
- Both models successfully simulate complete transformation patterns by correctly capturing the material hardening (i.e. fully martensitic phase) observed at the end of the upper superelastic plateau (Figures 5.11 and 5.14).
- Despite the fact that chemical composition, thermomechanical treatments and manifacturing processes may result in showing a different material behavior under the same loading conditions, the capability of the models to describe the hysteresis size reduction at high frequency levels is always noticed.

5.7 Concluding Remarks

In this section, we proposed two uniaxial constitutive models able to reproduce the rate-dependent superelastic effect exhibited by SMAs and able to take into account the different elastic properties between austenite and martensite.

In the following, we summarize the major outcomes based on the numerical tests as well as on the comparisons with experimental data.

- The viscous model is based on two scalar internal variables, the static and dynamic martensite fraction, while the thermo-mechanical model is based only on the actual martensite fraction. For both models, three different rate-independent evolutionary equations written in rate form are presented.
- The coupling of the rate-independent kinetic rules with either the viscous term, when considering the viscous model, or the heat equation, when considering the thermo-mechanical model, allows for the modelling of the SMAs' rate-dependent behavior.
- Both models require a limited number of mechanical parameters which can be determined from typical uniaxial tests conducted on either wires or bars. They are the Young's modulus of austenite and martensite, the plateau length and the stress levels at which the phase transformations take place. On the other hand, the thermodynamic parameters are not straightforward to determine experimentally but can be easily found in the literature for typical SMAs.
- Both power and exponential kinetic rules are able to simulate the smooth transition occurring between the pure elastic behavior (either austenite or martensite) and the superelastic plateaus, as experimental evidences display.
- The capacity of the models to simulate experimental data has also been assessed. In particular, static tests have provided an excellent comparison between experiments and numerical results meanwhile the dynamic tests were strongly affected by the different rate-dependent response (i.e different material response exhibited by the considered SMAs for the same loading frequency) of the SMA material under study, probably due to the different chemical composition.

In conclusion, the advantages of the presented models are the simplicity, the possibility of implementing a robust solution algorithm and the ability to reproduce experimental data obtained at different frequency levels of excitation for seismic application purposes.

Table 5.1. Viscous model: overall strain-driven algorithm.

1. Detect loading or unloading

If $|\epsilon - \epsilon_n| > 0 \Rightarrow$ loading
If $|\epsilon - \epsilon_n| < 0 \Rightarrow$ unloading

2. Check phase transformation

If loading then
  check A $\rightarrow$ S phase transformation (Table 5.2)
else if unloading then
  check S $\rightarrow$ A phase transformation (Table 5.3)
end if

3. Solve evolutionary equations

Iterative strategy or closed-form solution

Table 5.2. Viscous model: solution scheme for A → S phase transformation.

If $|\epsilon - \epsilon_n| > 0$ then $\Rightarrow$ loading

$$\begin{aligned} \epsilon_s^{AS} &= \text{sgn}(\epsilon)\,\frac{\sigma_s^{AS}}{E} + \text{sgn}(\epsilon)\,\xi_n\,\epsilon_L \\ \epsilon_f^{AS} &= \text{sgn}(\epsilon)\,\frac{\sigma_f^{AS}}{E} + \text{sgn}(\epsilon)\,\epsilon_L \end{aligned}$$

if $|\epsilon - \epsilon_n| \leq \epsilon_s^{AS}$

$$\begin{aligned} \xi &= \xi_n \\ E &= \frac{E_A\,E_S}{E_S + \xi_n\,(E_A - E_S)} \\ \sigma &= E\,[\epsilon - \epsilon_L\,\xi_n\,\text{sgn}(\epsilon)] \end{aligned}$$

else if $|\epsilon - \epsilon_n| > \epsilon_s^{AS}$ and $|\epsilon - \epsilon_n| < \epsilon_f^{AS}$

$$\text{Solve } \mathcal{R}^{AS} = 0 \begin{cases} \text{Iterative strategy} \\ \text{Closed-form solution} \end{cases}$$

else

$$\begin{aligned} \xi &= 1 \\ E &= E_S \\ \sigma &= E\,[\epsilon - \epsilon_L \text{sgn}(\epsilon)] \end{aligned}$$

end

end if

Table 5.3. Viscous model: solution scheme for S → A phase transformation.

If $|\,\epsilon - \epsilon_n| < 0$ then $\Rightarrow$ unloading

$$\begin{aligned} \epsilon_s^{SA} &= \operatorname{sgn}(\epsilon)\,\frac{\sigma_s^{SA}}{E} + \operatorname{sgn}(\epsilon)\,\xi_n\,\epsilon_L \\ \epsilon_f^{SA} &= \operatorname{sgn}(\epsilon)\,\frac{\sigma_f^{SA}}{E} \end{aligned}$$

if $|\,\epsilon - \epsilon_n| \geq \epsilon_s^{SA}$

$$\begin{aligned} \xi &= \xi_n \\ E &= \frac{E_A\,E_S}{E_S\,+\xi_n\,(E_A - E_S)} \\ \sigma &= E\,[\epsilon - \epsilon_L\,\xi_n\,\operatorname{sgn}(\epsilon)] \end{aligned}$$

else if $|\,\epsilon - \epsilon_n| < \epsilon_s^{SA}$ and $|\,\epsilon - \epsilon_n| > \epsilon_f^{SA}$

$$\text{Solve } \mathcal{R}^{SA} = 0 \begin{cases} \text{Iterative strategy} \\ \text{Closed-form solution} \end{cases}$$

else

$$\begin{aligned} \xi &= 0 \\ E &= E_A \\ \sigma &= E\,\epsilon \end{aligned}$$

end

end if

Table 5.4. Thermo-mechanical model: overall solution algorithm.

1. Define G and G_n

$$G = |\epsilon| + \frac{A}{E}(T - T_U)$$
$$G_n = |\epsilon_n| + \frac{A}{E}(T_n - T_U)$$

2. Detect loading or unloading

If $|G - G_n| > 0 \Rightarrow$ loading
If $|G - G_n| < 0 \Rightarrow$ unloading

3. Check phase transformation

If loading then
  check A $\rightarrow$ S phase transformation (Table 5.5)
else if unloading then
  check S $\rightarrow$ A phase transformation (Table 5.6)
end if

4. Solve evolutionary equations

Iterative strategy or closed-form solution

5. Solve heat equation

Table 5.5. Thermo-mechanical model: solution scheme for A → S phase transformation.

If $|\,G - G_n| > 0$ then $\Rightarrow$ loading

$$\begin{aligned} \epsilon_s^{AS} &= \text{sgn}(\epsilon)\,\frac{R_s^{AS}}{E} + \text{sgn}(\epsilon)\,\xi_n\,\epsilon_L \\ \epsilon_f^{AS} &= \text{sgn}(\epsilon)\,\frac{R_f^{AS}}{E} + \text{sgn}(\epsilon)\,\epsilon_L \end{aligned}$$

if $|\,G - G_n| \leq \epsilon_s^{AS}$

$$\begin{aligned} \xi &= \xi_n \\ E &= \frac{E_A\,E_S}{E_S\,+\xi_n\,(E_A - E_S)} \\ \sigma &= E\,[\epsilon - \epsilon_L\,\xi_n\,\text{sgn}(\epsilon)] \end{aligned}$$

else if $|\,G - G_n| > \epsilon_s^{AS}$ and $|\,G - G_n| < \epsilon_f^{AS}$

$$\text{Solve } \mathcal{R}^{AS} = 0 \begin{cases} \text{Iterative strategy} \\ \text{Closed-form solution} \end{cases}$$

else

$$\begin{aligned} \xi &= 1 \\ E &= E_S \\ \sigma &= E\,[\epsilon - \epsilon_L \text{sgn}(\epsilon)] \end{aligned}$$

end

end if

Table 5.6. Thermo-mechanical model: solution scheme for S → A phase transformation.

If $|G - G_n| < 0$ then $\Rightarrow$ unloading

$$\begin{aligned} \epsilon_s^{SA} &= \operatorname{sgn}(\epsilon)\,\frac{R_s^{SA}}{E} + \operatorname{sgn}(\epsilon)\,\xi_n\,\epsilon_L \\ \epsilon_f^{SA} &= \operatorname{sgn}(\epsilon)\,\frac{R_f^{SA}}{E} \end{aligned}$$

if $|G - G_n| \geq \epsilon_s^{SA}$

$$\begin{aligned} \xi &= \xi_n \\ E &= \frac{E_A\,E_S}{E_S + \xi_n\,(E_A - E_S)} \\ \sigma &= E\,[\epsilon - \epsilon_L\,\xi_n\,\operatorname{sgn}(\epsilon)] \end{aligned}$$

else if $|G - G_n| < \epsilon_s^{SA}$ and $|G - G_n| > \epsilon_f^{SA}$

$$\text{Solve } \mathcal{R}^{SA} = 0 \begin{cases} \text{Iterative strategy} \\ \text{Closed-form solution} \end{cases}$$

else

$$\begin{aligned} \xi &= 0 \\ E &= E_A \\ \sigma &= E\,\epsilon \end{aligned}$$

end

end if

Table 5.7. Material parameters (L=linear kinetic rules, P=power kinetic rules, E=exponential kinetic rules).

		Set 1			Set 2		
		L	**P**	**E**	**L**	**P**	**E**
E_A	[MPa]	31000	31000	31000	61000	61000	61000
E_S	[MPa]	24600	24600	24600	30000	30000	30000
ϵ_L	[%]	4.10	4.10	4.10	4.80	4.80	4.80
$\sigma^{AS}_{ST,s}$	[MPa]	310	280	250	350	350	350
$\sigma^{AS}_{ST,f}$	[MPa]	370	350	350	370	370	370
$\sigma^{SA}_{ST,s}$	[MPa]	60	250	250	150	150	250
$\sigma^{SA}_{ST,f}$	[MPa]	40	40	40	135	135	135
σ^{AS}_{f}	[MPa]	620	620	620	500	500	500
σ^{SA}_{s}	[MPa]	330	330	330	300	300	300
π^{AS}_{ST}	[-]	-	0.18	-	-	1.5	-
π^{SA}_{ST}	[-]	-	0.12	-	-	1.5	-
β^{AS}_{ST}	[-]	-	-	6	-	-	15
β^{SA}_{ST}	[-]	-	-	9.8	-	-	4
π^{AS}	[-]	-	1.1	-	-	0.5	-
π^{SA}	[-]	-	1.1	-	-	0.2	-
β^{AS}	[-]	-	-	240	-	-	25
β^{SA}	[-]	-	-	200	-	-	10

Table 5.8. Material parameters (L=linear kinetic rules, P=power kinetic rules, E=exponential kinetic rules).

		Set 3			Set 4		
		L	**P**	**E**	**L**	**P**	**E**
E_A	[MPa]	35000	35000	35000	28500	28500	28500
E_S	[MPa]	28000	28000	28000	24000	24000	24000
ϵ_L	[%]	4.25	4.25	4.25	2.90	2.90	2.90
$\sigma_{ST,s}^{AS}$	[MPa]	320	340	340	270	210	210
$\sigma_{ST,f}^{AS}$	[MPa]	460	460	460	530	530	530
$\sigma_{ST,s}^{SA}$	[MPa]	260	400	400	350	420	420
$\sigma_{ST,f}^{SA}$	[MPa]	200	200	200	90	90	90
σ_f^{AS}	[MPa]	520	520	520	750	750	750
σ_s^{SA}	[MPa]	320	320	320	500	500	500
π_{ST}^{AS}	[-]	-	1	-	-	0.7	-
π_{ST}^{SA}	[-]	-	0.09	-	-	0.75	-
β_{ST}^{AS}	[-]	-	-	140	-	-	150
β_{ST}^{SA}	[-]	-	-	15	-	-	120
π^{AS}	[-]	-	1	-	-	0.8	-
π^{SA}	[-]	-	2	-	-	0.9	-
β^{AS}	[-]	-	-	50	-	-	180
β^{SA}	[-]	-	-	130	-	-	450

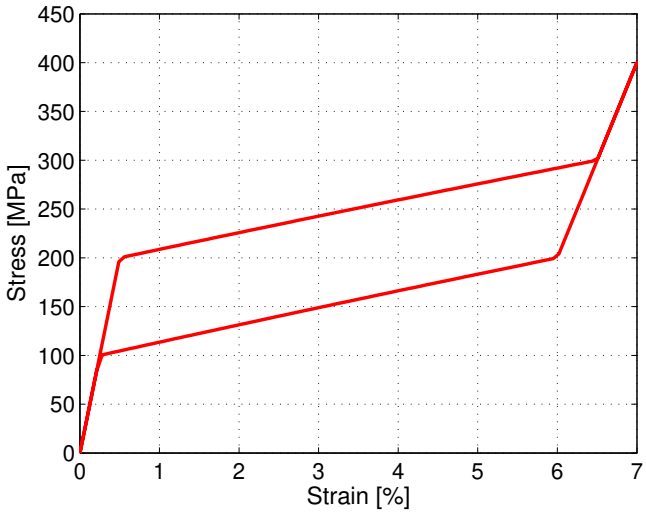

Figure 5.1. Viscous and thermo-mechanical models. Linear rules: stress-strain relationships for static loading-unloading conditions.

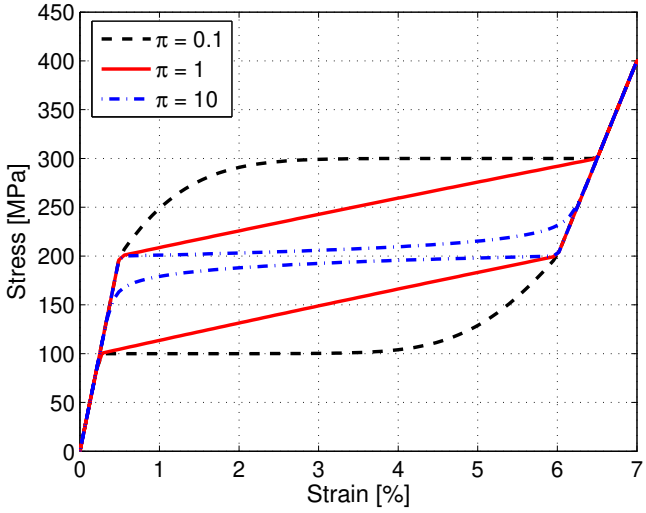

Figure 5.2. Viscous and thermo-mechanical models. Power rules: stress-strain relationships for static loading-unloading conditions.

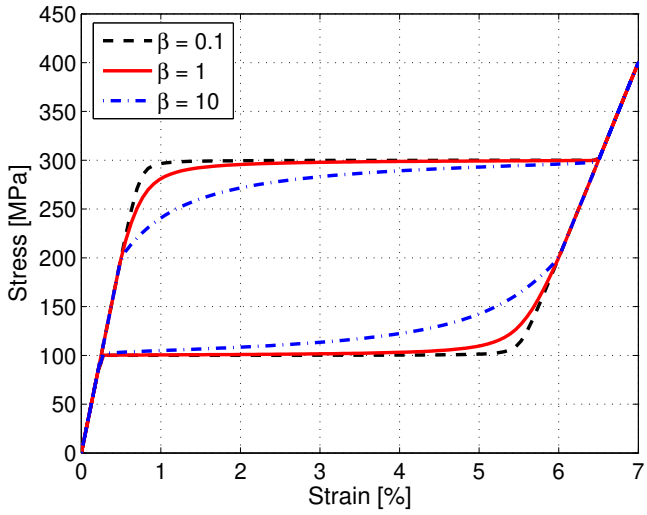

Figure 5.3. Viscous and thermo-mechanical models. Exponential rules: stress-strain relationships for static loading-unloading conditions.

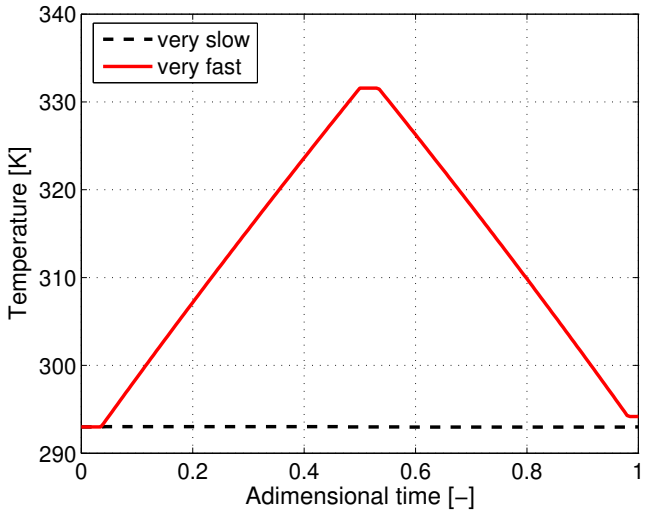

Figure 5.4. Thermo-mechanical model. Evolution of the material temperature for very slow and very fast loading-unloading conditions.

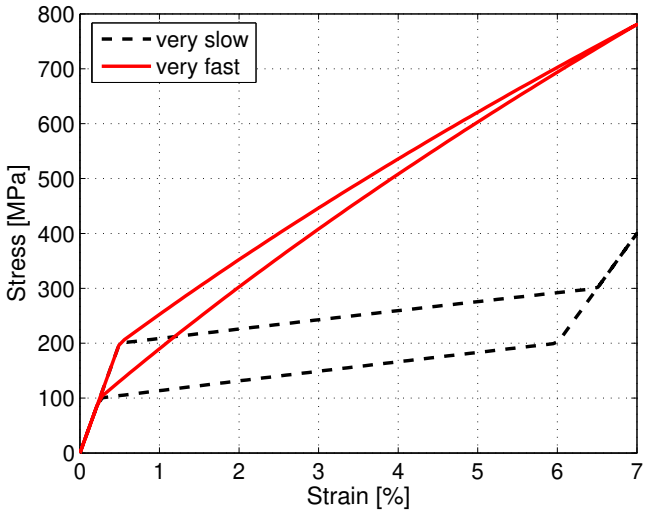

Figure 5.5. Viscous model. Linear rules: stress-strain relationship for very slow and very fast loading-unloading conditions.

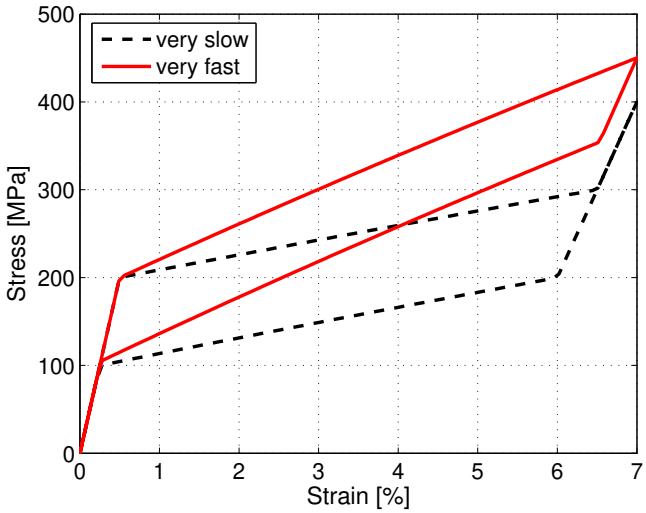

Figure 5.6. Thermo-mechanical model. Linear rules: stress-strain relationship for very slow and very fast loading-unloading conditions.

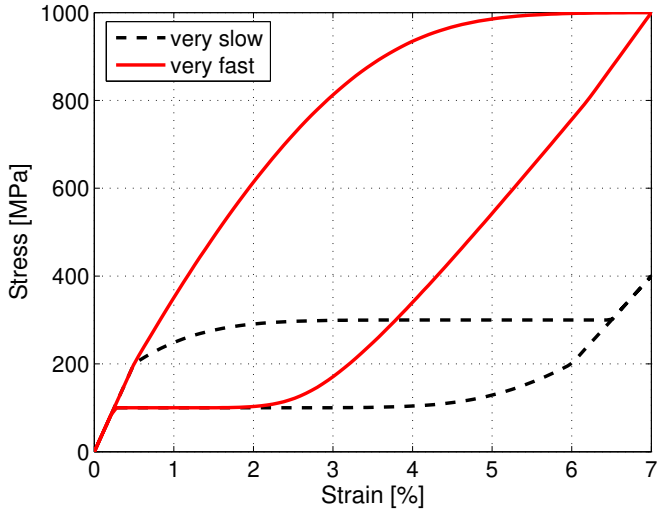

Figure 5.7. Viscous model. Power rules: stress-strain relationship for very slow and very fast loading-unloading conditions ($\pi = 0.1$).

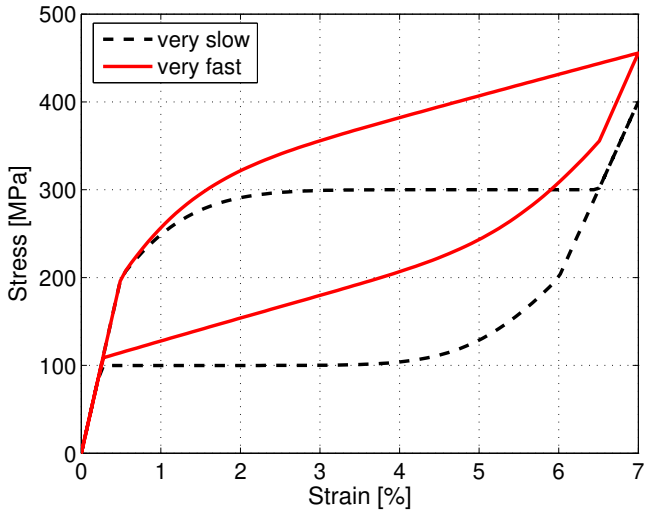

Figure 5.8. Thermo-mechanical model. Power rules: stress-strain relationship for very slow and very fast loading-unloading conditions ($\pi = 0.1$).

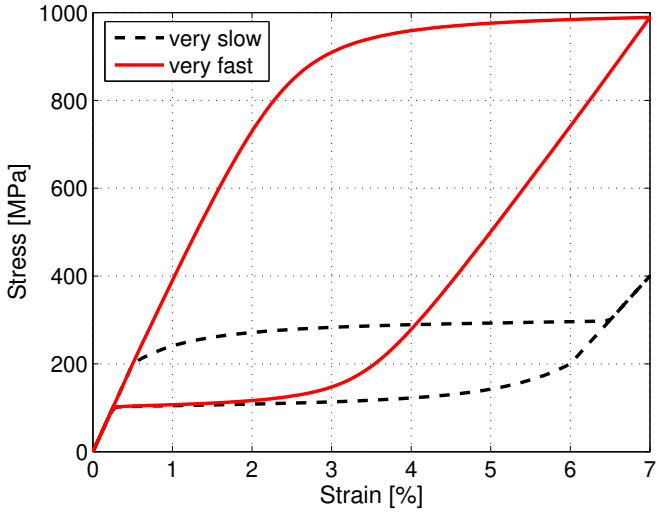

Figure 5.9. Viscous model. Exponential rules: stress-strain relationship for very slow and very fast loading-unloading conditions ($\beta = 10$).

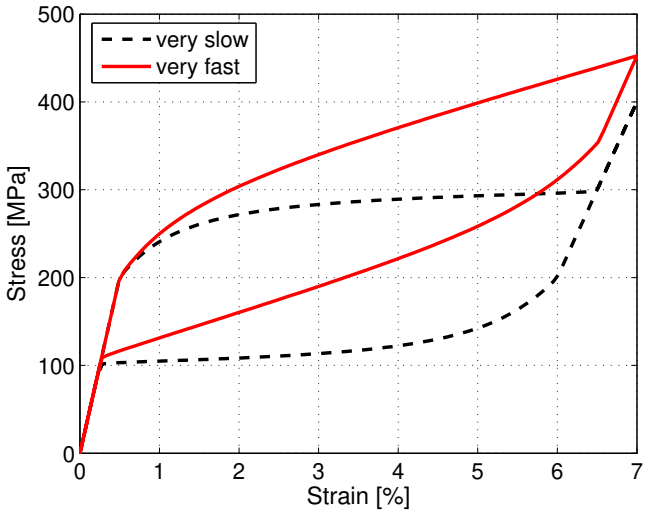

Figure 5.10. Thermo-mechanical model. Exponential rules: stress-strain relationship for very slow and very fast loading-unloading conditions ($\beta = 10$).

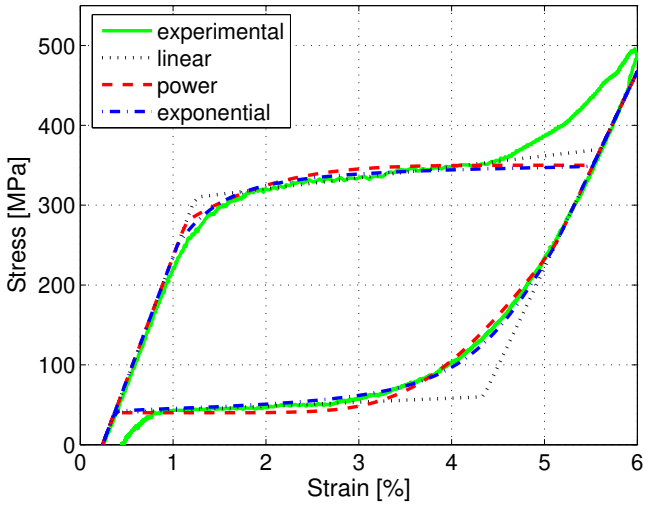

Figure 5.11. Viscous and thermo-mechanical models. Static loading conditions: experimental values (Set 1) vs. numerical results.

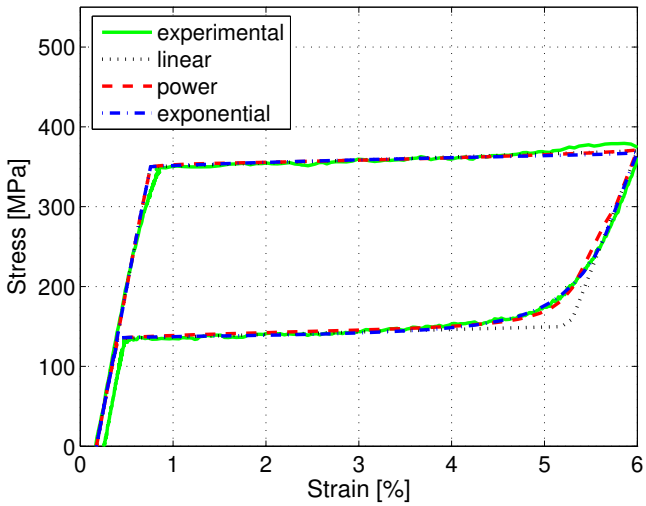

Figure 5.12. Viscous and thermo-mechanical models. Static loading conditions: experimental values (Set 2) vs. numerical results.

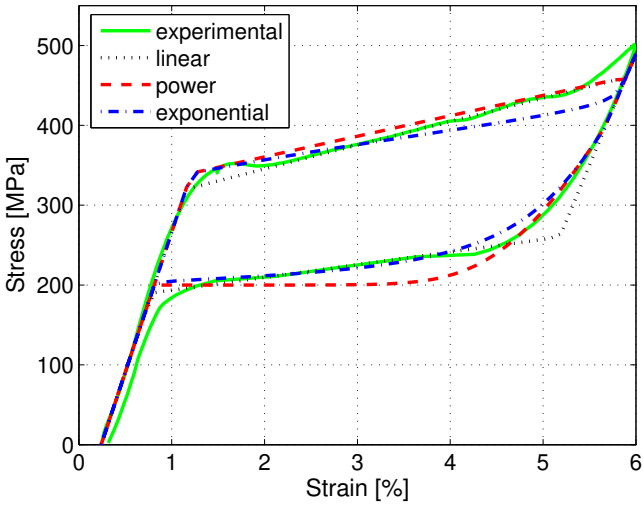

Figure 5.13. Viscous and thermo-mechanical models. Static loading conditions: experimental values (Set 3) vs. numerical results.

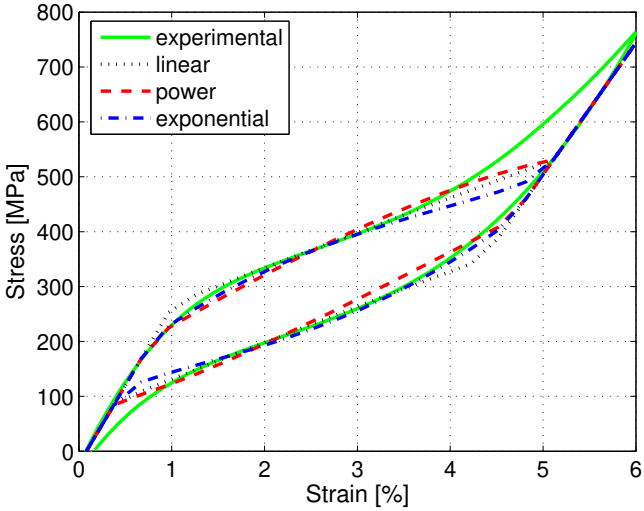

Figure 5.14. Viscous and thermo-mechanical models. Static loading conditions: experimental values (Set 4) vs. numerical results.

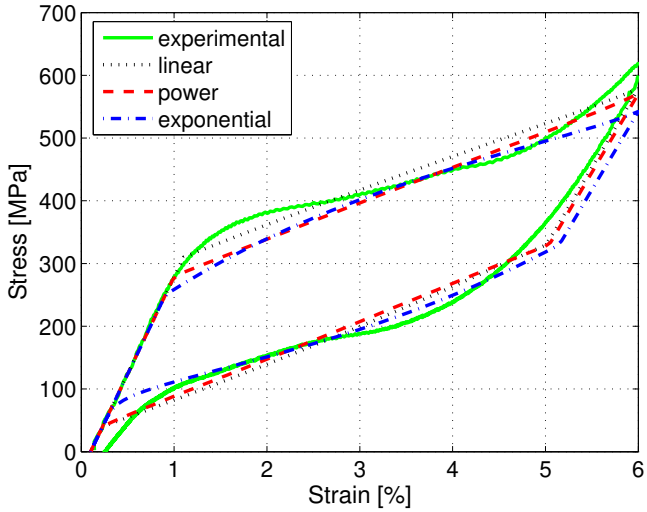

Figure 5.15. Viscous model. Dynamic loading conditions: experimental values (Set 1) vs. numerical results.

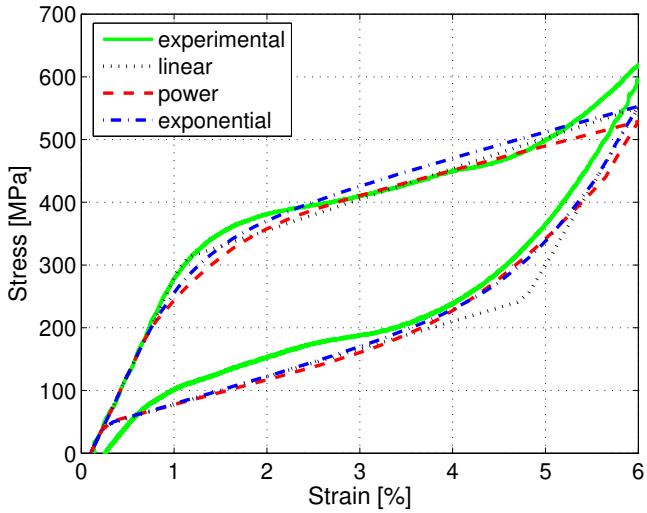

Figure 5.16. Thermo-mechanical model. Dynamic loading conditions: experimental values (Set 1) vs. numerical results.

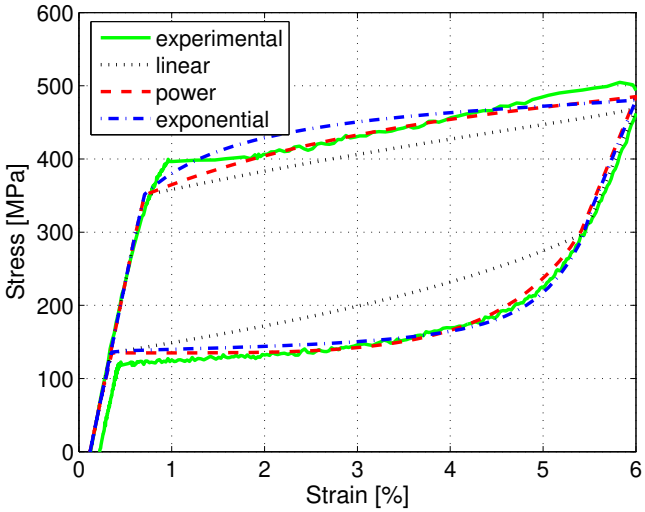

Figure 5.17. Viscous model. Dynamic loading conditions: experimental values (Set 2) vs. numerical results.

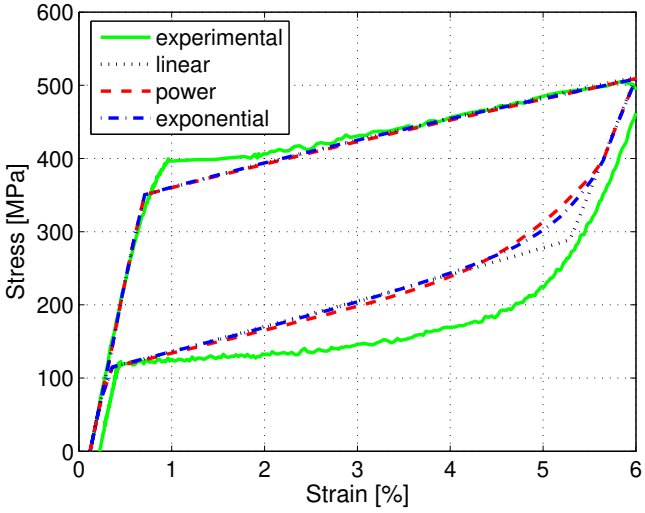

Figure 5.18. Thermo-mechanical model. Dynamic loading conditions: experimental values (Set 2) vs. numerical results.

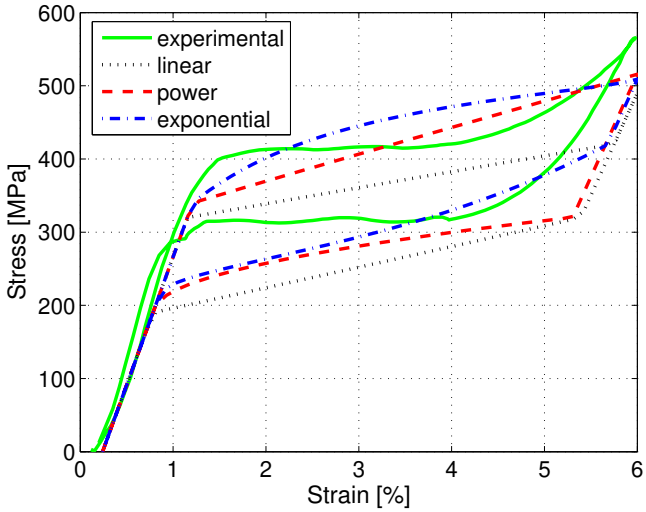

Figure 5.19. Viscous model. Dynamic loading conditions: experimental values (Set 3) vs. numerical results.

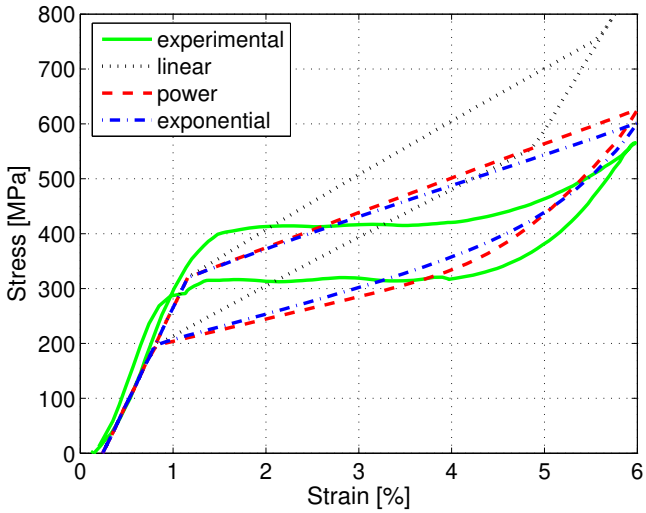

Figure 5.20. Thermo-mechanical model. Dynamic loading conditions: experimental values (Set 3) vs. numerical results.

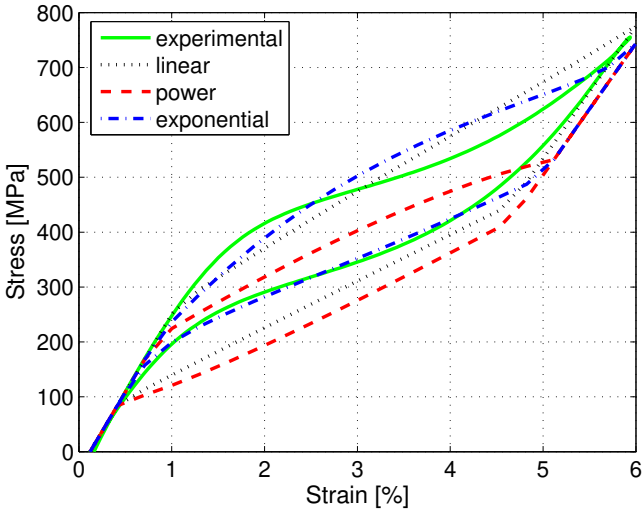

Figure 5.21. Viscous model. Dynamic loading conditions: experimental values (Set 4) vs. numerical results.

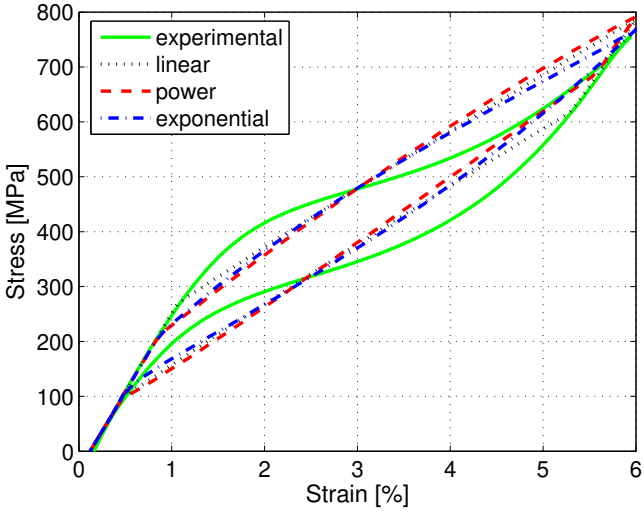

Figure 5.22. Thermo-mechanical model. Dynamic loading conditions: experimental values (Set 4) vs. numerical results.

6. SHAKE TABLE TESTS OF A REDUCED-SCALE FRAME EQUIPPED WITH SUPERELASTIC SHAPE-MEMORY ALLOY BRACES

6.1 Introduction

In this chapter, we present the preliminary results concerning the experimental investigation that considers shake-table tests of a reduced-scale frame equipped with superelastic SMA wires as bracing system. First, we focus attention on the dynamic behavior of the structure with and without braces undergoing a simulated earthquake then we provide the comparison between the experimental tests and the finite element simulations of the frame under study.

6.2 Experimental Setup

The experimental setup includes the 2-storey frame structure under study, the shake-table (457 mm by 457 mm) together with its control system (data acquisition board, power module and computer) and two accelerometers that will be mounted on the top of each floor.

The structural model (Figure 6.3) consists of 2 stories with constant storey heigth of 297 mm and a single bay of width 257 mm. The floors are made out of two plexi-glass sheets to create a rigid plan system and the columns are circular hollow brass rods of diameter 4.00 mm and thickness of 0.40 mm. A weight of approximatively 2.93 kg is placed on each floor in order to ensure the phase tranformations on the superelastic SMA braces during shaking. The structure is designed in such a way to carry superelastic wires installed in a cross-brace pattern running parallel to the direction of motion. They have been selected to have a diameter of 0.254 mm. Both the unbraced and the braced structure are tested on the shake table under the LA21 SAC earthquake (Figure 6.4).

6.3 Finite Element Model

After testing both structures (i.e. unbraced structure and braced structure), we develop a finite element model of the frames by use of OpenSEES, the software platform that was adopted for analyzing the full-scale steel structures described in Chapter 4. As a matter of fact, an analytical model possessing predictable capabilities could be useful to improve future design techniques and to reduce physical testing.

Due to the symmetry of the three-dimensional structure, only one braced bay is studied and the seismic weight is computed dividing the total floor weight by the number of braced frames in the direction of motion.

Columns and braces are modelled using *nonlinearBeamColumn* elements, while floors are simulated by using *elasticBeamColumn* elements with infinite axial stiffness in order to reproduce a rigid plan. Braces are pinned at both ends so that they can ideally carry axial loads only. P-Δ effects are taken into consideration. Also, a 5% Rayleigh damping is specified.

The uniaxial material model *steel01* is used to model the columns, while for the braces a modified version of the model for superelastic SMAs utilized in Chapter 4 is adopted. Specifically, since we do not consider the wires as being able to provide any compressive reaction, we assume zero stress in elements subjected to negative deformations.

Mechanical properties of brass, such as Young's modulus, E^{brass}, and yielding stress, σ^{brass}, as well as material parameters for the SMA model are provided in Table 6.1. They were all obtained from experimental tests performed at the Georgia Institute of Technology (Atlanta, USA) on brass and superelastic SMA specimens.

6.4 Experimental and Numerical Results

After performing the experiments and the numerical simulations, we may draw the following considerations.

- The acceleration results from the accelerometers placed on both floors show an increase in maximum acceleration (Figures 6.7 and 6.8) experienced when the SMA braces are installed, as a result of the higher stiffness associated with the braced structure as compared to the unbraced structure (Figures 6.5 and 6.6). Although the accelerations are higher for the braced structure, the damping and recentering capability of the wires tended to decrease the response at a faster rate

than the unbraced structure.

- For comparison purposes, numerical results are provided in terms of acceleration time-histories as well. As far as the unbraced structure is concerned, from Figures 6.5 and 6.6 we can observe a good prediction of the finite element study both in terms of absolute values and signal period. Furthermore, the chosen damping ratio seems to simulate with acceptable accuracy the oscillation reduction observed after the peak of the considered seismic input. When considering the braced structure, we instead notice a discrepancy between experiments and computer simulations. In particular, the finite element model overestimates the structural response, specially in the second floor of the frame.
- The model for buckling-allowed superelastic SMA elements successfully simulates the stress-strain relationship of the wires (Figures 6.9 and 6.10). As expected, large deformations occur when the braces are in compression meanwhile it reproduces the typical flag-shape exhibited by superelastic SMA materials when the braces are subjected to tensile forces.

6.5 Limitations of the Shake-Table Tests

Although the obtained results are encouraging, several are the limitations related to such an experimental study. In the following, we list and explain the points that should be taken into considerations to improve the outcomes of future investigations.

1. The connections between wires and rigid floors is very difficult to manage due to the small diameters of the SMA elements. After the tests, sliding between wires and screws was observed.
2. The position of the masses on each floor may have been slightly asymmetric. This caused a visible torsional movement during the shaking.
3. A concern comes from the measure of the brass column thickness. In particular, small differences were identified both along different section of the circumference and among the eight column elements with a consequent change of the overall stiffness of the structure.
4. Due to the small size of the braces, it was impossible to attach any strain gages for monitoring the deformation time-history of the wires during the experimental test. As a consequence, only the acceleration time-histories were recorded by means of two accelerometers.

Table 6.1. Material properties adopted for the numerical simulations.

Quantity		**Value**
E^{brass}	[MPa]	90000
E^{SMA}	[MPa]	30000
$\sigma_y^{columns}$	[MPa]	338
σ_s^{AS}	[MPa]	510
σ_f^{AS}	[MPa]	580
σ_s^{SA}	[MPa]	270
σ_f^{SA}	[MPa]	210
ϵ_L	[%]	4.10

Figure 6.1. Elevation view of the reduced-scale frame mounted on the shake table.

Figure 6.2. Close-up view of the top floor. Note the accelerometer, the steel masses and the connection between the plexi-glass sheet and the wire.

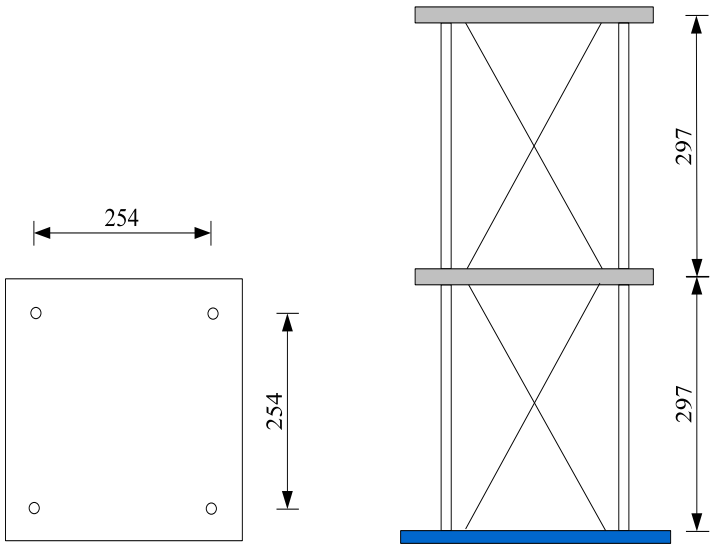

Figure 6.3. Plan and elevation view of the reduced-scale frame. Dimensions are expressed in mm.

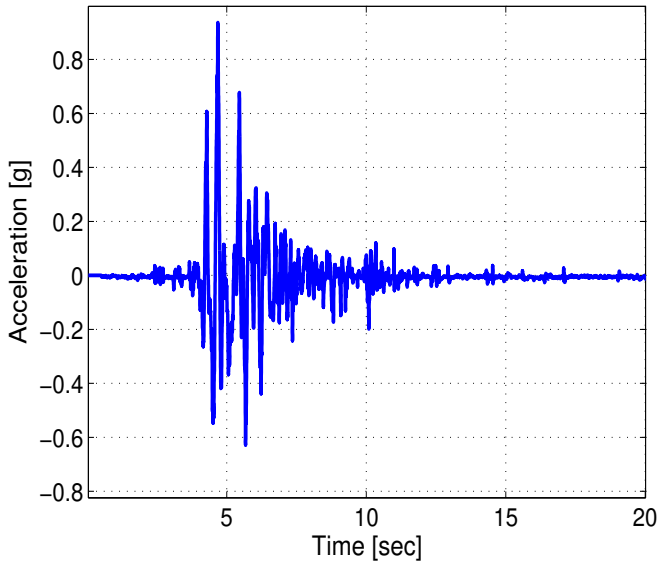

Figure 6.4. Acceleration time-history considered for the experimental investigation.

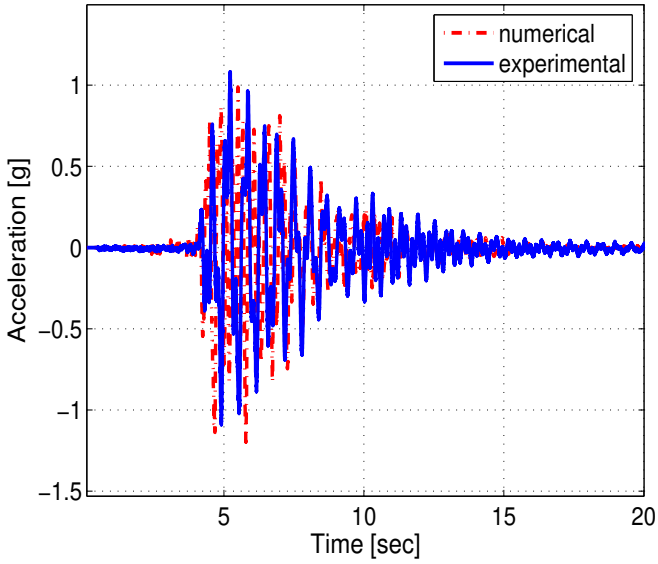

Figure 6.5. Unbraced structure. Acceleration time-history of the first floor.

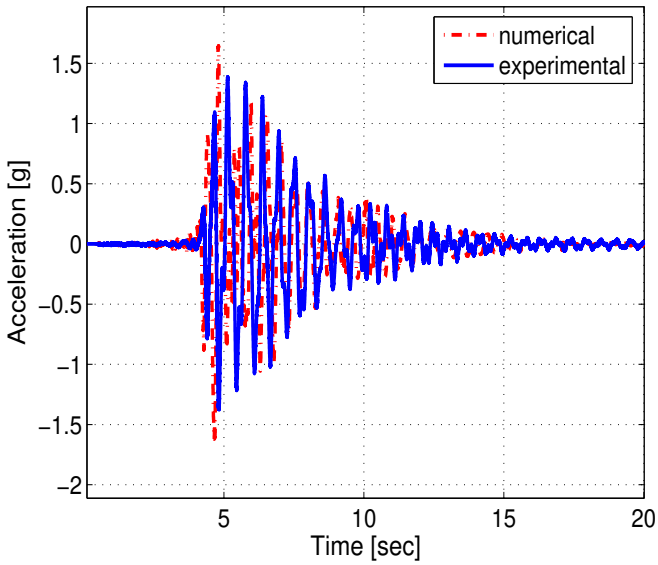

Figure 6.6. Unbraced structure. Acceleration time-history of the second floor.

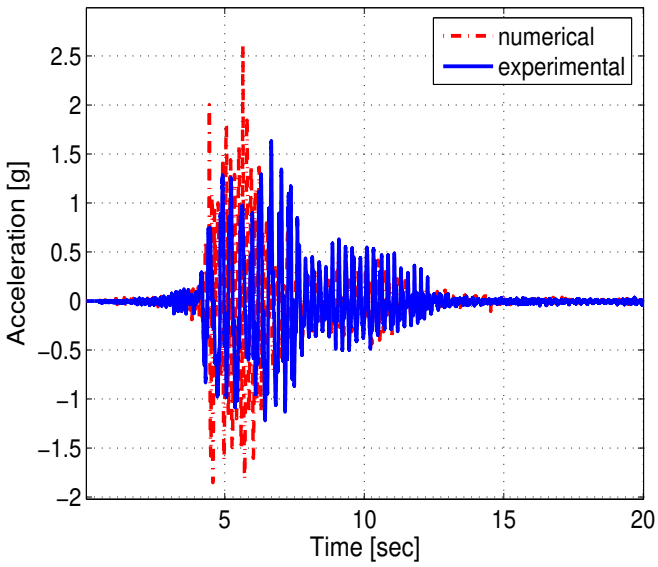

Figure 6.7. Braced structure. Acceleration time-history of the first floor.

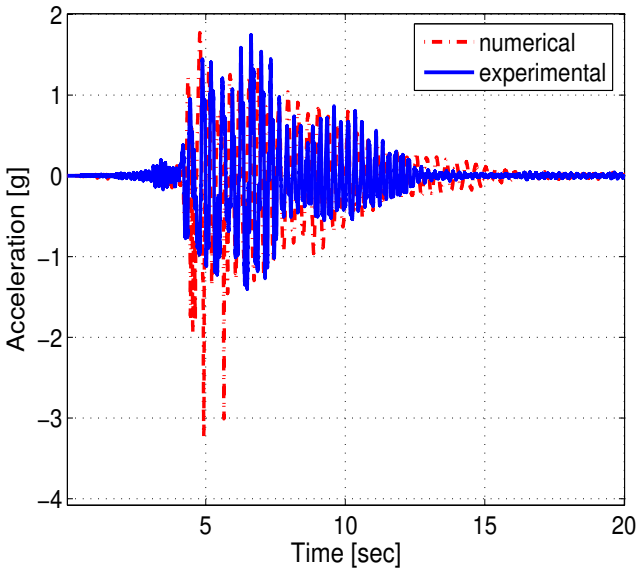

Figure 6.8. Braced structure. Acceleration time-history of the second floor.

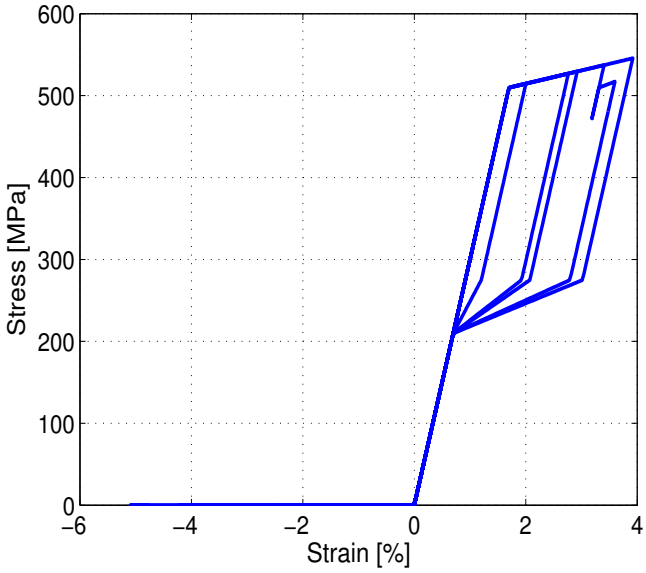

Figure 6.9. Braced structure. Numerical stress-strain relationship experienced by the lower left brace.

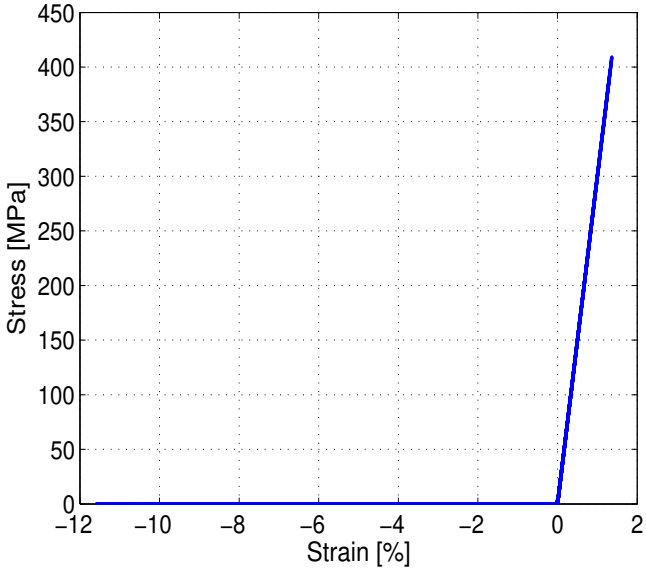

Figure 6.10. Braced structure. Numerical stress-strain relationship experienced by the upper left brace.

7. CONCLUSION AND FURTHER RESEARCH DIRECTIONS

The present dissertation evaluates the possibility of utilizing the SMA technology in earthquake engineering. In particular, the research work first investigates the structural performance of steel frames equipped with traditional and innovative bracing systems and then proposes two uniaxial constitutive equations for modelling their rate-dependent superelastic behavior. Finally, it presents an experimental investigation dealing with a reduced-scale frame tested on the shake-table.

After introducing SMA materials from a structural point of view (properties and mechanical behavior), in the first part of the thesis a state-of-the-art review on the use of SMAs for seismic applications is provided and the most promising numerical, experimental and existing applications are listed and described.

Then, structural analyses follow and the seismic performance of multi-storey steel frames equipped with either traditional steel braces or superelastic SMA braces is evaluated. A rate-independent uniaxial constitutive model for superelastic SMAs is implemented into the finite element software OpenSEES and a number of numerical simulations are carried out on a 3- and a 6-storey building. Numerical studies highlight how the proposed innovative bracing system provides better performance than the traditional one in terms of maximum interstory drift as well as residual drift.

Subsequently, two uniaxial rate-dependent constitutive models for superelastic SMAs are developed, implemented and numerically investigated. The first model includes a viscous term in the equation describing the evolution of the martensite fraction and it shows how it is bounded between two distinct rate-independent models. The second model, instead, is based on a rate-independent kinetic rule for the martensite fraction coupled with a thermal balance equation. Hence, it considers mechanical dissipation as well as latent heat and includes the temperature as a primary independent variable, which is responsible of the dynamic effects. Finally, the ability of both constitutive equations to simulate experimental data from uniaxial tests conducted at different frequency levels on

SMA wires and bars is assessed through several comparisons.

In the last part of the research work, the preliminary results of shake-table tests of a reduced-scale frame equipped with superelastic braces are presented and compared with a finite element study. Experimental results show the effectiveness in using superelastic SMA wires as new bracing system and the acceleration time-histories recorded by two accelerometers mounted on the frame are shown together with the numerical prediction. Finally, a critical discussion of the results highlights the limitations that emerge from such an investigation and provides advice for its improvement.

Different can be the directions that may be pursued for further research in the field:

- analysis of different braced structures such as frames with zippers,
- analysis of reinforced-concrete structures endowed with superelastic SMA braces,
- analysis of the considered frames using of a rate-dependent constitutive equation for the modelling of superelastic SMA braces,
- analysis of structures isolated by SMA-based devices.

All the proposed developments should be followed by an extensive experimental campaign aimed at evaluating both the feasibility of such innovative devices and the validation of the adopted numerical tools.

REFERENCES

Adachi, Y. and Unjoh, S. [1999] "Development of shape memory alloy damper for intelligent bridge systems," *SPIE Conference on Smart Systems for Bridges, Structures, and Highways*, pp. 31–42.

Andrawes, B., McCormick, J., and DesRoches, R. [2004] "Effect of cycling modeling parameters on the behavior of shape memory alloys for seismic applications," *SPIE Conference on Smart Structures and Materials*.

Auricchio, F. [1995] "Shape memory alloys: applications, micromechanics, macromodeling and numerical simulations," Ph.D. thesis, Department of Civil and Environmental Engineering, University of California at Berkeley.

Auricchio, F. and Sacco, E. [1997] "A one-dimensional model for superelastic shape-memory alloys with different elastic properties between austenite and martensite," *International Journal of Non-Linear Mechanics*, Vol. 32, pp. 1101–1114.

Auricchio, F. and Sacco, E. [1999] "Modelling of the rate-dependent superelastic behavior of shape-memory alloys," *ECCM '99, European Conference on Computational Mechanics, August 31-September 3, Munchen, Germany*.

Auricchio, F. and Sacco, E. [2001] "Thermo-mechanical modelling of a superelastic shape-memory wire under cyclic stretching-bending loadings," *International Journal of Solids and Structures*, Vol. 38, pp. 6123–6145.

Baratta, A. and Corbi, O. [2002] "On the dynamic behaviour of elastic-plastic structures equipped with pseudoelastic SMA reinforcements," *Computational Materials Science*, Vol. 25, pp. 1–13.

Barns, C. [2003] "Shape Memory and Superelastic Alloys. http://www.copper.org," web page.

Bernardini, D. and Brancaleoni, F. [1999] "Shape memory alloys modelling for seismic applications," *Atti del MANSIDE Project - Final Workshop - Memory Alloys for Seismic Isolation and Energy Dissipation Devices*, pp. 73–84, part II.

Bruno, S. and Valente, C. [2002] "Comparative response analysis of conventional and innovative seismic protection strategies," *Earthquake Engineering and Structural Dynamics*, Vol. 31, pp. 1067–1092.

Cardone, D., Dolce, M., Bixio, A., and Nigro, D. [1999] "Experimental tests on SMA elements," *Atti del MANSIDE Project - Final Workshop - Memory Alloys for Seismic Isolation and Energy Dissipation Devices*, pp. 85–104, part II.

Castellano, M. G. [2000] "Shaking table tests of masonry facade walls with and SMADs," *Proceedings of the Final Workshop of ISTECH Project - Shape Memory Alloy Devices for Seismic Protection of Cultural Heritage Structures*, pp. 99–109.

Clark, P. W., Aiken, I. D., and Kelly, J. M. [1995] "Experimental and analytical studies of shape memory alloy dampers for structural control," *Proceedings of Passive Damping*, Vol. 2445, pp. 241–251.

Corbi, O. [2003] "Shape memory alloys and their application in structural oscillations attenuation," *Simulation Modelling Practice and Theory*, Vol. 11, pp. 387–402.

Croci, G., Bonci, A., and Viskovic, A. [2000] "Use of shape memory alloy devices in the basilica of St Francis of Assisi," *Proceedings of the Final Workshop of ISTECH Project - Shape Memory Alloy Devices for Seismic Protection of Cultural Heritage Structures*, pp. 110–133.

DesRoches, R. [1999] "Seismic mitigations of bridges using smart restrainers," *SPIE Conference on Smart Systems for Bridges, Structures, and Highways*, pp. 11–20.

DesRoches, R. and Delemont, M. [2003] "Seismic retrofit of simply supported bridges using shape memory alloys," *Engineering Structures*, Vol. 24, pp. 325–332.

DesRoches, R., McCormick, J., and Delemont, M. [2004] "Cyclic properties of superelastic shape memory alloy wires and bars," *Journal of Structural Engineering*, Vol. 130, pp. 38–46.

DesRoches, R. and Smith, B. [2004] "Shape memory alloys in seismic resistant design and retrofit: a critical review of the state of the art, potential and limitations," *Journal of Earthquake Engineering*, Vol. 8, pp. 415–429.

Dolce, M. and Cardone, D. [2001a] "Mechanical behaviour of shape memory alloys for seismic applications 1. Martensite and austenite bars subjected to torsion," *International Journal of Mechanical Sciences*, Vol. 43, pp. 2631–2656.

Dolce, M. and Cardone, D. [2001b] "Mechanical behaviour of shape memory alloys for seismic applications 2. Austenite NiTi wires subjected to tension," *International Journal of Mechanical Sciences*, Vol. 43, pp. 2657–2677.

Dolce, M., Cardone, D., and Marnetto, R. [2000] "Implementation and testing of passive control devices based on shape memory alloys," *Earthquake Engineering and Structural Dynamics*, Vol. 29, pp. 945–968.

Dolce, M., Cardone, D., Ponzo, F. C., and Valente, C. [2005] "Shaking table tests on reinforced concrete frames without and with passive control systems," *Earthquake Engineering and Structural Dynamics (in press).*

Dolce, M., Nicoletti, M., and Ponzo, F. C. [2001] "Protezione sismica con dispositivi basate sulle leghe a memoria di forma: il progetto MANSIDE e gli ulteriori sviluppi," *Ingegneria Sismica*, Vol. 1, pp. 66–78.

Duerig, T., Melton, K., Stockel, D., and Wayman, C. [1990] *Engineering aspects of shape memory alloys*, Butterworth-Heinemann, London.

Feng, Z. C. and Li, D. Z. [1996] "Dynamics of a mechanical system with a shape memory alloy bar," *Journal of Intelligent Material Systems and Structures*, Vol. 7, pp. 399–410.

Fugazza, D. [2003] "Shape-memory alloy devices in earthquake engineering: mechanical properties, constitutive modelling and numerical simulations," Master's thesis, European School of Advanced Studies in Reduction of Seismic Risk (ROSE School).

Fugazza, D. [2005] "Experimental investigation on the cyclic behavior of superelastic NiTi shape-memory alloy wires and bars," *Individual study submitted to the European School for Advanced Studies in Reduction of Seismic Risk (ROSE School) in partial fulfilment of the requirements for the Doctor of Philosophy degree in Earthquake Engineering.*

Graesser, E. J. and Cozzarelli, F. A. [1991] "Shape-memory alloys as new materials for aseismic isolation," *Journal of Engineering Mechanics*, Vol. 117, pp. 2590–2608.

Han, Y.-L., Li, Q. S., Li, A.-Q., Leung, A. Y. Y., and Lin, P.-H. [2003] "Structural vibration control by shape memory alloy damper," *Earthquake Engineering and Structural Dynamics*, Vol. 32, pp. 483–494.

Humbeeck, J. V. [1999a] "General aspects of shape memory alloys," *Atti del MANSIDE Project - Final Workshop - Memory Alloys for Seismic Isolation and Energy Dissipation Devices*, pp. 9–44, part II.

Humbeeck, J. V. [1999b] "Non-medical applications of shape memory alloys," *Materials Science and Engineering*, pp. 134–148, A273–275.

Ikeda, T., Nae, F. A., Naito, H., and Matsuzaki, Y. [2004] "Constitutive model of shape memory alloys for unidirectional loading considering inner hysteresis loops," *Smart Materials and Structures*, Vol. 13, pp. 916–925.

Indirli, M. [2000] "The demo-intervention of the ISTECH Project: the bell tower of S. giorgio in Trignano (Italy)," *Proceedings of the Final Workshop of ISTECH Project - Shape Memory Alloy Devices for Seismic Protection of Cultural Heritage Structures*, pp. 134–146.

Indirli, M., Carpani, B., Martelli, A., Castellano, M. G., Infanti, S., Croci, G., Biritognolo, M., Bonci, A., Viskovic, A., and Viani, S. [2000] "Experimental tests on masonry structures provided with shape memory alloy antiseismic devices," *12th World Conference in Earthquake Engineering*, pp. 1–8.

Johnson Matthey [2005] "http://www.jmmedical.com," web page.

Krumme, R., Hayes, J., and Sweeney, S. [1995] "Structural damping with shape-memory alloys: one class of devices," *Proceedings of Passive Damping*, Vol. 2445, pp. 225–240.

Lemaitre, J. and Chaboche, J. [1990] *Mechanics of solid materials*, Cambridge University Press, Cambridge, MA, USA.

Lim, T. J. and McDowell, D. L. [1995] "Path dependence of shape memory alloys during cyclic loading," *Journal of Intelligent Material Systems and Structures*, Vol. 6, pp. 817–830.

Mazzolani, F. M. and Mandara, A. [2002] "Modern trends in the use of special metals for the improvement of historical and monumental structures," *Engineering Structures*, Vol. 24, pp. 843–856.

Mazzoni, S., McKenna, F., Scott, M., Fenves, G. L., and Jeremic, B. [2003] *Open System for Earthquake Engineering Simulations (OpenSEES) - Command Language Manual.*

Memory-Metalle GmbH [2005] "http://www.memory-metalle.de," web page.

Memry Corporation [2005] "http://www.memry.com," web page.

Moroni, M. O., Saldivia, R., Sarrazin, M., and Sepulveda, A. [2002] "Damping characteristics of a CuZnAlNi shape memory alloy," *Materials Science and Engineering*, pp. 313–319, A335.

Nitinol Devices & Components (NDC) [2005] "http://www.nitinol.com," web page.

Ocel, J., DesRoches, R., Leon, R. T., Hess, W. G., Krumme, R., Hayes, J. R., and Sweeney, S. [2004] "Steel beam-column connections using shape memory alloys," *Journal of Structural Engineering*, Vol. 130, pp. 732–740.

Piedboeuf, M. C., Gauvin, R., and Thomas, M. [1998] "Damping behaviour of shape memory alloys: strain amplitude, frequency and temperature effects," *Journal of Sound and Vibration*, Vol. 214, pp. 885–901.

Prahlad, H. and Chopra, I. [2001] "Comparative evaluation of shape memory alloy constitutive models with experimental data," *Journal of Intelligent Material Systems and Structures*, Vol. 12, pp. 1773–395.

Prahlad, H. and Chopra, I. [2003] "Development of a strain-rate dependent model for uniaxial loading of SMA wires," *Journal of Intelligent Material Systems and Structures*, Vol. 14, pp. 429–442.

Sabelli, R. [2001] "Research on improving the design and analysis of earthquake-resistant steel-braced frames," *The 2000 NEHRP Professional Fellowship Report.*

Sabelli, R., Mahin, S., and Chang, C. [2003] "Seismic demands on steel braced frame buildings with buckling-restrained braces," *Engineering Structures*, Vol. 25, pp. 655–666.

Sadat, S., Salichs, J., Noori, M., Hou, Z., Davoodi, H., Bar-on, I., Suzuki, Y., and Masuda, A. [2002] "An overview of vibration and seismic applications of NiTi shape memory alloy," *Smart Materials and Structures*, Vol. 11, pp. 218–229.

Seelecke, S., Heintze, O., and Masuda, A. [2002] "Simulation of earthquake-induced structural vibrations in systems with SMA damping elements," *SPIE Conference on Smart Structures and Materials.*

Shape Memory Applications Inc. [2005] "http://www.sma-inc.com," web page.

Special Metals Corporation [2005] "http://www.specialmetals.com," web page.

Strnadel, B., Ohashi, S., Ohtsuka, H., Ishihara, T., and Miyazaki, S. [1995] "Cyclic stress-strain characteristics of Ti-Ni and Ti-Ni-Cu shape memory alloys," *Materials Science and Engineering*, Vol. 202, pp. 148–156.

Tamai, H. and Kitagawa, Y. [2002] "Pseudoelastic behavior of shape memory alloy wire and its application to seismic resistance member for building," *Computational Materials Science*, Vol. 25, pp. 218–227.

Tobushi, H., Shimeno, Y., Hachisuka, T., and Tanaka, K. [1998] "Influence of strain rate on superelastic properties of TiNi shape memory alloy," *Mechanics of Materials*, Vol. 30, pp. 141–150.

Valente, C., Cardone, D., Lamonaca, B. G., and Ponzo, F. M. [1999] "Shaking table tests of structures with conventional and sma based protection devices," *Atti del MANSIDE Project - Final Workshop - Memory Alloys for Seismic Isolation and Energy Dissipation Devices*, pp. 177–194, part II.

Wilde, K., Gardoni, P., and Fujino, Y. [2000] "Base isolation system with shape memory alloy device for elevated highway bridges," *Engineering Structures*, Vol. 22, pp. 222–229.

Wilson, J. and Wesolowsky, M. [2005] "Shape memory alloys for seismic response modification: a state-of-the-art review," *Earthquake Spectra*, Vol. 21, pp. 569–601.

Wolons, D., Gandhi, F., and Malovrh, B. [1998] "Experimental investigation of the pseudoelastic hysteresis damping characteristics of shape memory alloy wires," *Journal of Intelligent Material Systems and Structures*, Vol. 9, pp. 116–126.

A. EARTHQUAKE RECORDS

Table A.1. Ground motion characteristics.

SAC name	Points	dt [sec]	Duration [sec]	PGA [g]
LA01	2674	0.02	53.46	0.461
LA02	2674	0.02	53.46	0.676
LA03	3939	0.01	39.38	0.394
LA04	3939	0.01	39.38	0.488
LA05	3909	0.01	39.08	0.301
LA06	3909	0.01	39.08	0.235
LA07	4000	0.02	79.08	0.421
LA08	4000	0.02	79.08	0.426
LA09	4000	0.02	79.08	0.520
LA10	4000	0.02	79.08	0.360
LA11	2000	0.02	39.98	0.665
LA12	2000	0.02	39.98	0.969
LA13	3000	0.02	59.98	0.678
LA14	3000	0.02	59.98	0.657
LA15	2990	0.005	14.945	0.533
LA16	2990	0.005	14.945	0.580
LA17	3000	0.02	59.98	0.569
LA18	3000	0.02	59.98	0.817
LA19	3000	0.02	59.98	1.019
LA20	3000	0.02	59.98	0.986

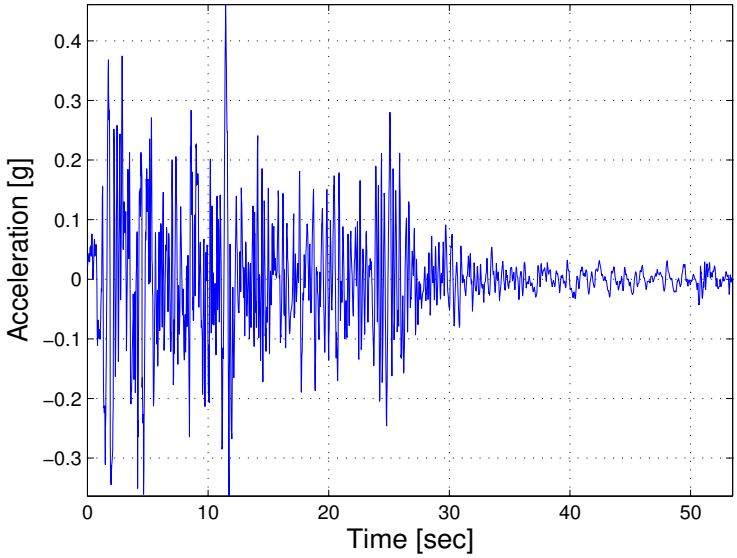

Figure A.1. Ground motion LA01.

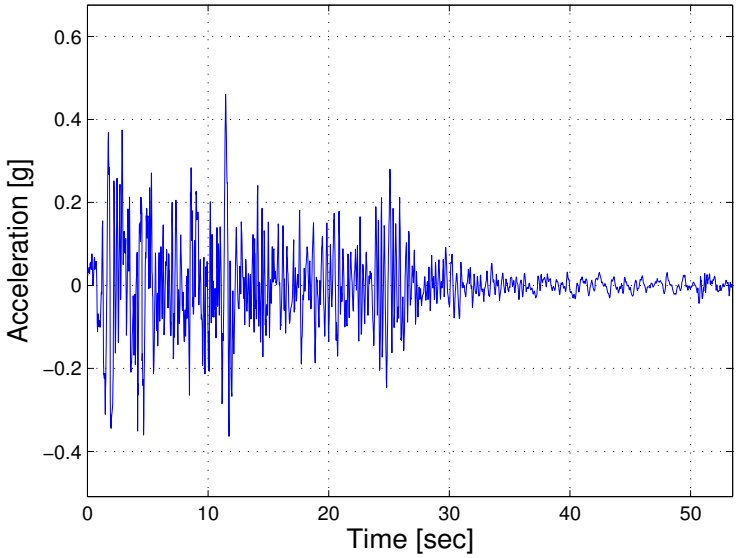

Figure A.2. Ground motion LA02.

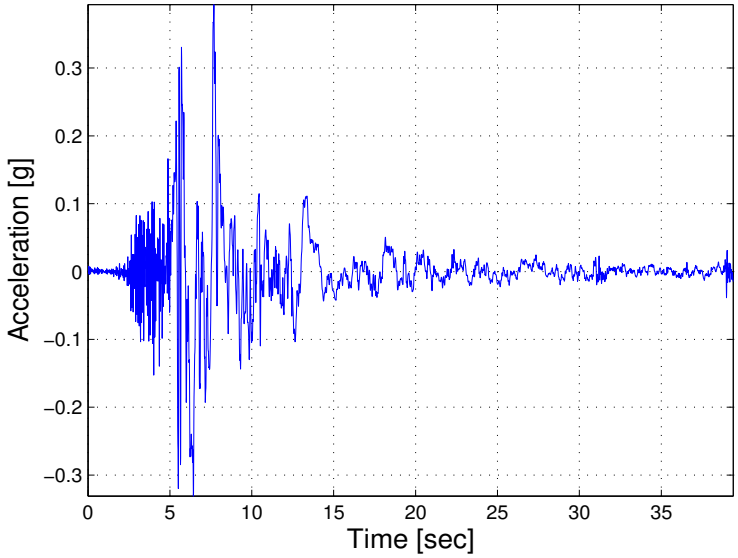

Figure A.3. Ground motion LA03.

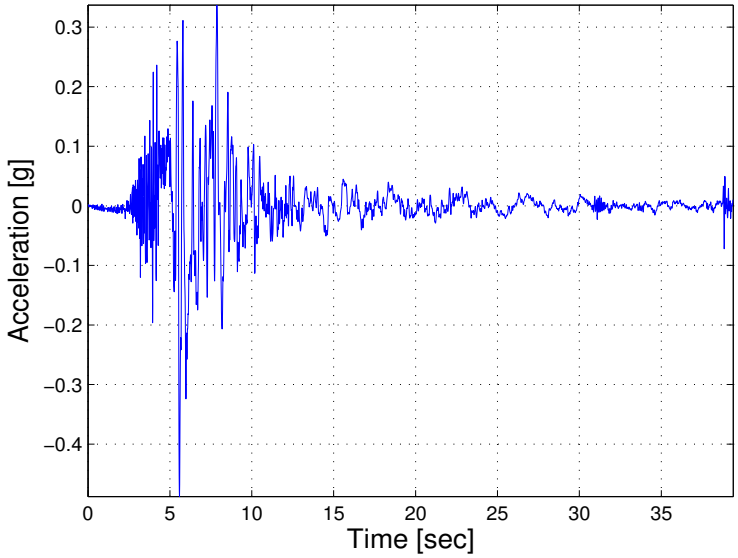

Figure A.4. Ground motion LA04.

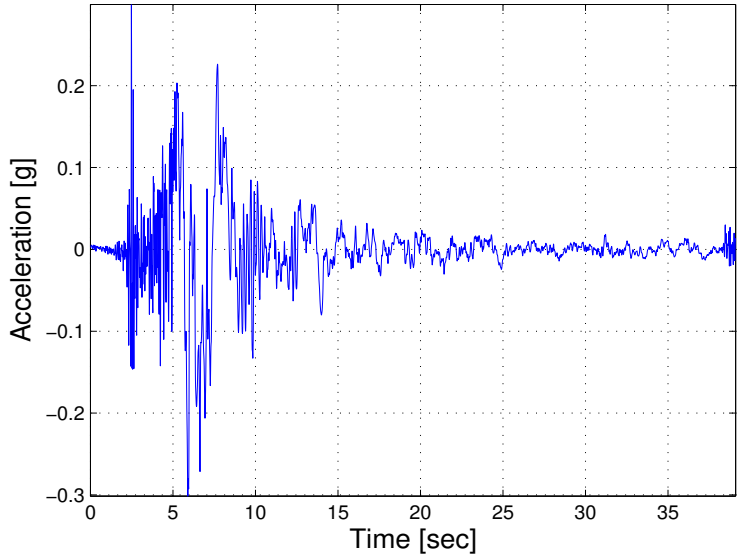

Figure A.5. Ground motion LA05.

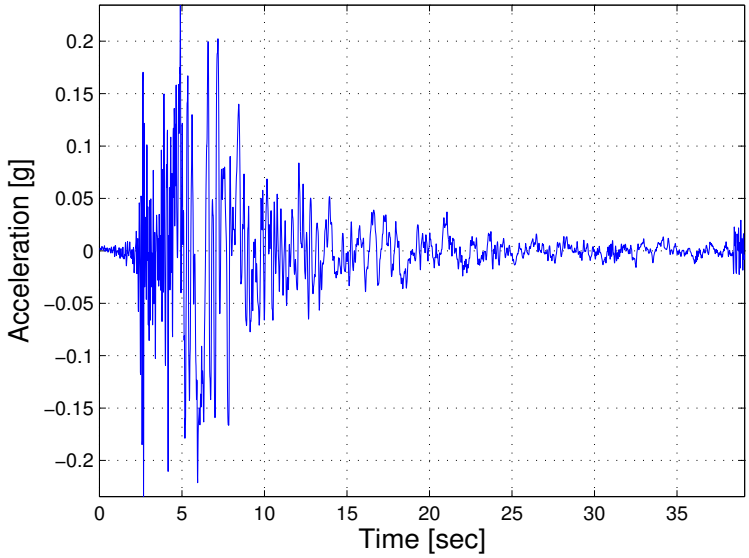

Figure A.6. Ground motion LA06.

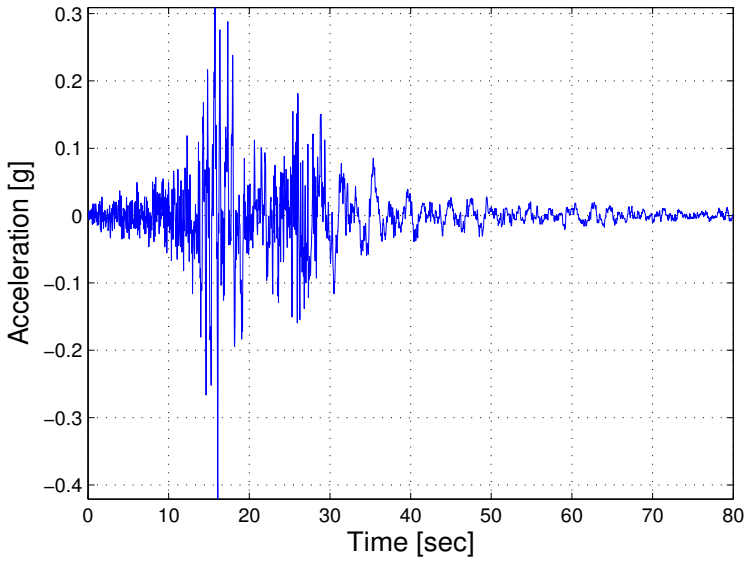

Figure A.7. Ground motion LA07.

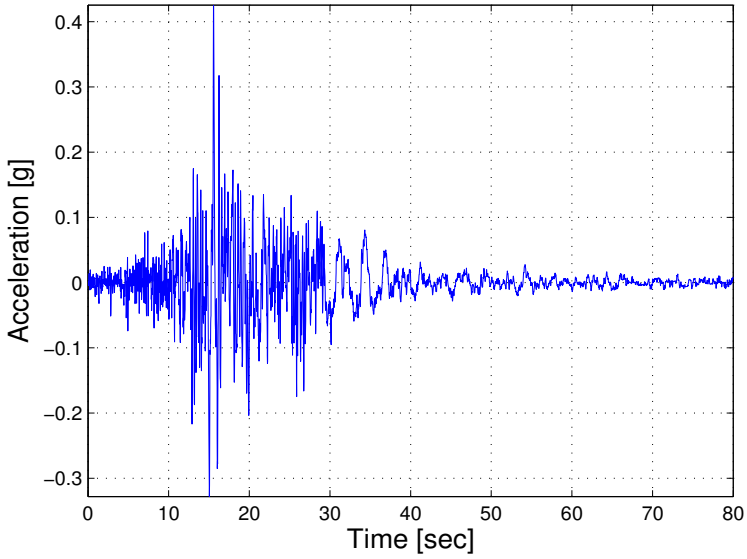

Figure A.8. Ground motion LA08.

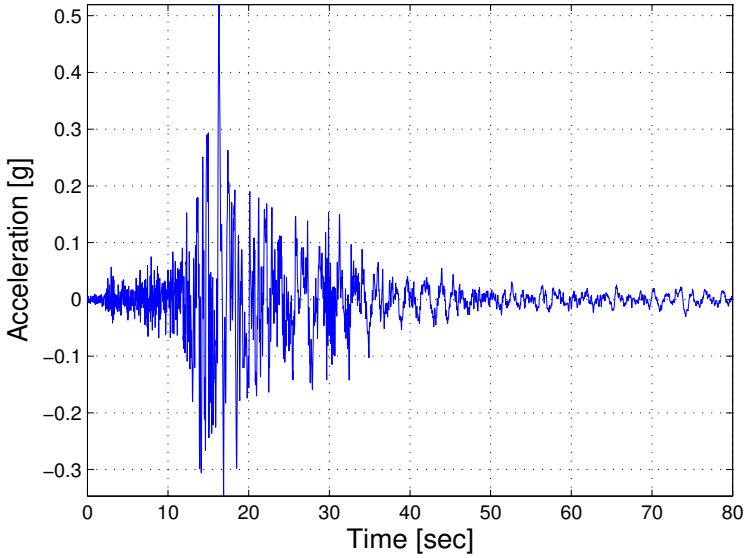

Figure A.9. Ground motion LA09.

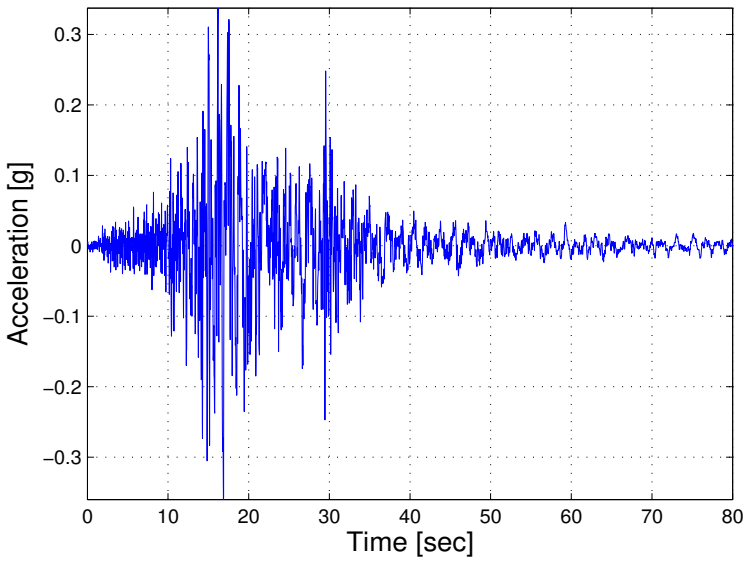

Figure A.10. Ground motion LA10.

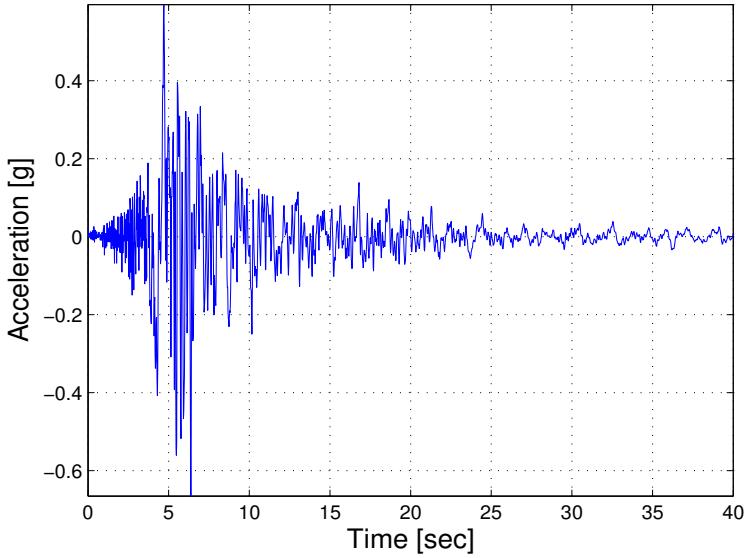

Figure A.11. Ground motion LA11.

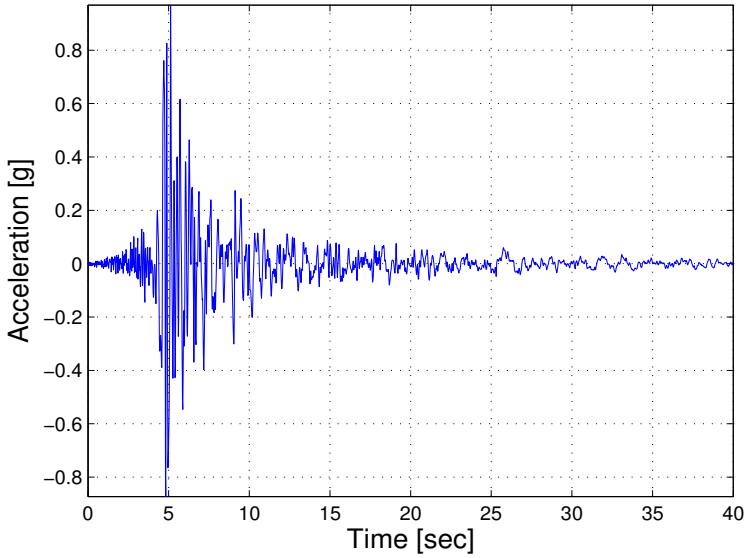

Figure A.12. Ground motion LA12.

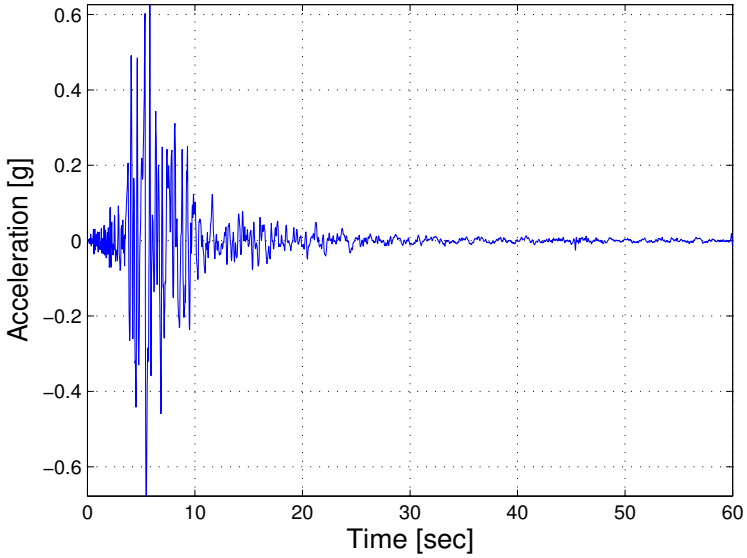

Figure A.13. Ground motion LA13.

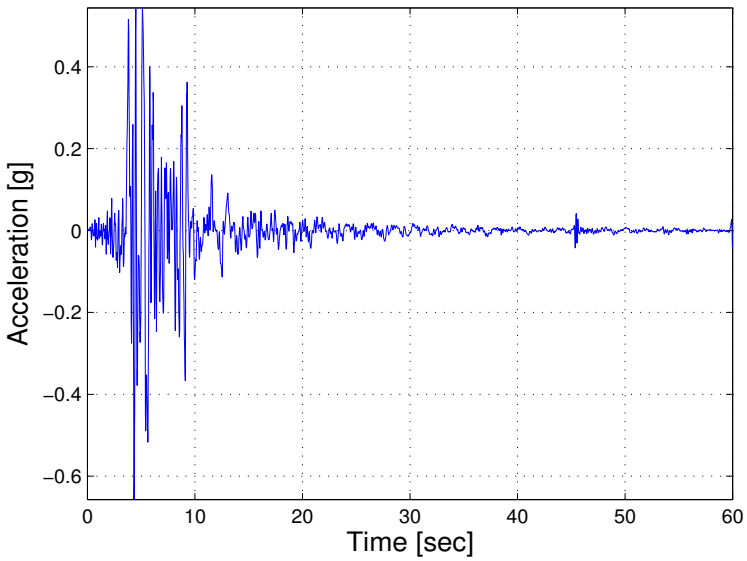

Figure A.14. Ground motion LA14.

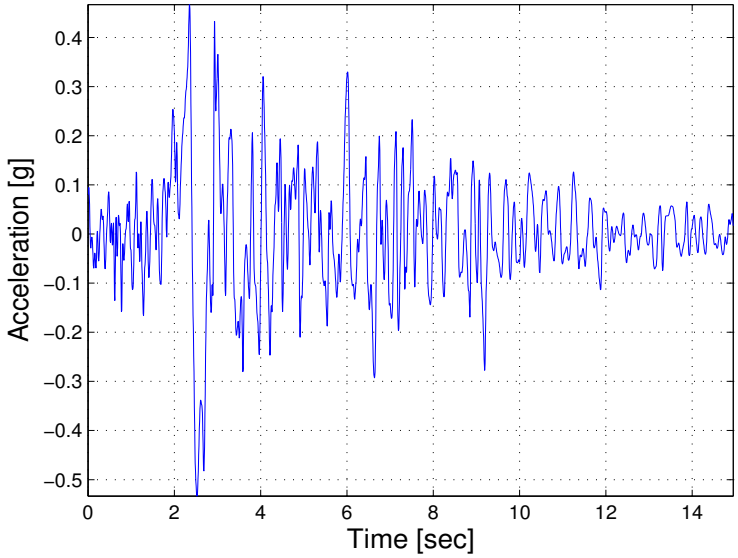

Figure A.15. Ground motion LA15.

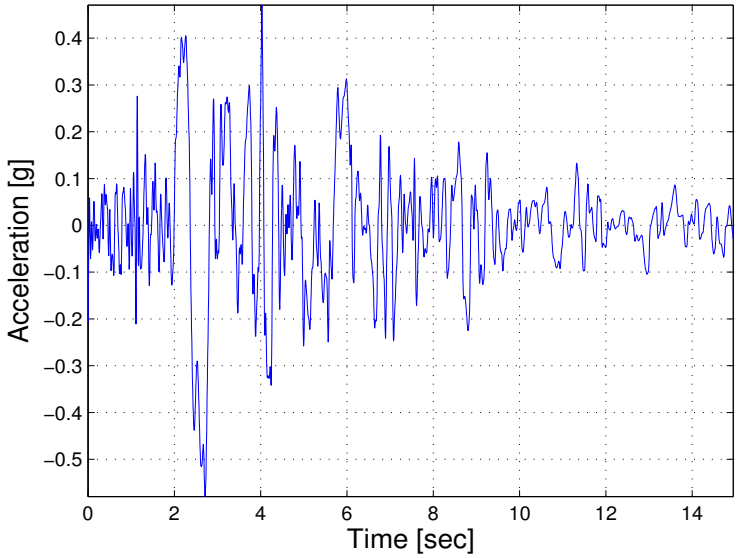

Figure A.16. Ground motion LA16.

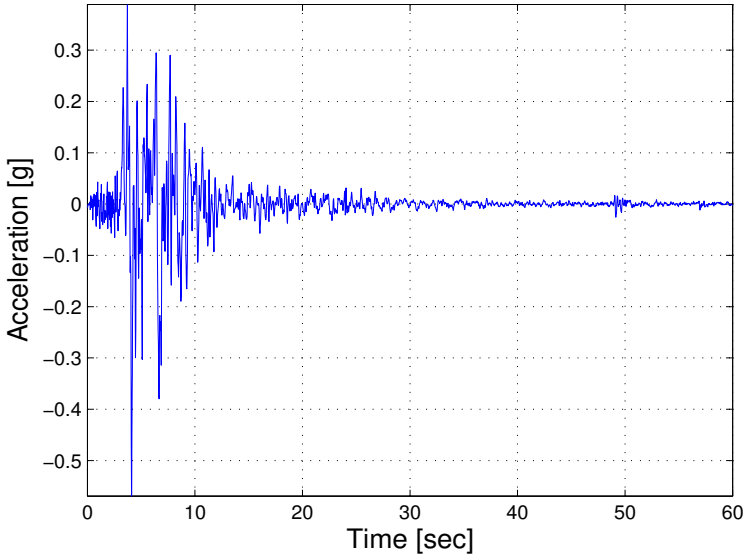

Figure A.17. Ground motion LA17.

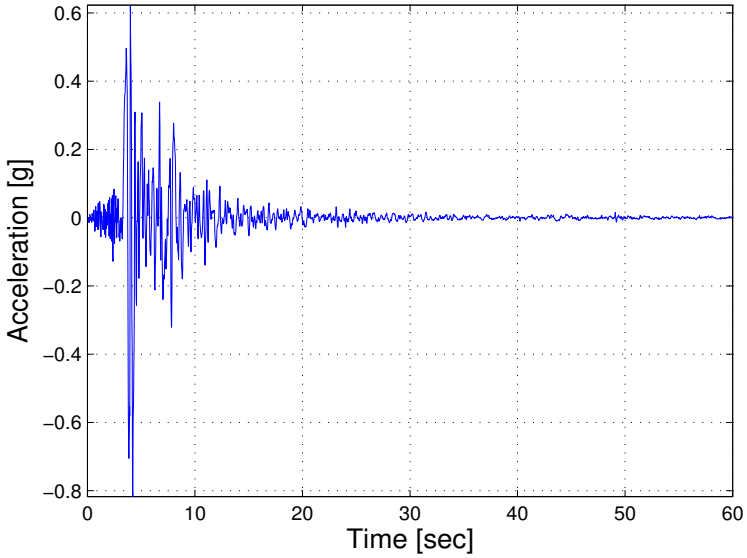

Figure A.18. Ground motion LA18.

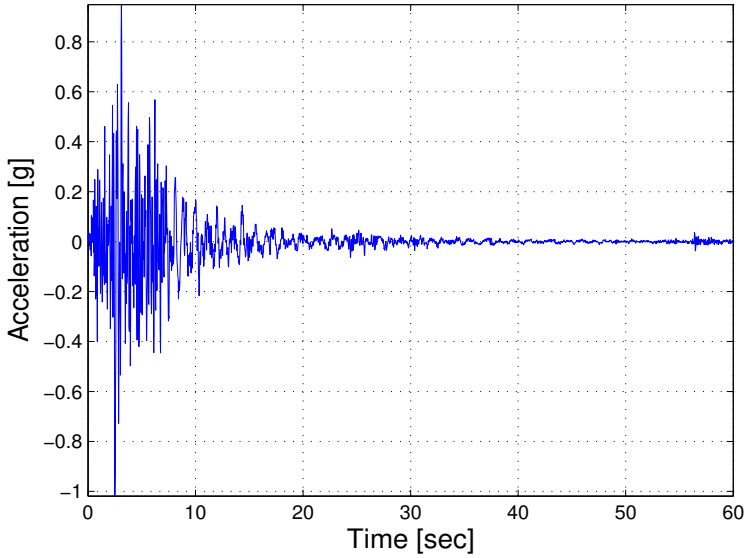

Figure A.19. Ground motion LA19.

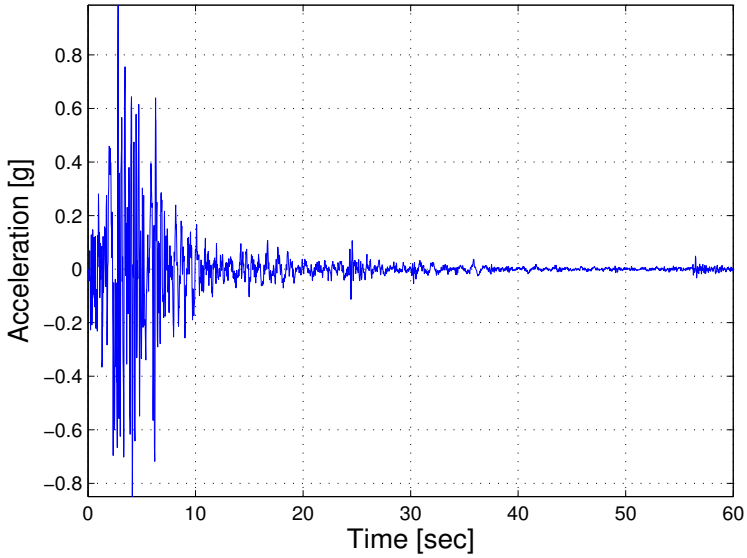

Figure A.20. Ground motion LA20.

B. CONSISTENT TANGENTS OF THE CONSTITUTIVE MODELS

B.1 Introduction

In this Appendix, we focus on the construction of the tangent moduli consistent with the time-discrete constitutive models developed in Chapter 5. The use of a consistent tangent preserves the quadratic convergence of the Newton-Raphson scheme adopted for solving the time-discrete evolutionary equations via iterative strategy.

B.2 Viscous Model

As far as the viscous model is concerned, we only need to compute the derivatives of the evolutionary equations written in residual form with respect to both the static and dynamic martensite fraction. In the following, each pair of equations refer to the linear, power and exponential rules respectively.

Conversion from austenite into martensite

$$\begin{aligned}
\frac{\partial \mathcal{R}_{ST}^{AS}}{\partial \xi_{ST}} &= (1-\xi_{ST,n})\,\frac{\partial|\sigma_{ST}|}{\partial \xi_{ST}} + (|\sigma_{ST,n}| - \sigma_{f,ST}^{AS}) \\
\frac{\partial \mathcal{R}^{AS}}{\partial \xi} &= (1-\xi_n)\,\frac{\partial|\sigma|}{\partial \xi} + \frac{\Delta t}{\tau}\,(\xi-\xi_{ST})\,\frac{\partial|\sigma|}{\partial \xi} + \frac{\Delta t}{\tau}\,(|\sigma| - \sigma_f^{AS}) + (|\sigma_n| - \sigma_f^{AS})
\end{aligned}$$

$$\begin{aligned}
\frac{\partial \mathcal{R}_{ST}^{AS}}{\partial \xi_{ST}} &= (\xi_{ST}-\xi_{ST,n})\,\frac{\partial|\sigma_{ST}|}{\partial \xi_{ST}} \;+\; \pi_{ST}^{AS}\,(1-\xi_{ST})\,\frac{\partial|\sigma_{ST}|}{\partial \xi_{ST}} \\
&+ (|\sigma_{ST}| - \sigma_{f,ST}^{AS}) \;-\; \pi_{ST}^{AS}\,(|\sigma_{ST}| - |\sigma_{ST,n}|) \\
\frac{\partial \mathcal{R}^{AS}}{\partial \xi} &= (\xi-\xi_n)\,\frac{\partial|\sigma|}{\partial \xi} \;+\; \pi^{AS}\,(1-\xi)\,\frac{\partial|\sigma|}{\partial \xi} + \frac{\Delta t}{\tau}\,(\xi-\xi_{ST})\,\frac{\partial|\sigma|}{\partial \xi} \\
&+ (|\sigma| - \sigma_f^{AS}) \;-\; \pi^{AS}\,(|\sigma| - |\sigma_n|) \;+\; \frac{\Delta t}{\tau}\,(|\sigma| - \sigma_f^{AS})
\end{aligned}$$

$$\begin{aligned}
\frac{\partial \mathcal{R}_{ST}^{AS}}{\partial \xi_{ST}} &= 2\,(\xi_{ST}-\xi_{ST,n})\,(|\sigma_{ST}| - \sigma_{f,ST}^{AS})\,\frac{\partial|\sigma_{ST}|}{\partial \xi_{ST}} - \beta_{ST}^{AS}\,(1-\xi_{ST})\,\frac{\partial|\sigma_{ST}|}{\partial \xi_{ST}} \\
&+ (|\sigma_{ST}| - \sigma_{f,ST}^{AS})^2 + \beta_{ST}^{AS}\,(|\sigma_{ST}| - |\sigma_{ST,n}|) \\
\frac{\partial \mathcal{R}^{AS}}{\partial \xi} &= 2\,(\xi-\xi_n)\,(|\sigma| - \sigma_f^{AS})\,\frac{\partial|\sigma|}{\partial \xi} + 2\,\frac{\Delta t}{\tau}\,(\xi-\xi_{ST})\,(|\sigma| - \sigma_f^{AS})\,\frac{\partial|\sigma|}{\partial \xi} \\
&+ (|\sigma| - \sigma_f^{AS})^2 - \beta^{AS}\,(1-\xi)\,\frac{\partial|\sigma|}{\partial \xi} + \beta^{AS}\,(|\sigma| - |\sigma_n|) + \frac{\Delta t}{\tau}\,(|\sigma| - \sigma_f^{AS})^2
\end{aligned}$$

Conversion from martensite into austenite

$$\frac{\partial \mathcal{R}_{ST}^{SA}}{\partial \xi_{ST}} = -\xi_{ST,n}\,\frac{\partial|\sigma_{ST}|}{\partial \xi_{ST}} + (|\sigma_{ST,n}| - \sigma_{f,ST}^{SA})$$

$$\frac{\partial \mathcal{R}^{SA}}{\partial \xi} = -\xi_n\,\frac{\partial|\sigma|}{\partial \xi} + \frac{\Delta t}{\tau}\,(\xi - \xi_{ST})\,\frac{\partial|\sigma|}{\partial \xi} + \frac{\Delta t}{\tau}\,(|\sigma| - \sigma_f^{SA}) + (|\sigma_n| - \sigma_f^{SA})$$

$$\begin{aligned}\frac{\partial \mathcal{R}_{ST}^{SA}}{\partial \xi_{ST}} &= (\xi_{ST} - \xi_{ST,n})\,\frac{\partial|\sigma_{ST}|}{\partial \xi_{ST}} - \pi_{ST}^{SA}\,\xi_{ST}\,\frac{\partial|\sigma_{ST}|}{\partial \xi_{ST}} \\ &+ (|\sigma_{ST}| - \sigma_{f,ST}^{SA}) - \pi_{ST}^{SA}\,(|\sigma_{ST}| - |\sigma_{ST,n}|)\end{aligned}$$

$$\begin{aligned}\frac{\partial \mathcal{R}^{SA}}{\partial \xi} &= (\xi - \xi_n)\,\frac{\partial|\sigma|}{\partial \xi} - \pi^{SA}\,\xi\,\frac{\partial|\sigma|}{\partial \xi} + \frac{\Delta t}{\tau}\,(\xi - \xi_{ST})\,\frac{\partial|\sigma|}{\partial \xi} \\ &+ (|\sigma| - \sigma_f^{SA}) - \pi^{SA}\,(|\sigma| - |\sigma_n|) + \frac{\Delta t}{\tau}\,(|\sigma| - \sigma_f^{SA})\end{aligned}$$

$$\begin{aligned}\frac{\partial \mathcal{R}_{ST}^{SA}}{\partial \xi_{ST}} &= 2\,(\xi_{ST} - \xi_{ST,n})\,(|\sigma_{ST}| - \sigma_{f,ST}^{SA})\,\frac{\partial|\sigma_{ST}|}{\partial \xi_{ST}} - \beta_{ST}^{SA}\,\xi_{ST}\,\frac{\partial|\sigma_{ST}|}{\partial \xi_{ST}} \\ &+ (|\sigma_{ST}| - \sigma_{f,ST}^{SA})^2 - \beta_{ST}^{SA}\,(|\sigma_{ST}| - |\sigma_{ST,n}|)\end{aligned}$$

$$\begin{aligned}\frac{\partial \mathcal{R}^{SA}}{\partial \xi} &= 2\,(\xi - \xi_n)\,(|\sigma| - \sigma_f^{SA})\,\frac{\partial|\sigma|}{\partial \xi} + 2\,\frac{\Delta t}{\tau}\,(\xi - \xi_{ST})\,(|\sigma| - \sigma_f^{SA})\,\frac{\partial|\sigma|}{\partial \xi} \\ &+ (|\sigma| - \sigma_f^{SA})^2 - \beta^{SA}\,\xi\,\frac{\partial|\sigma|}{\partial \xi} - \beta^{SA}\,(|\sigma| - \sigma_n) + \frac{\Delta t}{\tau}\,(|\sigma| - \sigma_f^{SA})^2\end{aligned}$$

B.3 Thermo-Mechanical Model

We first need to linearize the heat equation, where the only non-trivial term comes from the linearization of the heat source, b_d, as highlighted by Eq. 5.42:

$$\mathrm{d}b_d = \left(\frac{1}{t - t_n}\right) \mathrm{d}\Pi_1 \, \lambda + \Pi_1 \, \mathrm{d}\lambda + \mathrm{d}\Gamma_1 T + \Gamma_1 \, \mathrm{d}T$$

where, recalling Eqs. 5.59 and 5.60, we have:

$$\begin{aligned} \mathrm{d}\Pi_1 &= \epsilon_L \, \mathrm{sgn}(\epsilon) \, \mathrm{d}\sigma - \Delta\eta \, \mathrm{d}T \\ \mathrm{d}\Gamma_1 &= [\epsilon_n - \epsilon + \mathrm{sgn}(\epsilon) \, \epsilon_L \, \lambda] \, \mathrm{d}E + [E \, \alpha \, \epsilon_L \, \mathrm{sgn}(\epsilon) + \Delta\eta] \, \mathrm{d}\xi \end{aligned}$$

with

$$\mathrm{d}\sigma = \frac{\partial \sigma}{\partial \xi} \, \mathrm{d}\xi + \frac{\partial \sigma}{\partial T} \, \mathrm{d}T$$

and

$$\begin{aligned} \frac{\partial \sigma}{\partial \xi} &= -\frac{E_A E_S}{\left[E_A \, E_S + \xi \, (E_A - E_S)\right]^2} \cdot [\epsilon - \epsilon_L \, \xi \, \mathrm{sgn}(\epsilon) - \alpha \, (T - T_0)] - E \, \epsilon_L \, \mathrm{sgn}(\epsilon) \\ \frac{\partial \sigma}{\partial T} &= -E \, \alpha \end{aligned}$$

So far, the only unknown left is $\mathrm{d}\lambda$ (i.e. equal to $\mathrm{d}\xi$), which can be computed by linearizing the active evolutionary equation, generally written as $\mathcal{R}(\lambda, T) = 0$. Accordingly:

$$\mathrm{d}\mathcal{R} = \frac{\partial \mathcal{R}}{\partial \lambda} \, \mathrm{d}\lambda + \frac{\partial \mathcal{R}}{\partial T} \, \mathrm{d}T$$

from which we obtain:

$$\mathrm{d}\lambda = \left[-\left(\frac{\partial \mathcal{R}}{\partial \lambda}\right)^{-1} \frac{\partial \mathcal{R}}{\partial T} \right] \mathrm{d}T$$

We also need the derivatives of the driving force with respect to both the martensite fraction and temperature:

$$\begin{aligned} \frac{\partial F}{\partial \xi} &= \frac{\partial |\sigma|}{\partial \xi} = \mathrm{sgn}(\epsilon) \frac{\partial \sigma}{\partial \xi} \\ \frac{\partial F}{\partial T} &= \frac{\partial |\sigma|}{\partial T} - A = \mathrm{sgn}(\epsilon) \frac{\partial \sigma}{\partial T} - A \end{aligned}$$

Finally, we have to compute the derivatives of the evolutionary equations. In particular, each pair of expressions still refer to linear, power and exponential rules respectively.

Conversion of austenite into martensite

$$\begin{aligned}\frac{\partial \mathcal{R}^{AS}}{\partial \xi} &= (1-\xi_n)\,\frac{\partial F}{\partial \xi} + \left(F_n - R_f^{AS}\right)\\ \frac{\partial \mathcal{R}^{AS}}{\partial T} &= (1-\xi_n)\,\frac{\partial F}{\partial T}\end{aligned}$$

$$\begin{aligned}\frac{\partial \mathcal{R}^{AS}}{\partial \xi} &= \left[(\xi-\xi_n) + \pi^{AS}\,(1-\xi)\right]\frac{\partial F}{\partial \xi} + \left(F_n - R_f^{AS}\right) - \pi^{AS}\,(F-F_n)\\ \frac{\partial \mathcal{R}^{AS}}{\partial T} &= \left[(\xi-\xi_n) + \pi^{AS}\,(1-\xi)\right]\frac{\partial F}{\partial T}\end{aligned}$$

$$\begin{aligned}\frac{\partial \mathcal{R}^{AS}}{\partial \xi} &= \left[2\,(\xi-\xi_n)\left(F-R_f^{AS}\right) - \beta^{AS}\,(1-\xi)\right]\frac{\partial F}{\partial \xi} + \left(F_n - R_f^{AS}\right)^2 + \beta^{AS}\,(F-F_n)\\ \frac{\partial \mathcal{R}^{AS}}{\partial T} &= \left[2\,(\xi-\xi_n)\left(F-R_f^{AS}\right) - \beta^{AS}\,(1-\xi)\right]\frac{\partial F}{\partial T}\end{aligned}$$

Conversion of martensite into austenite

$$\begin{aligned}\frac{\partial \mathcal{R}^{SA}}{\partial \xi} &= -\,\xi_n\,\frac{\partial F}{\partial \xi} + \left(F_n - R_f^{SA}\right)\\ \frac{\partial \mathcal{R}^{SA}}{\partial T} &= -\,\xi_n\,\frac{\partial F}{\partial T}\end{aligned}$$

$$\begin{aligned}\frac{\partial \mathcal{R}^{SA}}{\partial \xi} &= \left[(\xi-\xi_n) - \pi^{SA}\,\xi\right]\frac{\partial F}{\partial \xi} + \left(F_n - R_f^{SA}\right) - \pi^{SA}\,(F-F_n)\\ \frac{\partial \mathcal{R}^{SA}}{\partial T} &= \left[(\xi-\xi_n) - \pi^{SA}\,\xi\right]\frac{\partial F}{\partial T}\end{aligned}$$

$$\begin{aligned}\frac{\partial \mathcal{R}^{SA}}{\partial \xi} &= \left[2\,(\xi-\xi_n)\left(F-R_f^{SA}\right) - \beta^{SA}\,\xi\right]\frac{\partial F}{\partial \xi} + \left(F_n - R_f^{SA}\right)^2 - \beta^{SA}\,(F-F_n)\\ \frac{\partial \mathcal{R}^{SA}}{\partial T} &= \left[2\,(\xi-\xi_n)\left(F-R_f^{SA}\right) - \beta^{SA}\,\xi\right]\frac{\partial F}{\partial T}\end{aligned}$$

C. CLOSED-FORM SOLUTION OF THE CONSTITUTIVE MODELS

C.1 Introduction

In this Appendix, we provide the coefficients of the algebraic equations needed to compute the martensite fraction in closed-form. As far as the viscous model is concerned, for brevity we only report the coefficients related to the dynamic martensite fraction since the ones related to the static martensite fraction can be computed similarly. For both phase transformations, we present three groups of expressions that refer to linear, power and exponential rules respectively.

C.2 Viscous Model

Conversion from austenite into martensite

$$
\begin{aligned}
A &= (E_A - E_S)\left[|\sigma_n| - \sigma_f^{AS}\left(1 + \frac{\Delta\, t}{\tau}\right)\right] - \frac{\Delta\, t}{\tau}\, E_A\, E_S\, \epsilon_L \\
B &= (E_A - E_S)\left[-|\sigma_n| + \sigma_f^{AS}\left(\xi_n + \frac{\Delta\, t}{\tau}\, \xi_{ST}\right)\right] + E_S\left[[|\sigma_n| - \sigma_f^{AS}\left(1 + \frac{\Delta\, t}{\tau}\right)\right] \\
&+ E_A\, E_S\left[\epsilon_L\left(\xi_n - 1 + \frac{\Delta\, t}{\tau}\, \xi_{ST}\right) + \frac{\Delta\, t}{\tau}\, \epsilon\, \mathrm{sgn}(\epsilon)\right] \\
C &= E_A\, E_S\, \epsilon\, \mathrm{sgn}(\epsilon)\left(-\xi_n + 1 - \frac{\Delta\, t}{\tau}\, \xi_{ST}\right) + E_S\left[\sigma_f^{AS}\left(\xi_n + \frac{\Delta\, t}{\tau}\, \xi_{ST}\right) - |\sigma_n|\right]
\end{aligned}
$$

$$
\begin{aligned}
A &= (E_A - E_S)\left[\pi^{AS}\,|\sigma_n| - \sigma_f^{AS}\,\left(1+\frac{\Delta\,t}{\tau}\right)\right] - E_A\,E_S\,\epsilon_L\left(-1+\pi^{AS}-\frac{\Delta\,t}{\tau}\right)\\
B &= (E_A - E_S)\left[-\pi^{AS}|\sigma_n| + \sigma_f^{AS}\,\left(\xi_n+\frac{\Delta\,t}{\tau}\,\xi_{ST}\right)\right] + E_S\left[\pi^{AS}|\sigma_n| - \sigma_f^{AS}\,\left(1+\frac{\Delta\,t}{\tau}\right)\right]\\
&+ E_A\,E_S\left[\epsilon_L\left(\xi_n-\pi^{AS}+\frac{\Delta\,t}{\tau}\,\xi_{ST}\right)+\epsilon\,\mathrm{sgn}(\epsilon)\left(1-\pi^{AS}+\frac{\Delta\,t}{\tau}\right)\right]\\
C &= E_A\,E_S\,\epsilon\,\mathrm{sgn}(\epsilon)\left(-\xi_n+\pi^{AS}-\frac{\Delta\,t}{\tau}\,\xi_{ST}\right) + E_S\left[\sigma_f^{AS}\left(\xi_n+\frac{\Delta\,t}{\tau}\,\xi_{ST}\right)-\pi^{AS}|\sigma_n|\right]
\end{aligned}
$$

$$
\begin{aligned}
A &= (E_A - E_S)^2\left[-\beta^{AS}\,|\sigma_n| + \sigma_f^{AS^2}\left(1+\frac{\Delta\,t}{\tau}\right)\right] + (E_A\,E_S\,\epsilon_L)^2\left(1+\frac{\Delta\,t}{\tau}\right)\\
&+ E_A\,E_S\,(E_A-E_S)\,\epsilon_L\left[2\,\sigma_f^{AS}+\left(1+\frac{\Delta\,t}{\tau}\right)-\beta^{AS}\right]\\
B &= (E_A - E_S)^2\left[\beta^{AS}\,|\sigma_n| - \sigma_f^{AS^2}\left(\xi_n+\frac{\Delta\,t}{\tau}\,\xi_{ST}\right)\right]\\
&+ (E_A\,E_S)^2\left[-\epsilon_L^2\left(\xi_n+\frac{\Delta\,t}{\tau}\,\xi_{ST}\right)-2\,\epsilon_L\,\epsilon\,\mathrm{sgn}(\epsilon)\left(1+\frac{\Delta\,t}{\tau}\right)\right]\\
&+ (E_A\,E_S)(E_A-E_S)\left\{\beta^{AS}\,[\epsilon_L+\epsilon\,\mathrm{sgn}(\epsilon)]-2\,\sigma_f^{AS}\epsilon\,\mathrm{sgn}(\epsilon)\left(1+\frac{\Delta\,t}{\tau}\right)-2\,\sigma_f^{AS}\epsilon_L\left(1+\frac{\Delta\,t}{\tau}\right)\right\}\\
&+ E_A\,E_S^2\left[-\beta^{AS}\epsilon_L+2\,\sigma_f^{AS}\epsilon_L\left(1+\frac{\Delta\,t}{\tau}\right)\right]\\
&+ 2\,E_S\,(E_A-E_S)\left[-\beta^{AS}\,|\sigma_n|+\sigma_f^{AS^2}+\left(1+\frac{\Delta\,t}{\tau}\right)\right]\\
C &= (E_AE_S)^2\left[\epsilon^2\left(1+\frac{\Delta\,t}{\tau}\right)+2\,\epsilon_L\,\mathrm{sgn}(\epsilon)\,\epsilon_L\left(\xi_n+\frac{\Delta\,t}{\tau}\,\xi_{ST}\right)\right]\\
&+ E_S^2\left[\beta^{AS}\,|\sigma_n|+\sigma_f^{AS^2}\,\left(1+\frac{\Delta\,t}{\tau}\right)\right]\\
&+ E_A\,E_S^2\left\{-2\,\sigma_f^{AS}\,\epsilon\,\mathrm{sgn}(\epsilon)\left(1+\frac{\Delta\,t}{\tau}\right)-2\,\sigma_f^{AS}\,\epsilon_L\left(\xi_n+\frac{\Delta\,t}{\tau}\,\xi_{ST}\right)+\beta^{AS}\,[\epsilon_L+\epsilon\,\mathrm{sgn}(\epsilon)]\right\}\\
&+ (E_A\,E_S)(E_A-E_S)\left[2\,\sigma_f^{AS}\,\epsilon\,\mathrm{sgn}(\epsilon)\left(\xi_n+\frac{\Delta\,t}{\tau}\,\xi_{ST}\right)-\beta^{AS}\epsilon\,\mathrm{sgn}(\epsilon)\right]\\
&+ 2\,E_S\,(E_A-E_S)\left[\beta^{AS}\,|\sigma_n|-\sigma_f^{AS^2}\left(\xi_n+\frac{\Delta\,t}{\tau}\,\xi_{ST}\right)\right]
\end{aligned}
$$

$$
\begin{aligned}
D &= -(E_A\,E_S\,\epsilon)^2\left(\xi_n+\frac{\Delta\,t}{\tau}\,\xi_{ST}\right)+E_S^2\left[\beta^{AS}\,|\sigma_n|-\sigma_f^{AS^2}\left(\xi_n+\frac{\Delta\,t}{\tau}\,\xi_{ST}\right)\right]\\
&+ E_A\,E_S^2\left[2\,\sigma_f^{AS}\,\epsilon\,\mathrm{sgn}(\epsilon)\left(\xi_n+\frac{\Delta\,t}{\tau}\,\xi_{ST}\right)-\beta^{AS}\,\epsilon\,\mathrm{sgn}(\epsilon)\right]
\end{aligned}
$$

Conversion from martensite into austenite

$$
\begin{aligned}
A &= (E_A-E_S)\left[|\sigma_n|-\sigma_f^{SA}\,\left(1+\frac{\Delta\,t}{\tau}\right)\right]-\frac{\Delta\,t}{\tau}\,E_A\,E_S\,\epsilon_L\\
B &= \sigma_f^{SA}(E_A-E_S)\left(\xi_n+\frac{\Delta\,t}{\tau}\,\xi_{ST}\right)+E_S\left[|\sigma_n|-\sigma_f^{SA}\,\left(1+\frac{\Delta\,t}{\tau}\right)\right]\\
&+ E_A\,E_S\left[\epsilon_L\left(\xi_n+\frac{\Delta\,t}{\tau}\,\xi_{ST}\right)+\frac{\Delta\,t}{\tau}\,\epsilon\,\mathrm{sgn}(\epsilon)\right]\\
C &= E_A\,E_S\,\epsilon\,\mathrm{sgn}(\epsilon)\left(-\xi_n-\frac{\Delta\,t}{\tau}\,\xi_{ST}\right)+E_S\,\sigma_f^{SA}\left(\xi_n+\frac{\Delta\,t}{\tau}\,\xi_{ST}\right)
\end{aligned}
$$

$$
\begin{aligned}
A &= (E_A-E_S)\left[\pi^{SA}\,|\sigma_n|-\sigma_f^{SA}\,\left(1+\frac{\Delta\,t}{\tau}\right)\right]+E_A\,E_S\,\epsilon_L\left(\pi^{SA}-1-\frac{\Delta\,t}{\tau}\right)\\
B &= \sigma_f^{SA}\,(E_A-E_S)\left(\xi_n+\frac{\Delta\,t}{\tau}\,\xi_{ST}\right)+E_S\left[\pi^{SA}|\sigma_n|-\sigma_f^{SA}\,\left(1+\frac{\Delta\,t}{\tau}\right)\right]\\
&+ E_A\,E_S\left[\epsilon_L\left(\xi_n+\frac{\Delta\,t}{\tau}\,\xi_{ST}\right)+\epsilon\,\mathrm{sgn}(\epsilon)\left(1-\pi^{SA}+\frac{\Delta\,t}{\tau}\right)\right]\\
C &= E_A\,E_S\,\epsilon\,\mathrm{sgn}(\epsilon)\left(-\xi_n-\frac{\Delta\,t}{\tau}\,\xi_{ST}\right)+E_S\,\sigma_f^{SA}\left(\xi_n+\frac{\Delta\,t}{\tau}\,\xi_{ST}\right)
\end{aligned}
$$

$$
\begin{aligned}
A &= (E_A-E_S)^2\left[\beta^{SA}\,|\sigma_n|+\sigma_f^{SA^2}\left(1+\frac{\Delta\,t}{\tau}\right)\right]+(E_A\,E_S\,\epsilon_L)^2\left(1+\frac{\Delta\,t}{\tau}\right)\\
&+ E_A\,E_S\,(E_A-E_S)\,\epsilon_L\left(1+\frac{\Delta\,t}{\tau}\right)
\end{aligned}
$$

$$
\begin{aligned}
B &= -\sigma_f^{SA\,2}\,(E_A - E_S)^2 \left(\xi_n + \frac{\Delta\, t}{\tau}\,\xi_{ST}\right) \\
&+ (E_A\,E_S)^2 \left[-\epsilon_L^2 \left(\xi_n + \frac{\Delta\, t}{\tau}\,\xi_{ST}\right) - 2\epsilon_L\,\epsilon\,\mathrm{sgn}(\epsilon)\left(1 + \frac{\Delta\, t}{\tau}\right)\right] \\
&+ (E_A\,E_S)\,(E_A - E_S)\left[\beta^{AS}\epsilon\,\mathrm{sgn}(\epsilon) - 2\sigma_f^{AS}\epsilon\,\mathrm{sgn}(\epsilon)\left(1 + \frac{\Delta\, t}{\tau}\right) - 2\sigma_f^{AS}\epsilon_L\left(1 + \frac{\Delta\, t}{\tau}\right)\right] \\
&+ E_A\,E_S^2\left[\beta^{SA}\epsilon_L + 2\,\sigma_f^{SA}\epsilon_L\left(1 + \frac{\Delta\, t}{\tau}\right)\right] \\
&+ 2\,E_S\,(E_A - E_S)\left[\beta^{SA}\,|\sigma_n| + \sigma_f^{SA\,2} + \left(1 + \frac{\Delta\, t}{\tau}\right)\right] \\
C &= (E_A\,E_S)^2\left[\epsilon^2\left(1 + \frac{\Delta\, t}{\tau}\right) + 2\,\epsilon_L\,\mathrm{sgn}(\epsilon)\,\epsilon_L\left(\xi_n + \frac{\Delta\, t}{\tau}\,\xi_{ST}\right)\right] \\
&+ E_S^2\left[\beta^{SA}\,|\sigma_n| + \sigma_f^{SA\,2}\,\left(1 + \frac{\Delta\, t}{\tau}\right)\right] \\
&+ E_A\,E_S^2\left[-2\,\sigma_f^{SA}\,\epsilon\,\mathrm{sgn}(\epsilon)\left(1 + \frac{\Delta\, t}{\tau}\right) - 2\,\sigma_f^{SA}\,\epsilon_L\left(\xi_n + \frac{\Delta\, t}{\tau}\,\xi_{ST}\right) - \beta^{SA}\epsilon\,\mathrm{sgn}(\epsilon)\right] \\
&+ 2\,(E_A\,E_S)\,(E_A - E_S)\,\sigma_f^{SA}\,\epsilon\,\mathrm{sgn}(\epsilon)\left(\xi_n + \frac{\Delta\, t}{\tau}\,\xi_{ST}\right) \\
&+ 2\,E_S\,(E_A - E_S)\,\sigma_f^{AS\,2}\left(\xi_n + \frac{\Delta\, t}{\tau}\right) \\
D &= -(E_A\,E_S\,\epsilon)^2\left(\xi_n + \frac{\Delta\, t}{\tau}\,\xi_{ST}\right) - E_S^2\,\sigma_f^{AS\,2}\left(\xi_n + \frac{\Delta\, t}{\tau}\,\xi_{ST}\right) \\
&+ 2\,E_A\,E_S^2\,\sigma_f^{SA}\,\epsilon\,\mathrm{sgn}(\epsilon)\left(\xi_n + \frac{\Delta\, t}{\tau}\,\xi_{ST}\right)
\end{aligned}
$$

C.3 Thermo-Mechanical Model

Conversion from austenite into martensite

$$
\begin{aligned}
A &= (E_A - E_S)\,(F_n - R_f^{AS}) \\
B &= E_A\,E_S\,\epsilon_L\,(\xi_n - 1) + E_S\,(F_n - R_f^{AS}) + (E_A - E_S)\,\left[A\,(\xi_n - 1)\,(T - T_U)\; - F_n + \xi_n\,R_f^{AS}\right] \\
C &= -E_A\,E_S\,\epsilon\,\mathrm{sgn}(\epsilon)\,(\xi_n - 1) + E_S\,\left[A\,(\xi_n - 1)\,(T - T_U)\; - F_n + \xi_n\,R_f^{AS}\right]
\end{aligned}
$$

$$
\begin{aligned}
A &= E_A\,E_S\,\epsilon_L\,(\pi^{AS} - 1) + (E_A - E_S)\left[A\,(T - T_U)(\pi^{AS} - 1) + \pi^{AS}\,F_n - R_f^{AS}\right] \\
B &= E_A\,E_S\,\epsilon\,\mathrm{sgn}(\epsilon)(1 - \pi^{AS}) + E_A\,E_S\,\epsilon_L\,(\xi_n - \pi^{AS}) + E_S\,(\pi^{AS}\,F_n - R_f^{AS}) \\
&- A\,E_S\,(T - T_U)(1 - \pi^{AS}) + (E_A - E_S)\;\left[A\,(\xi_n - \pi^{AS})\,(T - T_U)\; - \pi^{AS}\,F_n + \xi_n\,R_f^{AS}\right] \\
C &= -E_A\,E_S\,\epsilon\,\mathrm{sgn}(\epsilon)\,(\xi_n - \pi^{AS}) + E_S\,\left[A\,(\xi_n - \pi^{AS})\,(T - T_U)\; - \pi^{AS}\,F_n + \xi_n\,R_f^{AS}\right]
\end{aligned}
$$

$$
\begin{aligned}
A &= (E_A\,E_S\,\epsilon_L)^2 + (E_A - E_S)^2\{\left[A\,(T - T_U) + R_f^{AS}\right]^2\} \\
&- \beta^{AS}\;[A\,(T - T_U) + F_n]\} + E_A\,E_S\,(E_A - E_S)\,\epsilon_L\,\{2\left[A\,(T - T_U) + R_f^{AS}\right] - \beta^{AS}\} \\
B &= (E_A\,E_S)^2\{-\epsilon_L\,[2\,\epsilon\,\mathrm{sgn}(\epsilon) + \xi_n\,\epsilon_L]\} + 2\,E_S\,(E_A - E_S)\{\left[A\,(T - T_U) + R_f^{AS}\right]^2 \\
&- \beta^{AS}\;[A\,(T - T_U) + F_n]\} + E_A\,E_S\,(E_A - E_S)\{-2A\,(T - T_U)\,[\epsilon\,\mathrm{sgn}(\epsilon) + \xi_n\,\epsilon_L] \\
&+ \epsilon\,\mathrm{sgn}(\epsilon)\left[\beta^{AS} - 2R_f^{AS}\right] - \epsilon_L\left[\beta^{AS} - 2\,\xi_n\,R_f^{AS}\right]\} - (E_A\,E_S)^2\{\xi_n\left[A\,(T - T_U) + R_f^{AS}\right] \\
&- \beta^{AS}\;[A\,(T - T_U) + F_n] + E_A\,E_S^2\,\epsilon_L\{2\left[A\,(T - T_U) + R_f^{AS}\right] - \beta^{AS}\} \\
C &= (E_A\,E_S)^2\epsilon\,\{[\epsilon + 2\,\xi_n\,\epsilon_L\,\mathrm{sgn}(\epsilon)]\} + E_S^2\{\left[A\,(T - T_U) + R_f^{AS}\right]^2 \\
&- \beta^{AS}\;[A\,(T - T_U) + F_n]\} + E_A\,E_S\,(E_A - E_S)\,\epsilon\,\mathrm{sgn}(\epsilon)\,\{2\,\xi_n\left[A\,(T - T_U) + R_f^{AS}\right] - \beta^{AS}\} \\
&- E_S\,(E_A - E_S)\,\{2\,\xi_n\left[A\,(T - T_U) + R_f^{AS}\right]^2 - 2\,\beta^{AS}\,[A\,(T - T_U) + F_n]\} \\
&- E_A\,E_S^2\{2\,A\,(T - T_U)\,[\epsilon\,\mathrm{sgn}(\epsilon) + \xi_n\,\epsilon_L] + \epsilon\,\mathrm{sgn}(\epsilon)\left[2\,R_f^{AS} - \beta^{AS}\right] + \epsilon_L\left[2\,\xi_n\,R_f^{AS} - \beta^{AS}\right]\} \\
D &= -\xi_n\,(E_A\,E_S\epsilon)^2 - E_S^2\{\xi_n\left[A\,(T - T_U) + R_f^{AS}\right]^2 - \beta^{AS}\;[A\,(T - T_U) + F_n]\} \\
&+ E_A\,E_S^2\,\epsilon\,\mathrm{sgn}(\epsilon)\{2\,\xi_n\left[A\,(T - T_U) + R_f^{AS}\right] - \beta^{AS}\}
\end{aligned}
$$

Conversion from martensite into austenite

$$
\begin{aligned}
A &= (E_A - E_S)\,(F_n - R_f^{SA}) \\
B &= E_A\,E_S\,\epsilon_L\,\xi_n + E_S\,(F_n - R_f^{SA}) + (E_A - E_S)\,\left[A\,\xi_n\,(T - T_U) + \xi_n\,R_f^{SA}\right] \\
C &= -E_A\,E_S\,\epsilon\,\mathrm{sgn}(\epsilon)\,\xi_n + E_S\,\xi_n\left[A\,(T - T_U) + \xi_n\,R_f^{SA}\right]
\end{aligned}
$$

$$
\begin{aligned}
A &= E_A\,E_S\,\epsilon_L\,(\pi^{SA} - 1) + (E_A - E_S)\left[A\,(T - T_U)(\pi^{SA} - 1) + \pi^{SA}\,F_n - R_f^{SA}\right] \\
B &= E_A\,E_S\,\epsilon\,\mathrm{sgn}(\epsilon)(1 - \pi^{SA}) + E_A\,E_S\,\epsilon_L\,\xi_n + E_S\,(\pi^{SA}\,F_n - R_f^{SA}) \\
&- A\,E_S\,(T - T_U)(1 - \pi^{SA}) + (E_A - E_S)\,\left[A\,\xi_n\,(T - T_U) + \xi_n\,R_f^{SA}\right] \\
C &= -E_A\,E_S\,\epsilon\,\mathrm{sgn}(\epsilon)\,\xi_n + E_S\,\xi_n\left[A\,(T - T_U) + R_f^{SA}\right]
\end{aligned}
$$

$$
\begin{aligned}
A &= (E_A\,E_S\,\epsilon_L)^2 + (E_A - E_S)^2\{\left[A\,(T - T_U) + R_f^{SA}\right]^2\} \\
&+ \beta^{SA}\,[A\,(T - T_U) + F_n]\} + E_A\,E_S\,(E_A - E_S)\,\epsilon_L\,\{2\left[A\,(T - T_U) + R_f^{SA}\right] - \beta^{SA}\} \\
B &= (E_A\,E_S)^2\{-\epsilon_L\,[2\,\epsilon\,\mathrm{sgn}(\epsilon) + \xi_n\,\epsilon_L]\} + 2\,E_S\,(E_A - E_S)\{\left[A\,(T - T_U) + R_f^{SA}\right]^2 \\
&+ \beta^{SA}\,[A\,(T - T_U) + F_n]\} + E_A\,E_S\,(E_A - E_S)\{-2A\,(T - T_U)\,[\epsilon\,\mathrm{sgn}(\epsilon) + \xi_n\,\epsilon_L] \\
&- \epsilon\,\mathrm{sgn}(\epsilon)\left[\beta^{SA} + 2\,R_f^{SA}\right] - 2\,\epsilon_L\,\xi_n\,R_f^{SA}\} - (E_A\,E_S)^2\,\xi_n\left[A\,(T - T_U) + R_f^{SA}\right]^2 \\
&+ E_A\,E_S^2\,\epsilon_L\{2\left[A\,(T - T_U) + R_f^{SA}\right] + \beta^{SA}\} \\
C &= (E_A\,E_S)^2\epsilon\,\{[\epsilon + 2\,\xi_n\,\epsilon_L\,\mathrm{sgn}(\epsilon)]\} + E_S^2\{\left[A\,(T - T_U) + R_f^{SA}\right]^2 \\
&+ \beta^{SA}\,[A\,(T - T_U) + F_n]\} + 2\,\xi_n\,E_A\,E_S\,(E_A - E_S)\,\epsilon\,\mathrm{sgn}(\epsilon)\left[A\,(T - T_U) + R_f^{AS}\right]\} \\
&+ 2\,\xi_n\,E_S\,(E_A - E_S)\,\left[A\,(T - T_U) + R_f^{AS}\right]^2 \\
&- E_A\,E_S^2\{2\,A\,(T - T_U)\,[\epsilon\,\mathrm{sgn}(\epsilon) + \xi_n\,\epsilon_L] + \epsilon\,\mathrm{sgn}(\epsilon)\left[2\,R_f^{AS} + \beta^{SA}\right] + 2\,\xi_n\,R_f^{SA}\,\epsilon_L\} \\
D &= -\xi_n\,(E_A\,E_S\,\epsilon)^2 - E_S^2\{\xi_n\left[A\,(T - T_U) + R_f^{SA}\right]^2\} + 2\,E_A\,E_S^2\,\epsilon\,\mathrm{sgn}(\epsilon)\,\xi_n\left[A\,(T - T_U) + R_f^{SA}\right]
\end{aligned}
$$